

# IDENTIFYING MICROBIAL DRIVERS IN BIOLOGICAL PHENOTYPES WITH A BAYESIAN NETWORK REGRESSION MODEL

**Samuel Ozminkowski**

Department of Statistics  
Wisconsin Institute for Discovery  
University of Wisconsin-Madison  
Madison, WI

**Claudia Solís-Lemus**

Department of Plant Pathology  
Wisconsin Institute for Discovery  
University of Wisconsin-Madison  
Madison, WI  
[solislemus@wisc.edu](mailto:solislemus@wisc.edu)

## Abstract

In Bayesian Network Regression models, networks are considered the predictors of continuous responses. These models have been successfully used in brain research to identify regions in the brain that are associated with specific human traits, yet their potential to elucidate microbial drivers in biological phenotypes for microbiome research remains unknown. In particular, microbial networks are challenging due to their high-dimension and high sparsity compared to brain networks. Furthermore, unlike in brain connectome research, in microbiome research, it is usually expected that the presence of microbes have an effect on the response (main effects), not just the interactions. Here, we develop the first thorough investigation of whether Bayesian Network Regression models are suitable for microbial datasets on a variety of synthetic and real data under diverse biological scenarios. We test whether the Bayesian Network Regression model that accounts only for interaction effects (edges in the network) is able to identify key drivers (microbes) in phenotypic variability. We show that this model is indeed able to identify influential nodes and edges in the microbial networks that drive changes in the phenotype for most biological settings, but we also identify scenarios where this method performs poorly which allows us to provide practical advice for domain scientists aiming to apply these tools to their datasets. We implement the model in an easy-to-use, publicly available Julia package at <https://github.com/solislemuslab/BayesianNetworkRegression.jl>.

**Keywords:** High-dimensional, Influential edges, Influential nodes, Microbiome, Networks, Sparsity

## Introduction

Microbial communities are among the main driving forces of biogeochemical processes in the biosphere. For one, many critical soil processes such as mineral weathering and soil cycling of mineral-sorbed organic matter are governed by mineral-associated microbes (Fierer et al., 2012; Whitman et al., 2018; Cates et al., 2019; Kranz and Whitman, 2019; Whitman et al., 2019). Additionally, plant and soil microbiome drive phenotypic variation related to plant health and crop production (Allsup and Lankau, 2019; Rioux et al., 2019; Lankau et al., 2020b,a). Lastly, the human gut microbiome plays a key role in the regulation of human health and behaviour (Young, 2017; Dupont et al., 2020; Siddiqui et al., 2021) and similar host-microbe associations have been studied for lung (Sulaiman et al., 2020; Stavropoulou et al., 2021) or skin microbiome (Callewaert et al., 2020). Understanding the composition of microbial communities and how these compositions shape specific biological phenotypes is crucial to comprehend complex biological processes in soil, plants and humans alike.

Standard approaches to study the connection between microbial communities and biological phenotypes rely on abundance matrices to represent the microbial compositions (Kunin et al., 2008; Holmes et al., 2012; Sankaran and Holmes, 2018; Holmes, 2019; Martin et al., 2020; Minot and Willis, 2019; Sankaran and Holmes, 2019; Williamson et al., 2019). Different experimental settings are defined and then microbial compositions are measured (as abundances) on each experimental setting. Next, the abundance matrices are used as input in a regression-type (or machine-learning) analysis to relate the microbial community to phenotypes of interest.

This standard pipeline, however, has limitations to find real connections between microbes and phenotypes. Many times, these standard approaches focus on the relationship between a single microbial OTU and the phenotype, adjusting for possible confounders like soil mineral characteristics. This univariate procedure has multiple assumptions that are violated by the complexity of the microbiome and can lead to elevated type-I error rates as well as reduced power. For example, univariate analyses of individual OTUs ignore correlations and interactions among the microbial communities, which could lead to power loss if the tested OTU is weakly correlated with an unmeasured relevant OTU. In contrast, high-dimensional regression models allow the inclusion of multiple microbial OTUs simultaneously (Xia et al., 2013; Lin et al., 2014; Tang and Chen, 2019; Grantham et al., 2020; Subedi et al., 2020), yet these models can be complicated by multicollinearity (Zou and Hastie, 2005) or instability due to overfitting. Furthermore, standard regression analyses rarely account for interactions among microbes or ignore potential epistasis (Cordell, 2009; McKinney et al., 2009; Fan et al., 2011; McKinney and Pajewski, 2012) among genes across the microbiome that can reduce power if not properly modeled (Kraft et al., 2007; Broadaway et al., 2015). Finally, microbial OTUs are usually represented as relative abundances (compositional data) which is restricted to sum to 1 and this affects how proportions behave in different experimental settings (e.g. changes in proportions in the microbial composition does not necessarily reflect actual biological changes in the interactions (Blanchet et al., 2020)).

Given that relative abundances only provide a snapshot of the composition of the community at the specific time of sampling and do not account for correlations between microbes, microbial interaction networks have been recently

preferred to represent microbial communities (Hsu et al., 2019; Zhou et al., 2020; Zhang et al., 2020; Benidire et al., 2020). Yet models to connect a microbial network to a biological phenotype remain unknown. On one side, recent years have seen an explosion of methods to infer microbial networks from a variety of data types (Peixoto, 2019; Fang et al., 2017; Kurtz et al., 2015a; Friedman and Alm, 2012). However, these methods aim to reconstruct *one* microbial network and do not attempt to connect this network to any biological phenotypes. On the other side, novel statistical theory has been developed to study samples of networks (Durante et al., 2017; Durante and Dunson, 2018; Guha and Guhaniyogi, 2021), yet again, these methods do not aim to understand the connection between the networks and a phenotype of interest. There has only been a handful of new methods that aim to identify associations between a sample of networks (predictors) and a phenotype (response) via a regression framework (Ma et al., 2019; Wang et al., 2019; Guha and Rodriguez, 2021). These methods, however, have only been studied for brain connectome networks which, unlike microbial networks, are intrinsically dense, and thus, methods to find associations between a sample of microbial networks and a biological phenotype remain unknown.

In this paper, we introduce a Bayesian Network Regression (BNR) model that uses the microbial network as the predictor of a biological phenotype (Fig. 1). This model intrinsically accounts for the interactions among microbes and is able to identify influential edges (interactions) and influential nodes (microbes) that drive the phenotypic variability. While the model itself is not new (Ma et al., 2019; Wang et al., 2019; Guha and Rodriguez, 2021), it has only been studied for brain connectome networks, and thus, its applicability to microbial networks which are inherently more high-dimensional and sparser has not been studied. Here, we test the BNR model on a variety of simulated scenarios with varying degrees of sparsity and effect sizes, as well as different biological assumptions on the effect of the microbes on the phenotype such as additive effects, interactions effects or functional redundancy (Rosenfeld, 2002). We show that this model is able to identify influential nodes and edges in the microbial networks that drive changes in the phenotype for most biological settings, but we also identify scenarios where this method performs poorly which allows us to provide practical advice for domain scientists aiming to apply these tools to their datasets. In addition, we implement the method in an open-source publicly available and easy-to-use new Julia package (`BayesianNetworkRegression.jl`) with online documentation and step-by-step tutorial which will allow scientists to easily apply this model on their own data. The computational speed and efficiency of the package makes it suitable to meet the needs of large datasets.

**Main contributions.** The Bayesian Network Regression (BNR) model is not new (Ma et al., 2019; Wang et al., 2019; Guha and Rodriguez, 2021), yet its applicability to microbial datasets has never been explored. Here, we develop the first thorough investigation of whether BNR models are suitable for microbial datasets on a variety of synthetic data that was generated under realistic biological scenarios. We also test the BNR model on real soil microbiome data and validate the findings with the published results (Wagg et al., 2019). In addition, we introduce a novel Julia package (`BayesianNetworkRegression.jl`) with extensive documentation that implements the BNR model and has broad applicability for the microbiome research community.

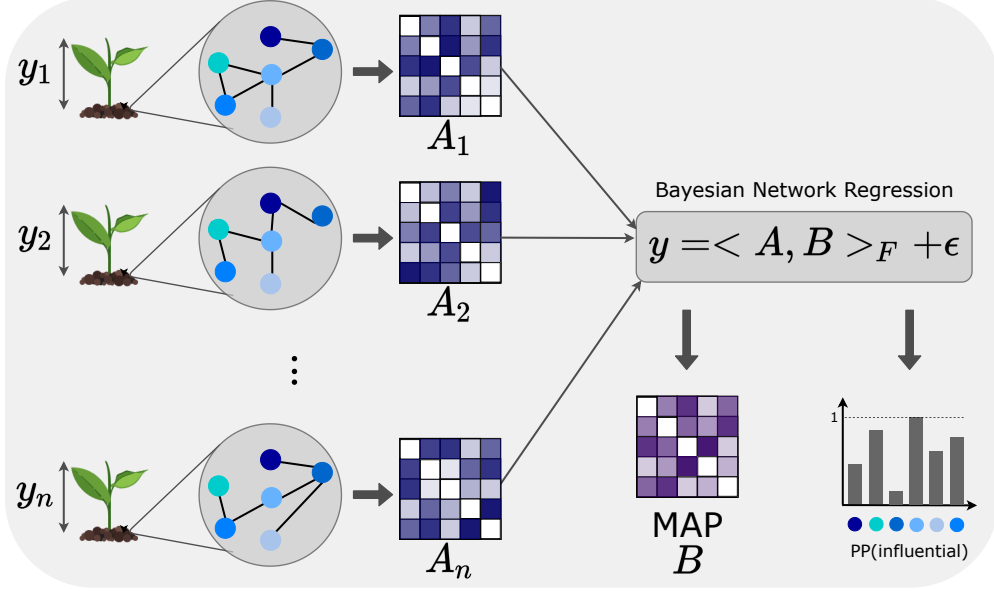


Figure 1: **Graphical abstract.** Samples contain a measured phenotype (e.g. height in plants)  $y_i$  and a microbial network as predictor which is converted into its adjacency matrix  $A_i$ . The Bayesian Network Regression model infers the regression coefficient matrix  $B$  with its maximum *a posteriori* (MAP) and the posterior probability of being an influential node for every node.

## Materials and methods

### Model and priors

We use the Bayesian Network Regression model initially defined in Guha and Rodriguez (2021) to elucidate associations between microbial drivers and biological phenotypes. We present below the theoretical details of the model and priors for the sake of completeness.

Let  $y_i$  denote the scalar continuous phenotype for sample  $i$  and let  $\mathcal{N}_i$  be the network that represents the microbial community in sample  $i$ . In this work, we assume that these networks have already been estimated and will be assumed to be known without error. That is, at this stage, we do not propagate statistical error in the inference of the microbial network (but see Discussion). For each microbial network, we can compute its adjacency matrix  $A_i \in \mathbb{R}^{V \times V}$  where  $V$  represents the number of nodes in the microbial network. While Guha and Rodriguez (2021) assume that all networks must have the same nodes (as is the case for brain connectome networks), here we allow different networks to have different nodes so that  $V$  represents the total number of nodes that appear in at least one network.

The network regression model is then defined as

$$y_i = \mu + \langle A_i, B \rangle_F + \epsilon_i$$

where  $\mu \in \mathbb{R}$  is the overall mean effect,  $\epsilon_i \sim N(0, \tau^2)$  is the error term,  $B \in \mathbb{R}^{V \times V}$  is the symmetric network coefficient matrix, and  $\langle \cdot \rangle_F$  represents the Frobenius inner product.

Given the symmetric structure of the predictor  $\mathbf{A}_i$ , we can rewrite this model with a design matrix  $\mathbf{X}$  where the  $i$ th row of  $\mathbf{X}$  is set to be the upper triangle of the  $i$ th adjacency matrix  $\mathbf{A}_i$  so that  $\mathbf{X} \in \mathbb{R}^{n \times q}$  with  $q = \frac{V(V-1)}{2}$ :

$$\mathbf{A}_i = \begin{bmatrix} a_{i,1,1} & a_{i,1,2} & \dots & a_{i,1,V} \\ \vdots & \ddots & \dots & \vdots \\ a_{i,V,1} & a_{i,V,2} & \dots & a_{i,V,V} \end{bmatrix}_{V \times V}$$

$$\mathbf{X} = \begin{bmatrix} a_{1,1,2} & a_{1,1,3} & \dots & a_{1,1,V} & a_{1,2,3} & \dots & a_{1,2,V} & \dots & a_{1,V-1,V} \\ \vdots & \vdots \\ a_{n,1,2} & a_{n,1,3} & \dots & a_{n,1,V} & a_{n,2,3} & \dots & a_{n,2,V} & \dots & a_{n,V-1,V} \end{bmatrix}_{n \times q}.$$

The responses  $\mathbf{y} \in \mathbb{R}^n$  then follow a Normal distribution  $\mathbf{y} \sim N(\mu + \mathbf{X}\gamma, \tau^2 \mathbb{I}_n)$  with an overall mean  $\mu \in \mathbb{R}$ , regression coefficients  $\gamma \in \mathbb{R}^q$  and error variance  $\tau^2 \in \mathbb{R}$ . Here,  $\mathbb{I}_n$  represents the identity matrix of dimension  $n$ . We note that the regression coefficients of this model ( $\gamma_{kl}$ ) represent the effect of the edge in the microbial network between node  $k$  and node  $l$  (interaction effects) in the response and they are connected to the original regression coefficient matrix  $\mathbf{B}$  as  $b_{ij} = \gamma_{ij}/2$ . The model implicitly assumes that there are no main effects for the presence of the microbes in the sample. While this could be a reasonable assumption for brain research where the model originated (Guha and Rodriguez, 2021), it is not appropriate for microbial research where the phenotype is expected to be affected by both the presence of the microbes and their interactions. At this stage, we implement the model as is (without main effects) to test its immediate applicability to microbial datasets. We will, however, extend the model to the inclusion of main effects as future work (see Discussion).

The prior for the regression coefficients  $\gamma \in \mathbb{R}^q$  is given by

$$\gamma_{kl} \sim N(\mathbf{u}_k^T \mathbf{\Lambda} \mathbf{u}_l, \tau^2 s_{kl}) \quad (1)$$

where  $\mathbf{u}_1, \dots, \mathbf{u}_V \in \mathbb{R}^R$  are latent variables corresponding to each of the  $V$  nodes,  $\mathbf{\Lambda} \in \mathbb{R}^{R \times R}$  is equal to  $\text{diag}(\lambda_1, \dots, \lambda_R)$  for  $\lambda_i \in \{-1, 0, 1\}$  and  $s_{kl} \in \mathbb{R}$  is a scale parameter. We note that the effect of the interaction between node  $k$  and node  $l$  on the response is positive if  $\mathbf{u}_k^T \mathbf{\Lambda} \mathbf{u}_l > 0$  (or similarly, negative if  $\mathbf{u}_k^T \mathbf{\Lambda} \mathbf{u}_l < 0$  or zero if  $\mathbf{u}_k^T \mathbf{\Lambda} \mathbf{u}_l = 0$ ). The dimension of the latent variable  $R$  is chosen by the user and we find in our simulations that it has a strong effect in the floating-point stability of the implementation (see Simulations).

The matrix  $\mathbf{\Lambda}$  governs which entries in the latent variables  $\mathbf{u}_k \in \mathbb{R}^R$  are informative and we set the following prior:

$$\lambda_r \sim \begin{cases} 0 & \text{with probability } \tilde{\pi}_{1r} \\ 1 & \text{with probability } \tilde{\pi}_{2r} \\ -1 & \text{with probability } \tilde{\pi}_{3r} \end{cases}$$

for  $r = 1, \dots, R$  and with hyper prior  $(\tilde{\pi}_{1r}, \tilde{\pi}_{2r}, \tilde{\pi}_{3r}) \sim \text{Dirichlet}(r^\eta, 1, 1)$  for  $\eta > 1$ . Note that the probability of 0 in the Dirichlet is governed by the index  $r$  (and  $\eta$ ) which is meant to bias inference towards lower dimensions. These  $\tilde{\pi}$  parameters control the sparsity of the regression coefficient matrix  $\mathbf{B}$ . It is traditionally assumed that only a subset of microbes in the sample are key drivers of the phenotype.

To determine which nodes are influential (non-zero effect on the response), we set a spike-and-slab prior (Ishwaran and Rao, 2005):

$$\mathbf{u}_k \sim \begin{cases} N(\mathbf{0}, \mathbf{M}) & \text{if } \xi_k = 1 \\ \delta_0 & \text{if } \xi_k = 0 \end{cases}$$

where  $\delta_0$  is the Dirac-delta function at 0,  $\mathbf{M} \in \mathbb{R}^{R \times R}$  is a covariance matrix,  $\mathbf{0}$  is an  $R$ -dimensional vector of zeros, and  $\xi \in \{0, 1\}^V$  is a column vector of dimension  $V$  where each value denotes whether that node is influential on the response or not. We assume that  $\xi_k \sim \text{Bernoulli}(\Delta)$  with hyper priors  $\Delta \sim \text{Beta}(a_\Delta, b_\Delta)$  for  $a_\Delta, b_\Delta \in \mathbb{R}$  and  $\mathbf{M} \sim \text{InverseWishart}(v, \mathbb{I}_R)$  for  $v \in \mathbb{R}$ .

Lastly, the prior for the scale parameters ( $\mathbf{s} \in \mathbb{R}^q$ ) is given by  $s_{kl} \sim \text{Exp}(\theta/2)$  with hyper prior  $\theta \sim \text{Gamma}(\zeta, \iota)$  for shape  $\zeta \in \mathbb{R}$  and rate  $\iota \in \mathbb{R}$ , and the prior for the overall mean ( $\mu$ ) and error variance ( $\tau^2$ ) is assumed to be non-informative  $\pi(\mu, \tau^2) \propto \frac{1}{\tau^2}$ .

Table 4 in the Appendix contains all parameters in the model and their descriptions.

## Posteriors

The posterior distribution of the overall mean and the error variance are given by

$$\mu | \mathbf{y}, \mathbf{X}, \gamma, \tau^2 \sim N \left( \frac{\mathbf{1}_n^T(\mathbf{y} - \mathbf{X}\gamma)}{n}, \frac{\tau^2}{n} \right) \quad (2)$$

$$\begin{aligned} \tau^2 | \mathbf{y}, \mathbf{X}, \mu, \gamma, \mathbf{W}, \mathbf{D} &\sim \text{InverseGamma}[(n/2 + V(V-1)/4), \\ &\quad \frac{1}{2}(\mathbf{y} - \mu\mathbf{1}_n - \mathbf{X}\gamma)^T(\mathbf{y} - \mu\mathbf{1}_n - \mathbf{X}\gamma) + (\gamma - \mathbf{W})^T \mathbf{D}^{-1}(\gamma - \mathbf{W})] \end{aligned} \quad (3)$$

where  $\mathbf{1}_n$  is an  $n$ -dimensional vector of ones,  $\mathbf{W} \in \mathbb{R}^q$  is a vector given by

$$\mathbf{W} = \begin{bmatrix} \mathbf{u}_1^T \boldsymbol{\Lambda} \mathbf{u}_2 \\ \vdots \\ \mathbf{u}_1^T \boldsymbol{\Lambda} \mathbf{u}_V \\ \vdots \\ \mathbf{u}_{V-1}^T \boldsymbol{\Lambda} \mathbf{u}_V \end{bmatrix}$$

and  $\mathbf{D} \in \mathbb{R}^{q \times q}$  is a diagonal matrix with the vector of scale parameters  $\mathbf{s}$  in the diagonal.

The posterior distributions for the scale parameters ( $s_{kl}$ ) and their hyper parameter ( $\theta$ ) are given by

$$s_{kl} | \gamma_{kl}, \mathbf{u}, \boldsymbol{\Lambda}, \tau^2, \theta \sim \text{GeneralizedInverseGaussian} \left[ \frac{1}{2}, \frac{(\gamma_{kl} - \mathbf{u}_k^T \boldsymbol{\Lambda} \mathbf{u}_l)^2}{\tau^2}, \theta \right] \quad (4)$$

$$\theta | \mathbf{s} \sim \text{Gamma} \left[ \left( \zeta + \frac{V(V-1)}{2} \right), \left( \iota + \sum_{k < l} \frac{s_{kl}}{2} \right) \right]. \quad (5)$$

The posterior distribution for the regression coefficients ( $\gamma$ ) is given by

$$\begin{aligned} \gamma | \mathbf{y}, \mathbf{X}, \mathbf{D}, \mathbf{W}, \mu, \tau^2 &\sim \\ N \left( (\mathbf{X}^T \mathbf{X} + \mathbf{D}^{-1})^{-1} (\mathbf{X}^T (\mathbf{y} - \mu \mathbf{1}_n) + \mathbf{D}^{-1} \mathbf{W}), \tau^2 (\mathbf{X}^T \mathbf{X} + \mathbf{D}^{-1})^{-1} \right). \end{aligned} \quad (6)$$

Next, for the auxiliary variables, the posterior distribution of the latent variables ( $\mathbf{u}_k$ ) is given by

$$\mathbf{u}_k | w_{\mathbf{u}_k}, \mathbf{m}_{\mathbf{u}_k}, \boldsymbol{\Sigma}_{\mathbf{u}_k} \sim w_{\mathbf{u}_k} \delta_0(\mathbf{u}_k) + (1 - w_{\mathbf{u}_k}) N(\mathbf{u}_k | \mathbf{m}_{\mathbf{u}_k}, \boldsymbol{\Sigma}_{\mathbf{u}_k}) \quad (7)$$

where

$$w_{\mathbf{u}_k} = \frac{(1 - \Delta) N(\boldsymbol{\gamma}_k | \mathbf{0}, \tau^2 \mathbf{H}_k)}{(1 - \Delta) N(\boldsymbol{\gamma}_k | \mathbf{0}, \tau^2 \mathbf{H}_k) + \Delta N(\boldsymbol{\gamma}_k | \mathbf{0}, \tau^2 \mathbf{H}_k + \mathbf{U}_k^* \mathbf{M} \mathbf{U}_k^{*T})} \quad (8)$$

for  $\boldsymbol{\gamma}_k = (\gamma_{1k}, \dots, \gamma_{k-1,k}, \gamma_{k,k+1}, \dots, \gamma_{kV}) \in \mathbb{R}^q$ , and  $N(x|m, v)$  corresponding to the Gaussian PDF evaluated on  $x$  for mean  $m$  and covariance  $v$ ,  $\Delta$  given by

$$\Delta | a_\Delta, b_\Delta, \xi \sim \text{Beta} \left[ \left( a_\Delta + \sum_{k=1}^V \xi_k \right), \left( b_\Delta + \sum_{k=1}^V (1 - \xi_k) \right) \right], \quad (9)$$

$\mathbf{H}_k = \text{diag}(s_{1k}, \dots, s_{k-1,k}, s_{k,k+1}, \dots, s_{kV}) \in \mathbb{R}^{(V-1) \times (V-1)}$ ,  $\mathbf{U}_k^* = (\mathbf{u}_1 : \dots : \mathbf{u}_{k-1} : \mathbf{u}_{k+1} : \dots : \mathbf{u}_V)^T \boldsymbol{\Lambda} \in \mathbb{R}^{(V-1) \times R}$ ,  $\mathbf{0}$  is the  $(V-1)$ -dimensional vector of zeros, and matrix  $\mathbf{M}$  sampled from the posterior distribution:

$$\mathbf{M} | \mathbf{u}, \boldsymbol{\Lambda}, v \sim \text{InverseWishart} \left[ \left( \mathbb{I}_R + \sum_{k: \mathbf{u}_k \neq \mathbf{0}} \mathbf{u}_k \boldsymbol{\Lambda} \mathbf{u}_k^T \right), \left( v + \sum_{k=1}^V \mathbf{1}(\mathbf{u}_k \neq \mathbf{0}) \right) \right] \quad (10)$$

where  $\mathbf{1}(\cdot)$  is the indicator function and  $\mathbb{I}_R$  is the identity matrix of dimension  $R$ .

In addition, the posterior mean ( $\mathbf{m}_{\mathbf{u}_k}$ ) and posterior covariance matrix ( $\boldsymbol{\Sigma}_{\mathbf{u}_k}$ ) are defined as

$$\begin{aligned} \mathbf{m}_{\mathbf{u}_k} &= \frac{1}{\tau^2} \boldsymbol{\Sigma}_{\mathbf{u}_k} \mathbf{U}_k^{*T} \mathbf{H}_k^{-1} \boldsymbol{\gamma}_k \\ \boldsymbol{\Sigma}_{\mathbf{u}_k} &= \left( \frac{1}{\tau^2} \mathbf{U}_k^{*T} \mathbf{H}_k^{-1} \mathbf{U}_k^* + \mathbf{M}^{-1} \right)^{-1}. \end{aligned}$$

The posterior probability of the vector  $\xi$  is given by

$$\xi_k | w_{\mathbf{u}_k} \sim \text{Bernoulli}(1 - w_{\mathbf{u}_k}) \quad (11)$$

with the same definition of  $w_{\mathbf{u}_k}$  as in Eq. 8.

The posterior distribution of the  $\lambda_r$  values is given by

$$\lambda_r | \gamma, \mathbf{u}, \mathbf{\Lambda}, \mathbf{D} \sim \begin{cases} 0 & \text{with probability } p_{1r} \\ 1 & \text{with probability } p_{2r} \\ -1 & \text{with probability } p_{3r} \end{cases} \quad (12)$$

with

$$\begin{aligned} p_{1r} &= \frac{\tilde{\pi}_{1r} N(\gamma | \mathbf{W}_0, \tau^2 \mathbf{D})}{\tilde{\pi}_{1r} N(\gamma | \mathbf{W}_0, \tau^2 \mathbf{D}) + \tilde{\pi}_{2r} N(\gamma | \mathbf{W}_1, \tau^2 \mathbf{D}) + \tilde{\pi}_{3r} N(\gamma | \mathbf{W}_{-1}, \tau^2 \mathbf{D})} \\ p_{2r} &= \frac{\tilde{\pi}_{2r} N(\gamma | \mathbf{W}_1, \tau^2 \mathbf{D})}{\tilde{\pi}_{1r} N(\gamma | \mathbf{W}_0, \tau^2 \mathbf{D}) + \tilde{\pi}_{2r} N(\gamma | \mathbf{W}_1, \tau^2 \mathbf{D}) + \tilde{\pi}_{3r} N(\gamma | \mathbf{W}_{-1}, \tau^2 \mathbf{D})} \\ p_{3r} &= 1 - p_{1r} - p_{2r} \end{aligned}$$

where  $N(x|m, v)$  corresponds to the Gaussian PDF evaluated at  $x$  for mean  $m$  and covariance  $v$  and

$$\begin{aligned} \mathbf{W}_0 &= [\mathbf{u}_1^T \mathbf{\Lambda}_0 \mathbf{u}_2, \dots, \mathbf{u}_1^T \mathbf{\Lambda}_0 \mathbf{u}_V, \dots, \mathbf{u}_{V-1}^T \mathbf{\Lambda}_0 \mathbf{u}_V]^T \in \mathbb{R}^q, \\ \mathbf{\Lambda}_0 &= \text{diag}(\lambda_1, \dots, \lambda_{r-1}, 0, \lambda_{r+1}, \dots, \lambda_R) \in \mathbb{R}^{R \times R}, \\ \mathbf{W}_1 &= [\mathbf{u}_1^T \mathbf{\Lambda}_1 \mathbf{u}_2, \dots, \mathbf{u}_1^T \mathbf{\Lambda}_1 \mathbf{u}_V, \dots, \mathbf{u}_{V-1}^T \mathbf{\Lambda}_1 \mathbf{u}_V]^T \in \mathbb{R}^q, \\ \mathbf{\Lambda}_1 &= \text{diag}(\lambda_1, \dots, \lambda_{r-1}, 1, \lambda_{r+1}, \dots, \lambda_R) \in \mathbb{R}^{R \times R}, \\ \mathbf{W}_{-1} &= [\mathbf{u}_1^T \mathbf{\Lambda}_{-1} \mathbf{u}_2, \dots, \mathbf{u}_1^T \mathbf{\Lambda}_{-1} \mathbf{u}_V, \dots, \mathbf{u}_{V-1}^T \mathbf{\Lambda}_{-1} \mathbf{u}_V]^T \in \mathbb{R}^q, \\ \mathbf{\Lambda}_{-1} &= \text{diag}(\lambda_1, \dots, \lambda_{r-1}, -1, \lambda_{r+1}, \dots, \lambda_R) \in \mathbb{R}^{R \times R}. \end{aligned}$$

Lastly, the posterior distribution of the hyper parameters  $(\tilde{\pi}_{1r}, \tilde{\pi}_{2r}, \tilde{\pi}_{3r})$  is given by

$$(\tilde{\pi}_{1r}, \tilde{\pi}_{2r}, \tilde{\pi}_{3r}) | \eta, \mathbf{\Lambda} \sim \text{Dirichlet} \left( r^\eta + \sum_{r=1}^R \mathbf{1}(\lambda_r = 0), 1 + \sum_{r=1}^R \mathbf{1}(\lambda_r = 1), 1 + \sum_{r=1}^R \mathbf{1}(\lambda_r = -1) \right) \quad (13)$$

where again  $\mathbf{1}(\cdot)$  represents the indicator function.

The main parameters of interest are the regression coefficients  $\gamma$  which represent the effect of the interactions among microbes on the response and the parameters  $\xi$  that represent whether each of the  $V$  microbes are influential on the response or not. We obtain the posterior probability that a node is influential by taking the mean of  $\xi$  over the samples. Samples of the posterior distributions are obtained using Gibbs sampling as described in the next section.

## Gibbs Sampling

We sample the posterior distributions using Gibbs sampling as described in Algorithm 1.

---

**Algorithm 1:** Posterior Gibbs Sampling

---

**Result:** MCMC samples of the posterior distribution of parameters of interest  
Initialization;

```

while not enough samples do
    Sample  $\tau^2 | \mathbf{y}, \mathbf{X}, \mu, \gamma, \mathbf{W}, \mathbf{D} \sim \text{InverseGamma}$  (Eq. 3);
    Sample  $\xi | w_{\mathbf{u}_k} \sim \text{Binomial}$  (Eq. 11);
    for  $k$  in  $1 : V$  do
        | Sample  $\mathbf{u}_k | w_{\mathbf{u}_k}, \mathbf{m}_{\mathbf{u}_k}, \Sigma_{\mathbf{u}_k} \sim \xi_k \times \text{Normal}$  (Eq. 7);
    end
    Sample  $\gamma | \mathbf{y}, \mathbf{X}, \mathbf{D}, \mathbf{W}, \mu, \tau^2 \sim \text{Normal}$  (Eq. 6);
    Sample  $s_{kl} | \gamma_{kl}, \mathbf{u}, \Lambda, \tau^2, \theta \sim \text{GeneralizedInverseGaussian}$  (Eq. 4);
    Sample  $\theta | \mathbf{s} \sim \text{Gamma}$  (Eq. 5);
    Sample  $\Delta \sim \text{Beta}$  (Eq. 9);
    Sample  $\mathbf{M} | \mathbf{u}, \Lambda, v \sim \text{InverseWishart}$  (Eq. 10);
    Sample  $\mu | \mathbf{y}, \mathbf{X}, \gamma, \tau^2 \sim \text{Normal}$  (Eq. 2);
    for  $r$  in  $1 : R$  do
        | Sample  $\lambda_r | \gamma, \mathbf{u}, \Lambda, \mathbf{D} \sim [0, 1, -1]$  (Eq. 12);
        | Sample  $(\tilde{\pi}_{1r}, \tilde{\pi}_{2r}, \tilde{\pi}_{3r}) | \eta, \Lambda \sim \text{Dirichlet}$  (Eq. 13);
    end
end

```

---

## Open-source software

We have released a package in the Julia programming language to perform the sampling scheme which provides posterior estimates and convergence statistics for the Bayesian Network Regression model available as `BayesianNetworkRegression.jl` at the GitHub repository <https://github.com/solislemuslab/BayesianNetworkRegression.jl>. In addition, we provide all reproducible scripts for the simulation study (described in the next section) in the GitHub repository [https://github.com/samozm/bayesian\\_network\\_regression\\_imp](https://github.com/samozm/bayesian_network_regression_imp).

## Simulations

One of the main objectives of this manuscript is to test the applicability of the Bayesian Network Regression model when facing sparse data that is ubiquitous in microbiome research. There are two main sources of sparsity: 1) the matrix of regression coefficients  $\mathbf{B}$  is assumed to be sparse (sparsity controlled by  $\pi$ ) which means that there are few microbial drivers that affect the phenotype and 2) the data matrix is sparse (represented by the adjacency matrix  $\mathbf{A}_i$  with sparsity controlled by the number of sampled microbes  $k$ ) because we do not have complete sampling of all microbes. We test different levels of sparsity both on the regression coefficient matrix  $\mathbf{B}$  ( $\pi = 0.3, 0.8$ ) and in the adjacency matrices  $\mathbf{A}_i$  ( $k = 8, 15, 22$  sampled microbes out of 30 total). In addition, we test two levels of effect sizes ( $\mu = 0.8, 1.6$ ) so that the entries in the regression coefficient matrix  $\mathbf{B}$  are distributed  $N(\mu, \sigma = 1.0)$ . For all simulation cases, all possible combinations of parameter values are tested.

We split the simulations into two scenarios: 1) theoretical simulations (graphical description in Fig. 2) and 2) realistic simulations (graphical description in Fig. 3). We describe both scenarios next.

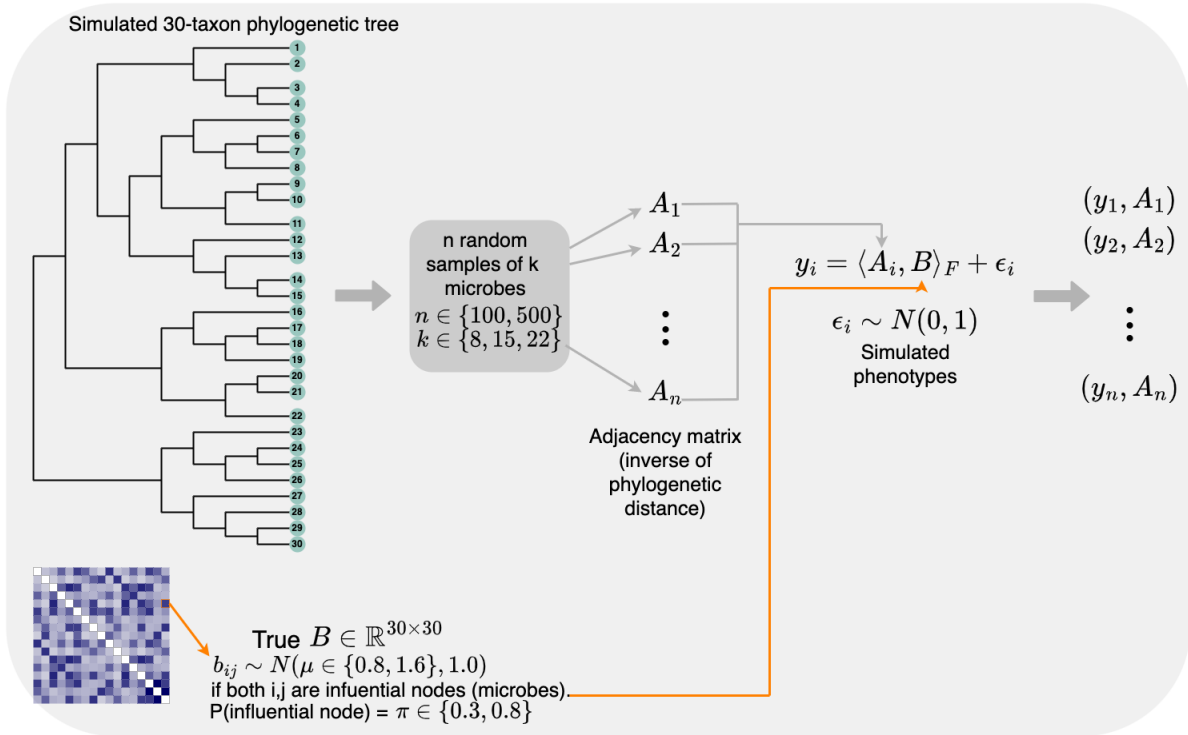


Figure 2: **Description of theoretical simulations.** We simulate a 30-taxon phylogenetic tree as the representation of the true microbial community, and then select  $k$  microbes per sample with which to build an adjacency matrix ( $A_i$ ) per sample. The phenotype  $y_i$  is then computed as the Frobenius product of the sample adjacency matrix ( $A_i$ ) and the true matrix of regression coefficients  $B$  plus Gaussian noise.

**Theoretical simulations.** We simulate a 30-taxon phylogenetic tree using the `rtree` function from the R package `ape` (Paradis and Schliep, 2019) that randomly splits edges until the desired number of leaves is attained. This tree represents the true community of microbes. We generate the true matrix of regression coefficients ( $B \in \mathbb{R}^{30 \times 30}$ ) by flipping a biased coin for every entry  $b_{ij}$  to determine if the edge connecting nodes  $i$  and  $j$  is an influential edge. We vary the probability of influential node as  $\pi = 0.3, 0.8$  as already mentioned above. If the edge is indeed set as influential, the entry  $b_{ij}$  is sampled from a Normal distribution with mean  $\mu = 0.3$  or  $0.8$  and variance equal to  $1.0$ .

For each sample, we randomly select  $k$  (set as 8, 15, or 22) microbes out of the 30 total microbes. We build the adjacency matrix for that sample using the phylogenetic distance between microbes. That is, the entry  $a_{ij}$  is equal to the inverse of the phylogenetic distance between microbe  $i$  and microbe  $j$  if both microbes are present in the sample (and zero otherwise). Note that we are not estimating the phylogenetic tree for a given sample given that we are not simulating sequences, and thus, we are ignoring estimation error in the phylogenetic pipeline at this point. Future work will incorporate this type of error to assess its implications downstream (see Discussion).

For each sample, we calculate the phenotype  $y_i$  as the Frobenius product between  $B$  and the adjacency matrix for that sample  $A_i$  plus a Gaussian random error with mean zero and variance of  $1.0$ . Because the generation of the phenotype follows the same model as the Bayesian Network Regression, we denote this scenario as “theoretical”.

We vary the sample size as  $n = 100, 500$ . The whole simulation process is illustrated in Fig. 2 and the mathematical details are described in the Appendix.

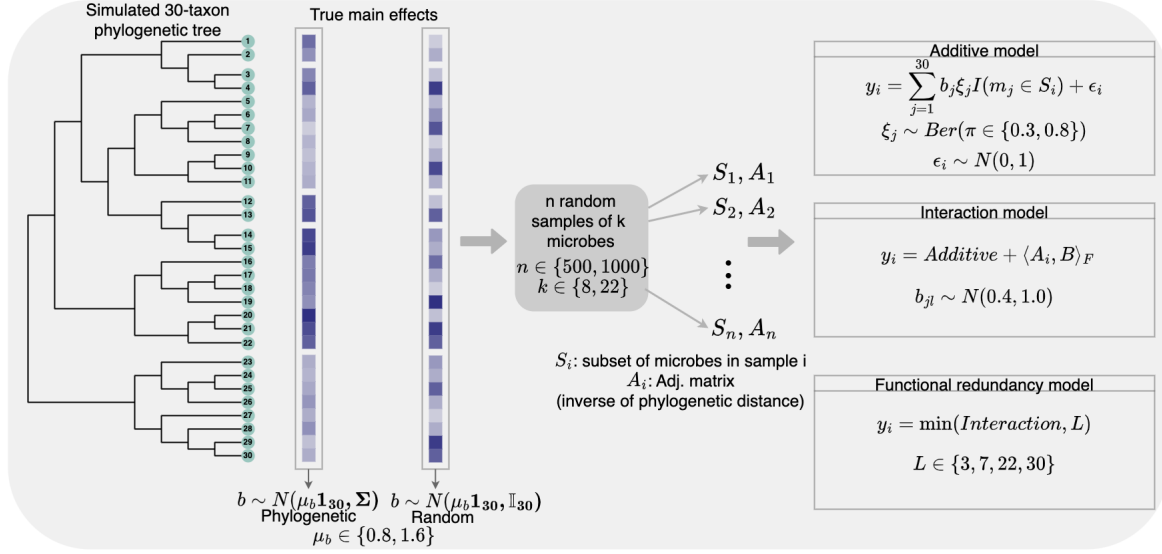


Figure 3: **Description of realistic simulations.** We simulate a 30-taxon phylogenetic tree as the true microbial community, and then select  $k$  microbes per sample with which to build an adjacency matrix ( $A_i$ ) per sample. The phenotype  $y_i$  is computed under three models: additive, interaction or functional redundancy. Within each model, there are two options for the generation of the true microbial effects: randomly sampled independently of other microbes or phylogenetically-informed in which related microbes have similar effects on the phenotype.

**Realistic simulations.** Again, we simulate a 30-taxon phylogenetic tree which represents the true community of microbes using the `rtree` function from the R package `ape` (Paradis and Schliep, 2019) that randomly splits edges until the desired number of leaves is attained. For each microbe, we simulate its true effect on the phenotype under two settings: 1) random in which each microbe has an effect  $b_i$  that is distributed Normal with mean  $\mu_b = 0.8$  or  $1.6$  and variance of  $1.0$  independently of other microbes, and 2) phylogenetic in which we simulate the whole vector of microbial effects  $\mathbf{b}$  as a Brownian motion on the phylogenetic tree using the Julia package `PhyloNetworks` (Solís-Lemus et al., 2017). That is,  $\mathbf{b} \sim N(\mu_b \mathbf{1}_{30}, \Sigma)$  where  $\mu_b = 0.8$  or  $1.6$ ,  $\mathbf{1}_{30}$  is a 30-dimensional vector of ones, and  $\Sigma$  is the covariance matrix imposed by the phylogenetic tree. In this last setting, microbes that are closely related have similar effects on the phenotype. In the random setting, the main effects of each microbe on the phenotype are generated without regard to the relationships between them.

The generation of the sample adjacency matrices ( $\mathbf{A}_i$ ) is the same as in the theoretical scenario. Namely, for each sample, we randomly select  $k$  (set as 8 or 22) microbes out of the 30 total microbes. We build the adjacency matrix for that sample using the phylogenetic distance between microbes. That is, the entry  $a_{ij}$  is equal to the inverse of the phylogenetic distance between microbe  $i$  and microbe  $j$  if both microbes are present in the sample (and zero otherwise).

For the computation of the phenotype, we test three settings:

*Additive model.* The phenotype  $y_i$  is computed as the sum of effects  $b_i$  for the influential microbes that are present in the sample plus Gaussian noise. As before, microbe is considered influential with probability  $\pi = 0.3$ , or  $0.8$ .

*Interaction model.* In addition to the main effects already described in the additive model, the phenotype also contains interaction terms  $a_{jl} \times b_{jl}$ , with  $b_{jl} \sim N(0.4, 1.0)$  if microbes  $j$  and  $l$  are both influential and  $a_{jl}$  as the inverse of phylogenetic distance between microbes  $j$  and  $l$  if both are in the sample. Since the interaction term is positive, this model is sometimes referred to as a super-additive model.

*Functional redundancy model.* Here, we assume that the effect of the microbes on the phenotype is not unbounded. That is, different microbes can have the same function, and thus, the phenotype is not affected by both microbes at the same time. We model this mathematically by imposing a threshold  $L$  on the phenotype after it was computed following the interaction model. In this setting, we cannot impose the same threshold on all combinations of  $\mu_b$  and  $\pi$  because the phenotype values will have different ranges. Therefore, we utilize different thresholds for each setting to try to guarantee that not all response values will be capped:  $L = 3$  for the  $\pi = 0.3, \mu = 0.8$  case,  $L = 7$  for the  $\pi = 0.3, \mu = 1.6$  case,  $L = 22$  for the  $\pi = 0.8, \mu = 0.8$  and  $L = 30$  for  $\pi = 0.8, \mu = 1.6$ . Values of  $L$  were chosen so that some but not all (and, generally, fewer than 50%) of responses were capped.

Because the phenotype is not computed using the Frobenius product directly (as in the theoretical simulations), but instead it is generated based on biologically reasonable settings (additive, interaction and functional redundancy models), we denote these scenarios as “realistic”.

We vary the sample size as  $n = 500, 1000$ . The whole simulation process is illustrated in Fig. 3 and the mathematical details are described in the Appendix.

### MCMC convergence

For each simulation setting, we run three MCMC chains and assess convergence using the  $\hat{R}$  convergence criterion proposed in Vehtari et al. (2019). We consider convergence to have been achieved if  $\hat{R} \leq 1.2$  for all of the  $\gamma$  and  $\xi$  variables as suggested in Vehtari et al. (2019). For most simulation settings, 30,000 burn-in followed by 20,000 samples (50,000 total generations) is enough to guarantee convergence. In eleven cases (Tables 1 and 2), longer chains are needed to achieve convergence. See Results for information on computing times.

$R$	$\mu$	$\pi$	$k$	Sample size	Burn-in	Total
5	0.8	0.3	15	500	260000	280000
5	1.6	0.3	8	500	60000	80000
5	1.6	0.3	22	100	160000	180000
5	1.6	0.8	22	100	200000	220000
7	0.8	0.3	15	500	340000	360000
7	1.6	0.3	22	100	240000	260000
9	1.6	0.0	22	100	100000	120000
9	1.6	0.3	22	100	60000	80000

Table 1: Theoretical simulation cases with more than 30,000 burn-in to achieve convergence. The number of MCMC samples post burn-in is 20,000 for all cases. All other simulation cases required 30,000 burn-in (50,000 total) generations to achieve convergence.

$R$	$\mu$	$\pi$	$k$	Sample size	Simulation type	Burn-in	Total
7	1.6	0.3	8	500	additive random	120000	140000
7	1.6	0.3	22	500	redundant phylogenetic	100000	120000
7	1.6	0.3	22	1000	redundant random	60000	80000

Table 2: Realistic simulation cases with more than 120,000 burn-in to achieve convergence. The number of MCMC samples post burn-in is 20,000 for all cases. All other simulation cases required 30,000 burn-in (50,000 total) generations to achieve convergence.

### Connections of Bacterial Microbiome to Phosphorous Leaching

We re-analyze the experimental data collected by Wagg et al. (2019) to study the fungal-bacterial interactions in soil microbiome and how they are connected to specific biological phenotypes. In this experiment, a soil diversity gradient was produced by filtering inoculum through different meshes from less than 5mm to less than 0.001mm. In addition, a number of indicators of soil microbiome functions were collected, of which we focus on phosphorous leaching as our response. Following Wagg et al. (2019), we construct the microbiome network for each sample as follows:

1. Remove all OTUs occurring fewer than 40 samples in the dataset
2. Construct a "meta-network" using data from all samples. This is done with the R package Spiec-Easi (Kurtz et al., 2015b).
3. For each sample, construct a "sample network" from the meta-network by including only edges between OTUs appearing in that sample. An OTU appears in a sample if its relative abundance is different than zero. If an edge does not appear in the sample, its edge coefficient is set to 0.

After removal of OTUs than do not appear in at least 40 samples, the resulting meta-network contains 90 OTUs, for a model matrix of dimension  $\mathbf{X} \in \mathbb{R}^{50 \times 4005}$  given that the experiment collected 50 samples. Our simulation results indicate that this number of samples will likely not be enough to achieve the necessary statistical power to detect influential microbes or edges. Therefore, we employ the following data augmentation technique to generate 50 more samples, for a total of 100 samples. For each of the 50 true samples, an augmented sample is created. First, to generate the response (phosphorous leaching), an offset is generated from  $N(0, s_P^2/4)$ , where  $s_P^2$  is the sample variance of phosphorous leaching in the 50 original samples. If this offset is negative and greater in magnitude than the original response (so that the augmented response is negative), a new value for the augmented response is generated from  $\frac{1}{15}\chi_3^2$ . The original phosphorous leaching values range from 0.0040 to 0.6840, with a mean of 0.1593 mg/L. The augmented phosphorous leaching values range from 0.0066 to 0.6760 with a mean of 0.1900 mg/L. To generate augmented microbiome data, each microbe is present in the augmented sample with probability 0.9 if it was in the original sample or 0.1 if it was not, independently of other microbes. For the original data, sample sizes of distinct OTUs range from 52 to 90 with a mean number of OTUs per sample of 82. For the augmented data, samples sizes of distinct OTUs range from 53 to 86 with a mean number of OTUs per sample of 75. Much of the sparsity in the data comes from the relationships between OTUs, rather than the number of OTUs collected in each sample. Only about 2% of the entries in the meta-matrix are non-zero.

## MCMC convergence

As in the simulation study, we run three MCMC chains and assess convergence using the  $\hat{R}$  convergence criterion proposed in Vehtari et al. (2019). We again consider convergence to have been achieved if  $\hat{R} \leq 1.2$  for all of the  $\gamma$  and  $\xi$  variables. We find that 10,000 burn-in followed by 10,000 samples (20,000 total generations) is enough to guarantee convergence in the real dataset.

## Results

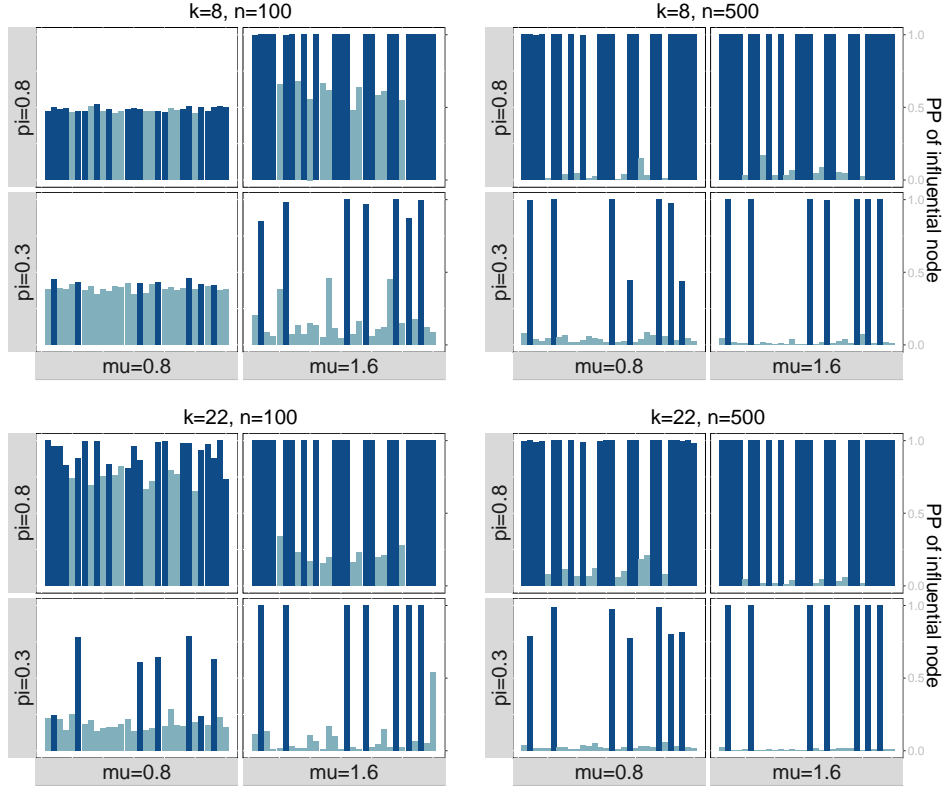
### Theoretical Simulations

Fig. 4 shows the posterior probability of being an influential node (key microbe) for different sample sizes ( $n = 100, 500$ ), number of sampled microbes ( $k = 8, 22$ ), effect sizes ( $\mu = 0.8, 1.6$ ) and sparsity ( $\pi = 0.3, 0.8$ ) in the regression coefficient matrix  $\mathbf{B}$ . Each bar corresponds to one node (microbe) and the bars are colored depending on whether the node is truly influential (dark) or not influential (light). For smaller sample size ( $n = 100$ ), the effect sizes need to be larger ( $\mu = 1.6$ ) for the nodes to be accurately detected as influential (tall dark bars). For a larger sample size ( $n = 500$ ), the model has a high PP for truly influential nodes (tall dark bars) and a low PP for non-influential nodes (short light bars) regardless of the values of  $k, \mu, \pi$ . There seem to be no major differences in the performance of the method in terms of regression coefficient sparsity ( $\pi$ ) or adjacency matrix sparsity ( $k$ ) with the exception that for smaller effect sizes ( $\mu = 0.8$ ) in small sample size setting ( $n = 100$ ), less sparsity in  $\mathbf{A}$  ( $k = 22$ ) improves the detection of influential nodes compared to  $k = 8$ .

We further compare the performance when changing the latent dimension ( $R$ ). In Fig. 4, we have a latent dimension of  $R = 7$  which produced more accurate results than  $R = 5$  (Fig. 15 in the Appendix). Latent dimension of  $R = 9$  (Fig. 16 in the Appendix) produces slightly better accuracy compared to  $R = 7$ , but it also creates floating-point instability in the code. As Guha and Rodriguez (2021) suggest, we aim to find the smallest  $R$  value that produces good performance to guarantee floating-point stability. In our case, we choose a latent dimension of  $R = 7$  for all the remaining of the simulations. Lastly, results for  $k = 15$  sampled microbes can be found in the Fig. 17 in the Appendix with no considerable differences with respect to  $R$ .

We conclude that the method is able to detect influential nodes (microbes) for a sufficiently large sample size ( $n = 500$  in here) regardless of the effect size ( $\mu$ ) and sparsity ( $\pi$ ) of the regression coefficient  $\mathbf{B}$  and regardless of the sparsity of the adjacency matrix ( $k$ ). For smaller sample size ( $n = 100$ ), either larger effect sizes are needed ( $\mu = 1.6$ ) or less sparsity in the adjacency matrix  $\mathbf{A}$  ( $k = 22$ ).

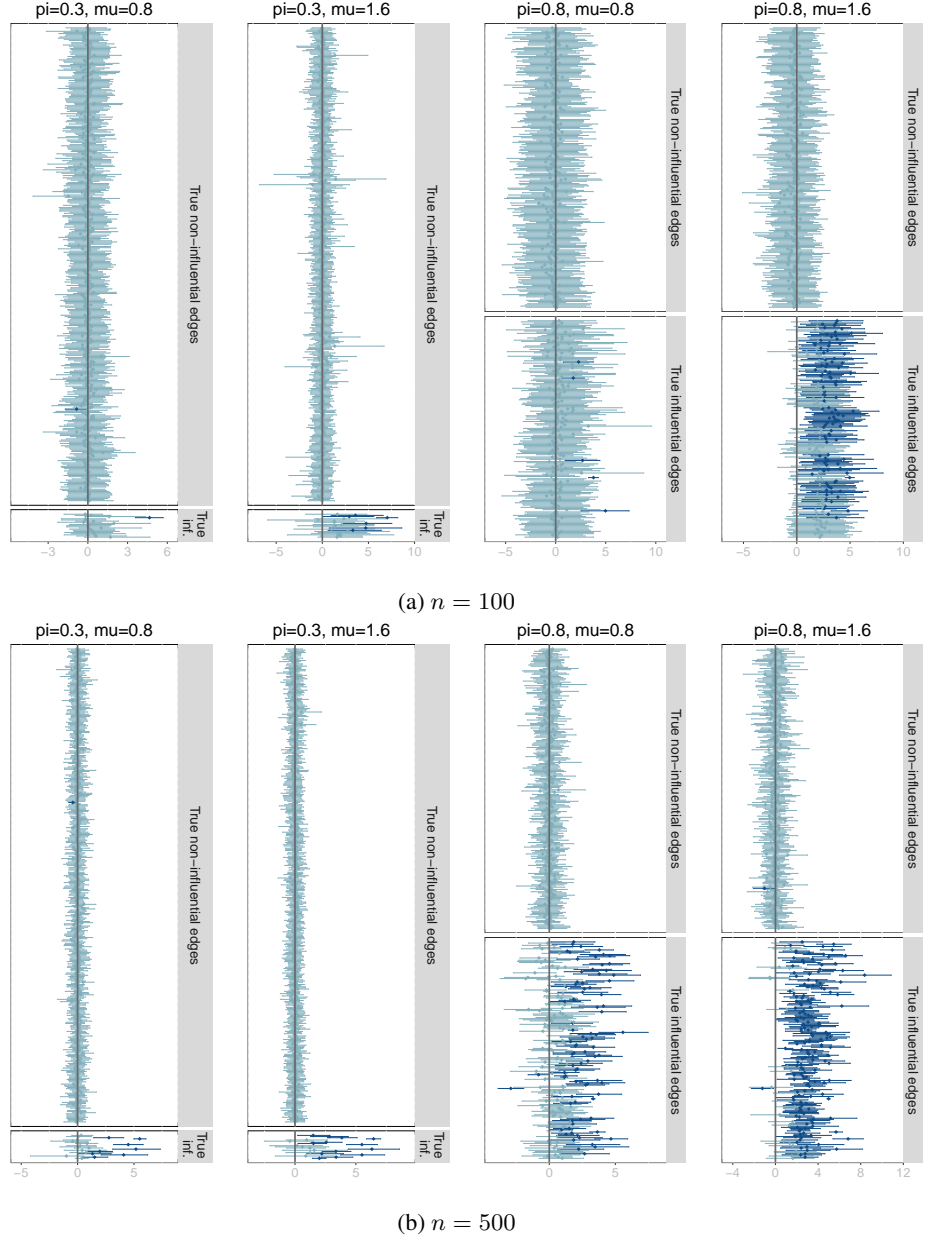
Fig. 5 shows the 95 % credible intervals for the regression coefficients per edge ordered depending on whether they are truly non-influential edges (top of each panel) or truly influential edges (bottom of each panel) for  $k = 8$  sampled microbes. The color of the intervals depends on whether it intersects zero (light) and hence estimated to be non-influential or does not intersect zero (dark) and hence estimated to be influential by the model. These panels allow



**Figure 4: Posterior probability of influential nodes (theoretical simulations).** Different panels represent different number of sampled microbes ( $k = 8, 22$ ) which controls the sparsity of the adjacency matrix and different sample sizes ( $n = 100, 500$ ). Within each panel, we have four plots corresponding to the two values of edge effect size ( $\mu = 0.8, 1.6$ ) and two values of probability of influential node ( $\pi = 0.3, 0.8$ ) which controls the sparsity of the regression coefficient matrix ( $\mathbf{B}$ ). Each bar corresponds to one node (microbe) and the bars are colored depending on whether the node is truly influential (dark) or not influential (light). As expected, the model has a high PP for truly influential nodes (tall dark bars) and a low PP for non-influential nodes (short light bars) for the case of  $n = 500$  regardless of the values of  $k, \mu, \pi$ .

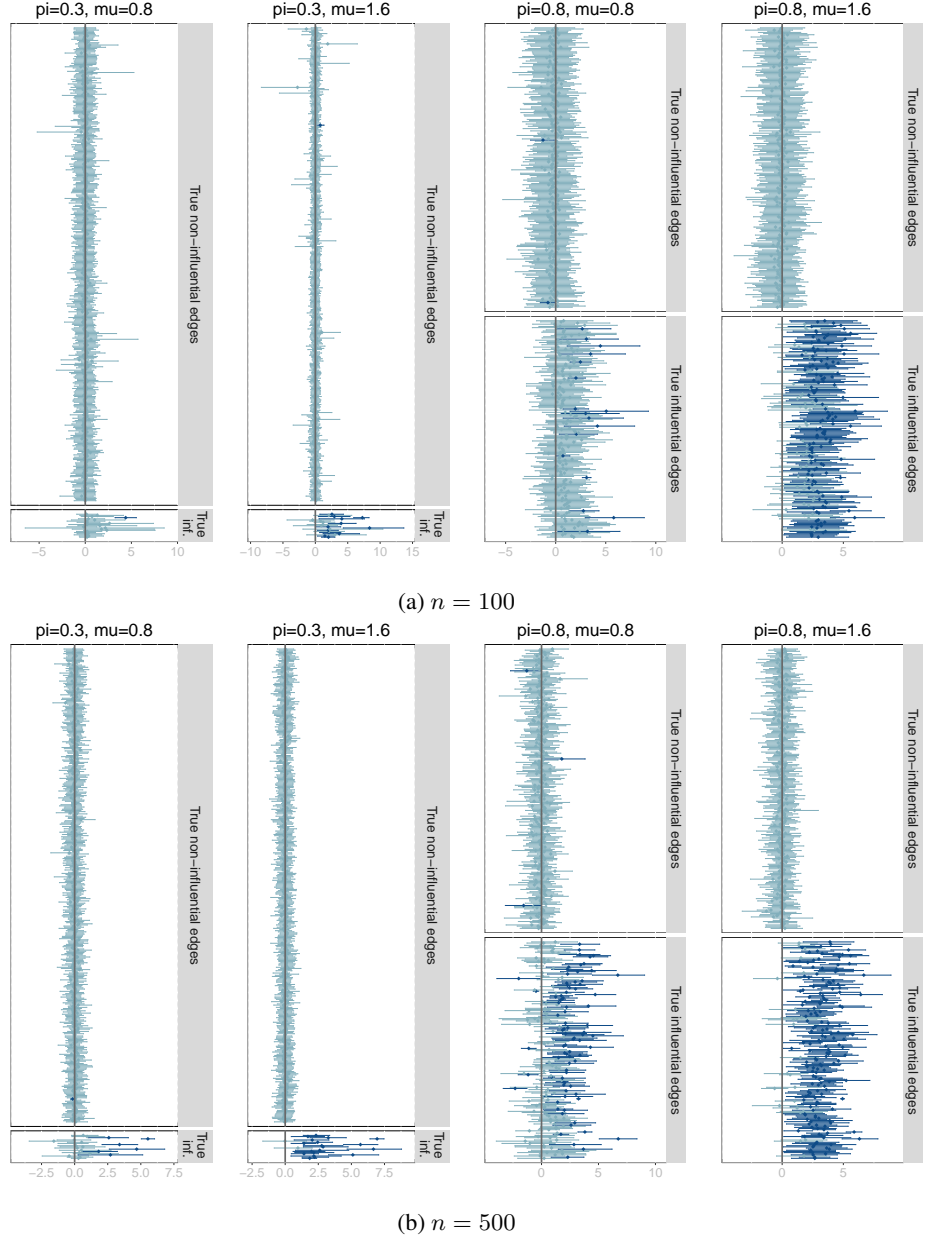
us to visualize false positives (dark intervals on the top panel) or false negatives (light intervals on the bottom panel) for all simulation settings ( $n, k, \pi, \mu$ ). Smaller samples size (top  $n = 100$ ) has considerably more false negatives compared to larger sample size (bottom  $n = 500$ ) as evidenced by the many light intervals in the “True influential edges” panels. This is true especially for the cases of high sparsity in  $\mathbf{B}$  ( $\pi = 0.3$  for both  $\mu = 0.8$  and  $1.6$ ) and low effect size with less sparsity in  $\mathbf{B}$  ( $\pi = 0.8, \mu = 0.8$ ). Overall, all simulation settings show controlled false positive rate as evidenced by few dark intervals on the “True non-influential edges” panels, regardless of sample size ( $n$ ), effect size ( $\mu$ ) and sparsity in  $\mathbf{B}$  ( $\pi$ ). Fig. 6 shows the same plot for  $k = 22$  sampled microbes instead of  $k = 8$ . The conclusions are the same which provides evidence that the identification of influential edges does not depend on the number of microbes in the samples.

Fig. 7 shows the heatmaps of MAP estimates of  $\mathbf{B}$  compared to the true heatmap of  $\mathbf{B}$ . The estimated  $\mathbf{B}$  matrix has a similar heatmap to the true  $\mathbf{B}$  in all settings of  $k, \pi, \mu$  for large sample size ( $n = 500$ ) and for large effect size ( $\mu = 1.6$ )



**Figure 5: 95 % credible intervals for edge effects for  $k = 8$  sampled nodes (theoretical simulations).** Top (a): Sample size of  $n = 100$ . Bottom (b): Sample size of  $n = 500$ . Each panel corresponds to a scenario of  $\pi = 0.3, 0.8$  (which controls the sparsity of the regression coefficient matrix  $\mathbf{B}$ ) and  $\mu = 0.8, 1.6$ . We plot the 95 % credible intervals for the regression coefficients per edge ordered depending on whether they are truly non-influential edges (top of each panel) or truly influential edges (bottom of each panel). The color of the intervals depends on whether it intersects zero (light) and hence estimated to be non-influential or does not intersect zero (dark) and hence estimated to be influential by the model. These panels allow us to visualize false positives (dark intervals on the top panel) or false negatives (light intervals on the bottom panel). Smaller samples size (top  $n = 100$ ) has considerably more false positives compared to larger sample size (bottom  $n = 500$ ) especially for the cases of high sparsity in  $\mathbf{B}$  ( $\pi = 0.3$  for both  $\mu = 0.8$  and  $1.6$ ) and low effect size with less sparsity in  $\mathbf{B}$  ( $\pi = 0.8$ ,  $\mu = 0.8$ ).

for smaller sample size ( $n = 100$ ). The actual  $\hat{b}_{ij}$  coefficients appear to be slightly overestimated based on the range (0-6 or 0-8 for the MAP and 0-4 for the true  $\mathbf{B}$ ).



**Figure 6: 95 % credible intervals for edge effects for  $k = 22$  sampled nodes (theoretical simulations).** Top (a): Sample size of  $n = 100$ . Bottom (b): Sample size of  $n = 500$ . Each panel corresponds to a scenario of  $\pi = 0.3, 0.8$  (which controls the sparsity of the regression coefficient matrix  $\mathbf{B}$ ) and  $\mu = 0.8, 1.6$ . We plot the 95 % credible intervals for the regression coefficients per edge ordered depending on whether they are truly non-influential edges (top of each panel) or truly influential edges (bottom of each panel). The color of the intervals depends on whether it intersects zero (light) and hence estimated to be non-influential or does not intersect zero (dark) and hence estimated to be influential by the model. These panels allow us to visualize false positives (dark intervals on the top panel) or false negatives (light intervals on the bottom panel). We find similar conclusions as Fig. 5: controlled false positive rate for all settings and improved false negative rate with increased sample size (bottom  $n = 500$ ).

Lastly, Fig. 18 (Appendix) shows the false positive and false negative rates for influential edges and nodes for different simulation settings in terms of  $n, k, \pi, \mu$ . With increased sample size ( $n = 500$ ), the false positive rates for edges and for nodes are zero as well as the false negative rate for nodes. Only the false negative rate for edges remains high

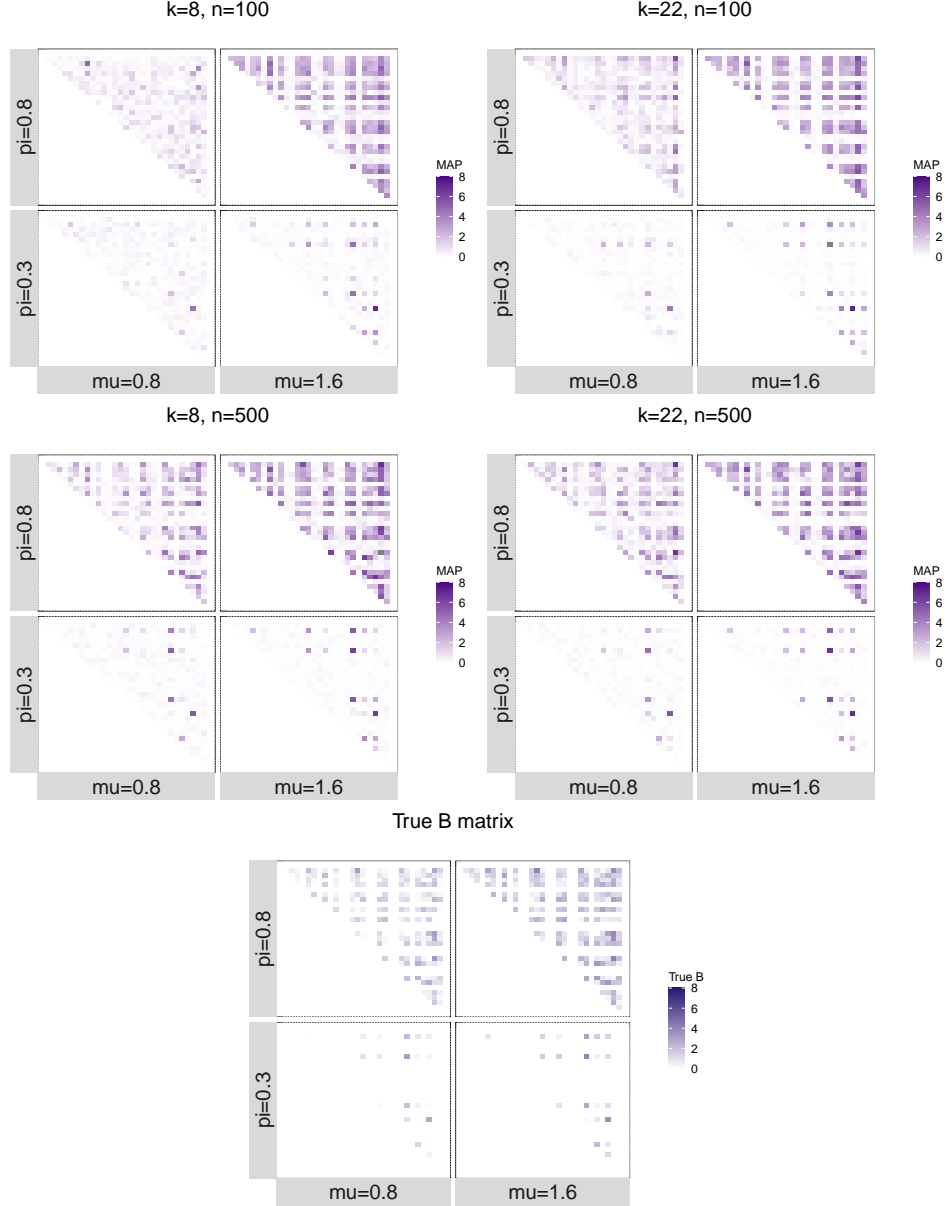


Figure 7: **Heatmap of MAP estimates for  $\mathbf{B}$  (theoretical simulations).** Different panels represent different number of sampled microbes ( $k = 8, 22$ ) which controls the sparsity of the adjacency matrix and different sample sizes ( $n = 100, 500$ ). Within each panel, we have four plots corresponding to the two values of edge effect size ( $\mu = 0.8, 1.6$ ) and two values of probability of influential node ( $\pi = 0.3, 0.8$ ) which controls the sparsity of the regression coefficient matrix ( $\mathbf{B}$ ). Each panel has a heatmap of the MAP estimates for  $\mathbf{B}$  and on the bottom, we have the true values of  $\mathbf{B}$ . The estimated  $\mathbf{B}$  matrix has a similar heatmap to the true  $\mathbf{B}$  in all settings of  $k, \pi, \mu$  for large sample size ( $n = 500$ ) and for large effect size ( $\mu = 1.6$ ) for smaller sample size ( $n = 100$ ). The actual  $\hat{b}_{ij}$  coefficients appear to be slightly overestimated based on the range (0-6 for the MAP and 0-4 for the true  $\mathbf{B}$ ).

for  $n = 500$  for the case of small effect size ( $\mu = 0.8$ ). The number of sampled microbes ( $k$ ) does not appear to have any effect in the rates, at least for the case of  $n = 500$ . Fig. 19 (Appendix) shows the mean square error for the estimated coefficients and the responses. The MSE of the coefficients seems to be better when the edge effects are

weaker ( $\mu = 0.8$ ) or when there is more sparsity ( $\pi = 0.3$ ) whereas the MSE of the responses is similar for all values of  $\pi$  and  $\mu$ .

## Realistic simulations

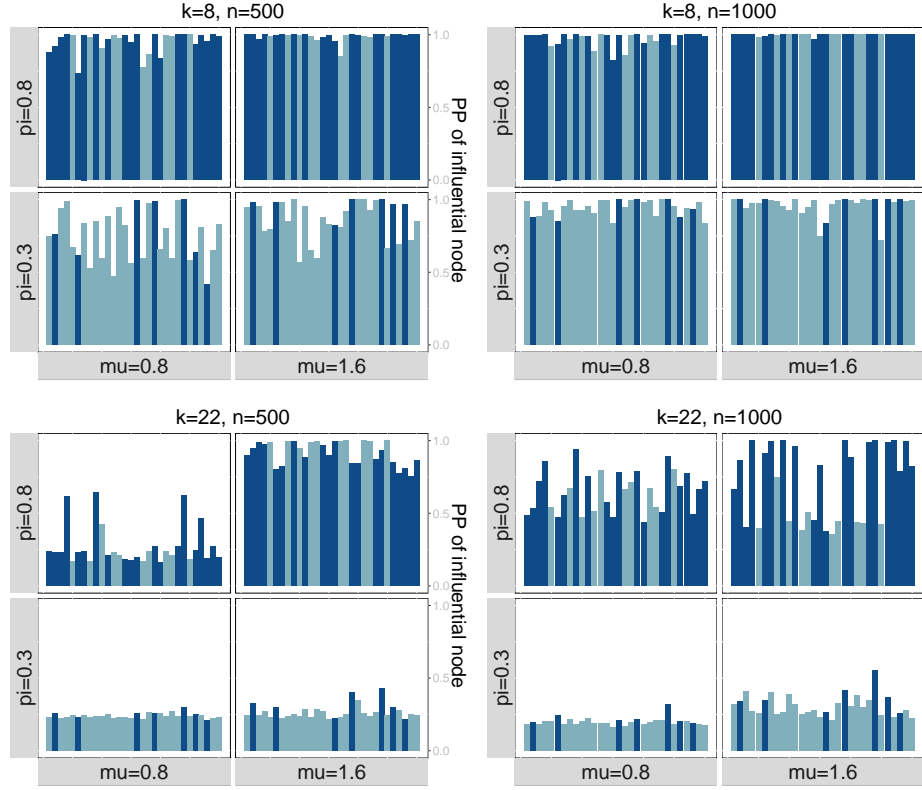
### Additive model

Fig. 8 and Fig. 21 (Appendix) show the posterior probability of influential nodes for random coefficients and phylogenetic coefficients respectively. Both types of coefficients produce similar results. The model performs poorly for  $k = 8$  sampled nodes as it is unable to identify influential nodes regardless of sample size ( $n$ ) and characteristics of  $\mathbf{B}$  ( $\pi, \mu$ ). For  $k = 22$  sampled microbes, the model behaves better for increased sample size ( $n = 1000$ ) except for high sparsity and low effect size ( $\pi = 0.3, \mu = 0.8$ ) for the case of random coefficients and high sparsity ( $\pi = 0.3$ ) for the case of phylogenetic coefficients. That is, if the biological phenotype is generated under an additive model with random or phylogenetic coefficients, the BNR model is able to successfully detect influential nodes only under large sample sizes ( $n = 1000$ ), large number of sampled microbes ( $k = 22$ ) and low sparsity in the regression coefficient matrix ( $\pi = 0.8$ ).

Fig. 9 shows the 95 % credible intervals for edge effects under the additive model with random coefficients for  $k = 22$  sampled microbes (see Fig. 23 in the Appendix for the case of phylogenetic coefficients which has very similar results). We observe a reduced false positive rate in all settings compared to  $k = 8$  sampled microbes (Fig. 20 for random coefficients and Fig. 22 for phylogenetic coefficients, both figures in the Appendix). Given that the additive model does not have interaction (edge) effects, these panels allow us to visualize false positives (dark intervals). The false positive rate does not appear to be affected by sample size (top vs bottom) with higher rate for the cases of larger effect sizes ( $\mu = 1.6$ ) or less sparsity ( $\pi = 0.8$ ). Note that the parameter  $\mu$  in the additive simulations corresponds to the effect of the nodes, not the effect of the edges (as in the theoretical simulations). So, here, we can conclude that larger main (node) effects also drive a higher false positive rate in the edge effects. That is, if the biological phenotype is generated under an additive model with random or phylogenetic coefficients, the BNR model is able to identify that there are indeed no interaction (edge) effects only when sufficiently many microbes have been sampled ( $k = 22$ ).

### Interaction model

Fig. 10 (for phylogenetic coefficients) shows the posterior probabilities of influential nodes under the interaction model (Fig. 24 for random coefficients is in the Appendix). Both types of coefficients show similar performance when there is low sparsity in the  $\mathbf{B}$  matrix ( $\pi = 0.8$ ). Namely, the method estimates a high PP for truly influential nodes (tall dark bars) and a low PP for non-influential nodes (short light bars) for all cases of low sparsity in  $\mathbf{B}$  ( $\pi = 0.8$ ) regardless of sample size ( $n$ ), number of sampled microbes ( $k$ ) or effect size ( $\mu$ ). For scenarios of high sparsity in  $\mathbf{B}$  ( $\pi = 0.3$ ), both types of coefficients behave differently with phylogenetic coefficients showing more signal to detect influential nodes when  $k = 22$  microbes are sampled for both values of effect size ( $\mu = 0.8, 1.6$ ) and any sample size ( $n = 500, 1000$ ). For random coefficients, sample size needs to be  $n = 1000$  for influential nodes to be detected under  $k = 22$  sampled



**Figure 8: Posterior probability of influential nodes (additive model with random coefficients).** Different panels represent different number of sampled microbes ( $k = 8, 22$ ) which controls the sparsity of the adjacency matrix and different sample sizes ( $n = 100, 500$ ). Within each panel, we have four plots corresponding to the two values of edge effect size ( $\mu = 0.8, 1.6$ ) and two values of probability of influential node ( $\pi = 0.3, 0.8$ ) which controls the sparsity of the regression coefficient matrix ( $\mathbf{B}$ ). Each bar corresponds to one node (microbe) and the bar are colored depending on whether the node is truly influential (dark) or not influential (light). The model performs poorly for  $k = 8$  sampled nodes as it is unable to identify influential nodes regardless of sample size ( $n$ ) and characteristics of  $\mathbf{B}$  ( $\pi, \mu$ ). For  $k = 22$  sampled microbes, the model behaves better for increased sample size ( $n = 1000$ ) except for high sparsity and low effect size ( $\pi = 0.3, \mu = 0.8$ ). Phylogenetic coefficients (Fig. 21) have similar performance.

microbes (Fig. 24). Sampling fewer nodes ( $k = 8$ ) produces worse results for both types of coefficients with high false positive rate for random coefficients for all sample sizes (Fig. 24) and high false positive rate for phylogenetic coefficients only under the  $\mu = 1.6, n = 1000$  setting (Fig. 10). It is interesting to note that under the phylogenetic coefficients with  $k = 8$  sampled microbes, the false positive rate is worse for  $n = 1000$  than for  $n = 500$  when  $\mu = 1.6$ . This implies that if few microbes are sampled, larger sample sizes produce a larger false positive rate when the effect of the nodes is large ( $\mu = 1.6$ ).

To conclude, when the biological phenotype is generated under an interaction model, the BNR method is able to accurately identify influential microbes under low sparsity settings ( $\pi = 0.8$ ) regardless of the type of coefficients (random vs phylogenetic), regardless of number of sampled microbes ( $k = 8, 22$ ) and regardless of sample size ( $n = 500, 1000$ ). For high sparsity settings ( $\pi = 0.3$ ), phylogenetic coefficients have more signal to identify influential nodes regardless of sample size ( $n$ ), number of microbes sampled ( $k$ ), or effect sizes ( $\mu$ ), yet there is an inflated false positive rate with larger sample sizes ( $n = 1000$ ) for the case of large effect size ( $\mu = 1.6$ ) with few sampled microbes

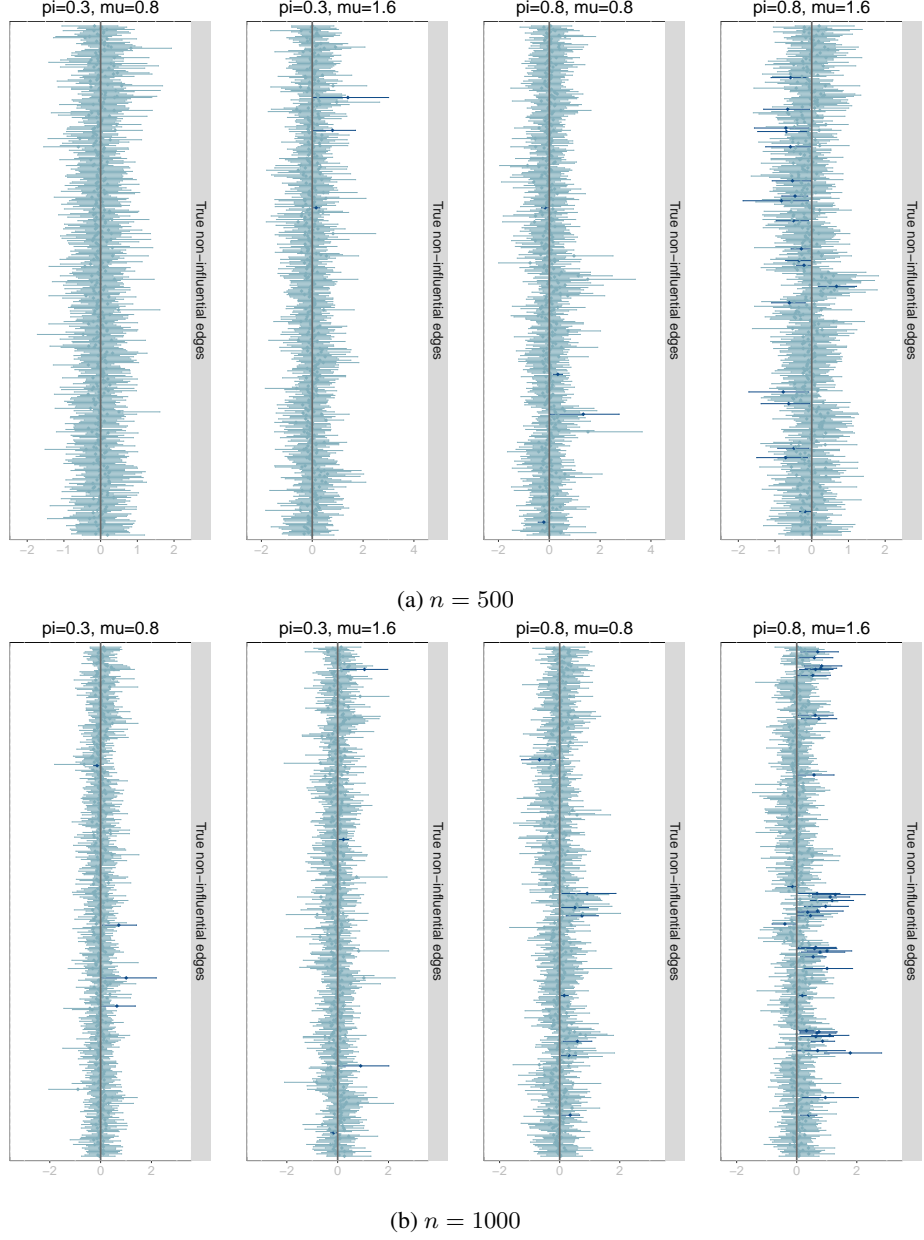


**Figure 9: 95 % credible intervals for edge effects (additive model with random coefficients) with  $k = 22$  sampled nodes.** Top (a): Sample size of  $n = 500$ . Bottom (b): Sample size of  $n = 1000$ . Each panel corresponds to a scenario of  $\pi = 0.3, 0.8$  (which controls the sparsity of the regression coefficient matrix  $\mathbf{B}$ ) and  $\mu = 0.8, 1.6$ . We plot the 95 % credible intervals for the regression coefficients per edge. In the additive model, all edges are non-influential. The color of the intervals depends on whether it intersects zero (light) and hence estimated to be non-influential or does not intersect zero (dark) and hence estimated to be influential by the model. Given that the additive model does not have interaction (edge) effects, these panels allow us to visualize false positives (dark intervals). We observe a decreased false positive rate when compared to  $k = 8$  sampled microbes (Fig. 20).

( $k = 8$ ). Random coefficients provide no strong signal to detect the influential nodes (high false positive rate) under high sparsity ( $\pi = 0.3$ ) unless there are  $k = 22$  microbes sampled with large sample size ( $n = 1000$ ).

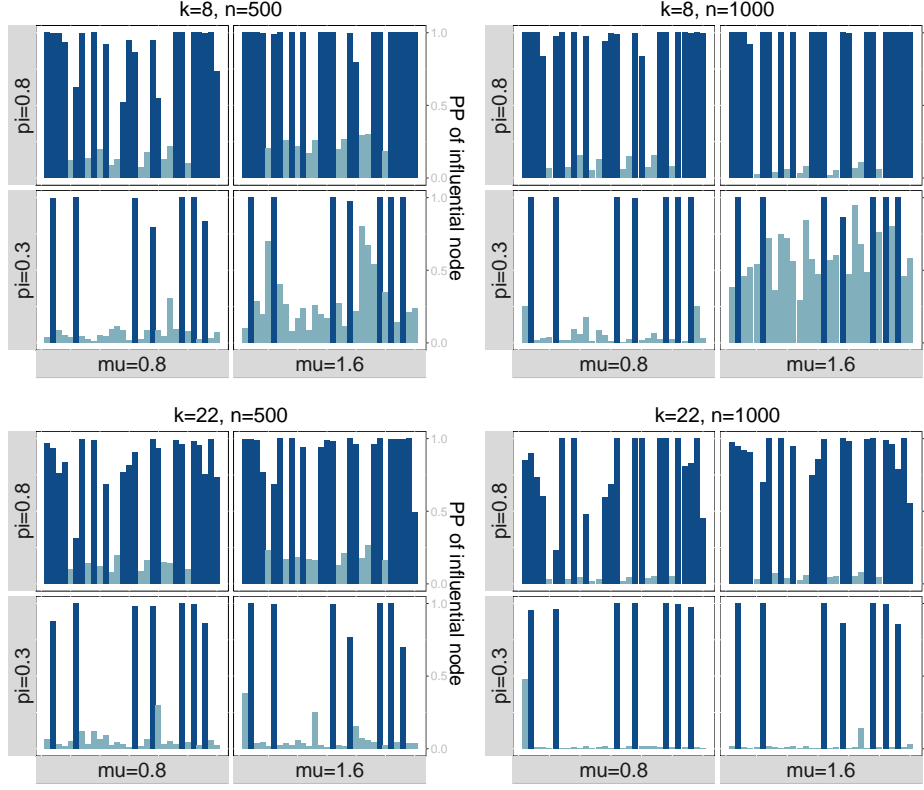


**Figure 10: Posterior probability of influential nodes (interaction model with phylogenetic coefficients).** Different panels represent different number of sampled microbes ( $k = 8, 22$ ) which controls the sparsity of the adjacency matrix and different sample sizes ( $n = 100, 500$ ). Within each panel, we have four plots corresponding to the two values of edge effect size ( $\mu = 0.8, 1.6$ ) and two values of probability of influential edge ( $\pi = 0.3, 0.8$ ) which controls the sparsity of the regression coefficient matrix ( $\mathbf{B}$ ). Each bar corresponds to one node (microbe) and the bar are colored depending on whether the node is truly influential (dark) or not influential (light). Just as in the case of random coefficients (Fig. 10), the model has a high PP for truly influential nodes (tall dark bars) a low PP for non-influential nodes (short light bars) for all cases of low sparsity in  $\mathbf{B}$  ( $\pi = 0.8$ ) regardless of sample size ( $n$ ), number of sampled microbes ( $k$ ), or effect size ( $\mu$ ). For high sparsity in  $\mathbf{B}$  ( $\pi = 0.3$ ), there is a high false positive rate (tall light bars) when  $k = 8$  microbes are sampled (top) only for large effect size ( $\mu = 1.6$ ) and large sample size ( $n = 1000$ ). Unlike with random coefficients (Fig. 24), the method with phylogenetic coefficients shows good performance in high sparsity settings ( $\pi = 0.3$ ) when  $k = 22$  microbes are sampled.

Fig. 11 shows the 95 % credible intervals for edge effects under the interaction model with random coefficients for  $k = 8$  sampled nodes. The results are very similar for  $k = 22$  sampled nodes (Fig. 25 in the Appendix) and for phylogenetic coefficients (Fig. 26 for  $k = 8$  and Fig. 27 for  $k = 22$ , both in the Appendix). Namely, the model displays a low false positive rate as evidenced by few dark intervals on the “True non-influential edges” panels for all sample sizes ( $n$ ), sparsity levels ( $\pi$ ) and effect sizes ( $\mu$ ). We highlight that it is expected that there will be few differences when comparing the two effect sizes ( $\mu = 0.8, 1.6$ ) as these quantities refer to the main (node) effects, not the interaction (edge) effects which was set as 0.4 for all simulations. The purpose of these simulations is to test if changes in the main (node) effects biased the performance of the BNR model to detect influential edges. It appears from these figures that there is no such bias. That is, when the biological phenotype is generated under the interaction model, the BNR has good performance to identify the influential edges regardless of the sample size ( $n$ ), the number of microbes sampled

( $k$ ), the sparsity level ( $\pi$ ), node effect sizes ( $\mu$ ), and type of coefficient (random vs phylogenetic) with controlled false positive and false negative rates in all settings.

### Functional redundancy model

Fig. 12 shows the posterior probability of influential nodes under the functional redundancy model with random coefficients. We observe that there is a high false positive rate in all settings (tall light bars) except for low sparsity ( $\pi = 0.8$ ) with few sampled nodes ( $k = 8$ ) or small effect size with high sparsity ( $\mu = 0.8, \pi = 0.3$ ) and more sampled nodes ( $k = 22$ ). This behavior is similar with phylogenetic coefficients (see Fig. 28 in the Appendix). This implies that the BNR model is unable to identify influential microbes under a model of functional redundancy unless there are very few sampled microbes ( $k = 8$ ), but many expected to be influential ( $\pi = 0.8$ ). This result could be explained by the fact that multiple sampled microbes could cause the phenotype to reach the threshold more easily and thus, there is less information on the variability of the response to estimate the effects and influential probabilities.

Fig. 13 shows the 95 % credible intervals for edge effects under the functional redundancy model with random coefficients for  $k = 8$  sampled nodes. The results are very similar for phylogenetic coefficients (Fig. 29 for  $k = 8$  in the Appendix). Namely, there is controlled false positive rate (dark intervals in the “True non-influential edges” top panels) for the case of small sample size (top:  $n = 500$ ) which strangely worsens slightly for larger sample size (bottom:  $n = 1000$ ) for all cases of  $\pi, \mu$ . False negative rate (light intervals in the “True influential edges” top panels) appears unaffected by  $n, \pi, \mu$ . When  $k = 22$  microbes are sampled instead, the model performs worse in all settings (Fig. 30 for random coefficients for  $k = 22$  sampled nodes and Fig. 31 for phylogenetic coefficients for  $k = 22$ , both in the Appendix). Namely, there are inflated false positive and false negative rates for all settings of  $n, \pi, \mu$ . Similarly to the identification of influential nodes, it seems that the BNR model is unable to accurately identify influential edges under a functional redundancy model when many nodes are sampled ( $k = 22$ ). That is, when the biological phenotype is generated under the functional redundancy model, the BNR has good performance to identify influential nodes and influential edges only when there are few microbes sampled ( $k = 8$ ) and low sparsity in  $\mathbf{B}$  ( $\pi = 0.8$ ).

### False positive and false negative rates

We present the plots for false positive and negative rates in the Appendix. Fig. 32 shows the false positive and false negative rates for edges and nodes for different simulation settings in terms of  $n, k, \pi, \mu$  for additive (top), interaction (middle) and functional redundancy (bottom) models with random coefficients. An interaction model with low sparsity in  $\mathbf{B}$  ( $\pi = 0.8$ ) shows the best performance in terms of controlled false positive and false negative rates for all settings of  $n$  and  $\mu$ . Under the interaction model, there is inflated false negative rate of edges which could be due to the fact that the model does not include main (node) effects. Overall, sampling more nodes ( $k = 22$ ) shows lower false positive rates than fewer sampled nodes ( $k = 8$ ), except for the functional redundancy model. Sample size ( $n = 500, 1000$ ) does not appear to have an influence given that both columns show similar rate patterns. False positive rates for edges (dark blue bars) seems to be controlled in all simulation settings showing that the BNR model is accurate in identifying

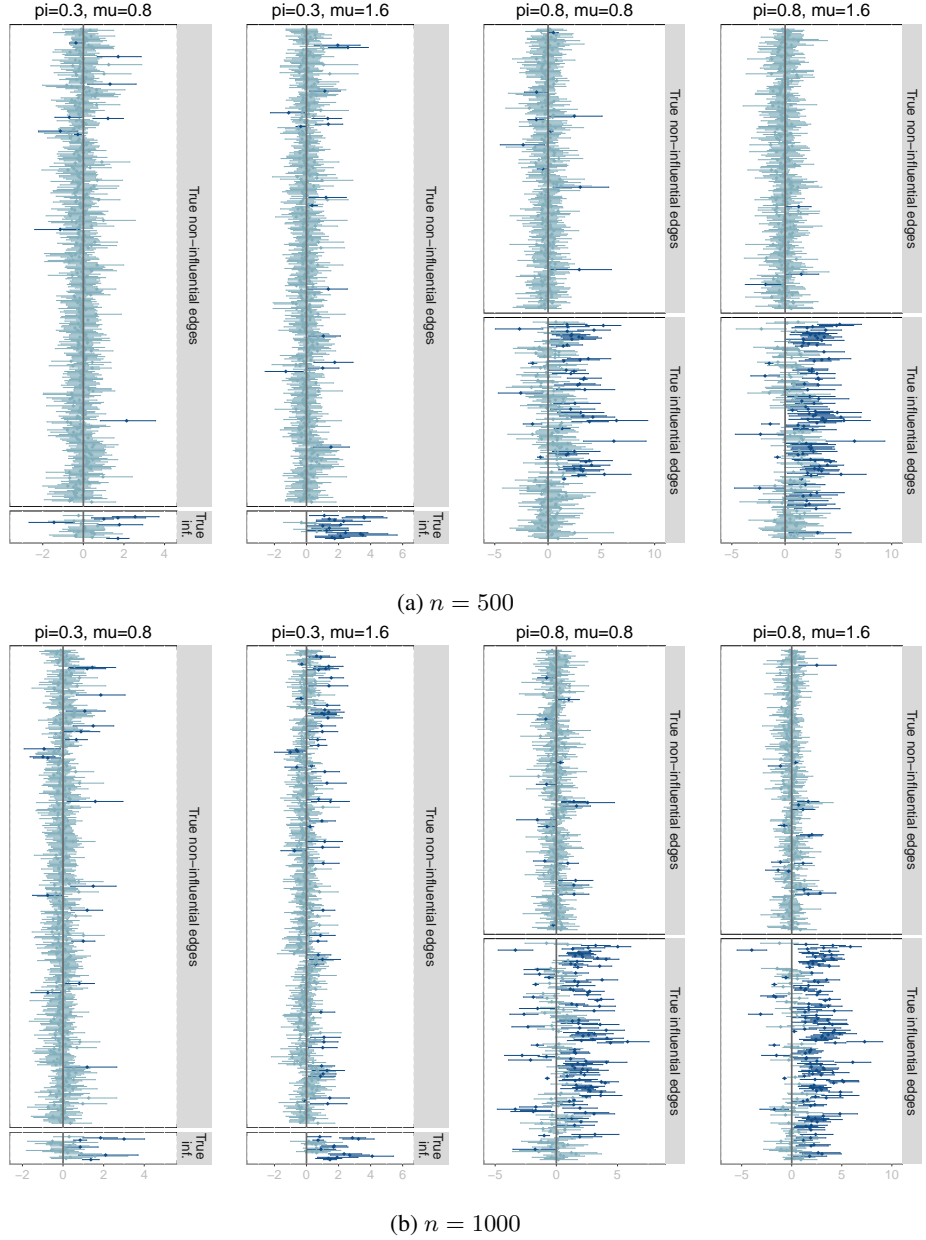
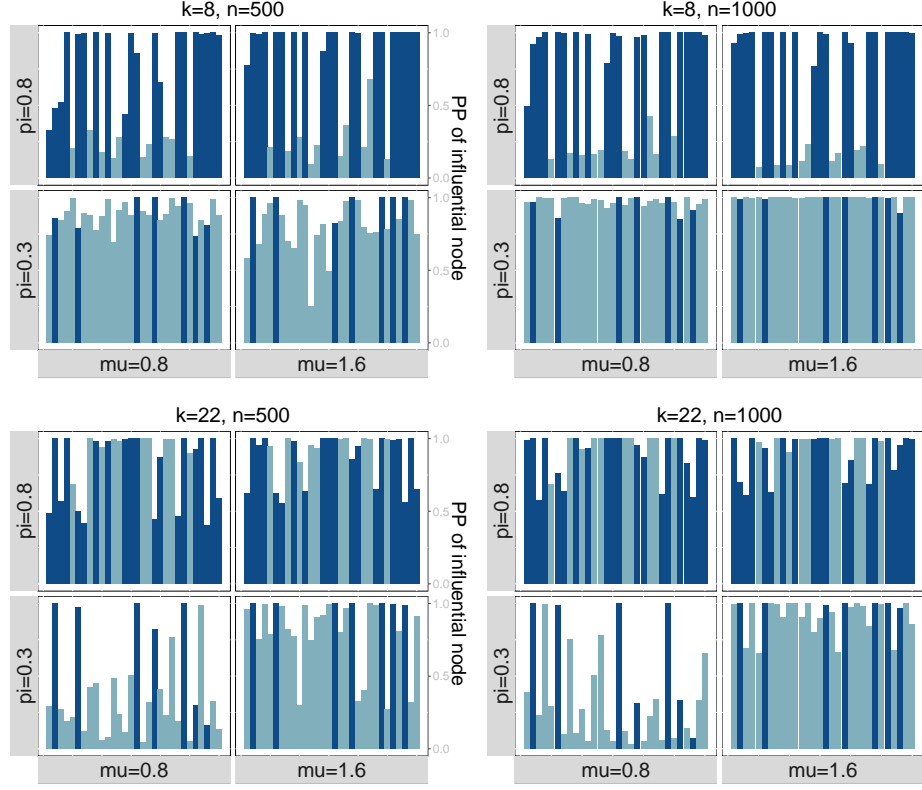


Figure 11: **95 % credible intervals for edge effects (interaction model with random coefficients) with  $k = 8$  sampled nodes.** Top (a): Sample size of  $n = 500$ . Bottom (b): Sample size of  $n = 1000$ . Each panel corresponds to a scenario of  $\pi = 0.3, 0.8$  (which controls the sparsity of the regression coefficient matrix  $\mathbf{B}$ ) and  $\mu = 0.8, 1.6$ . We plot the 95 % credible intervals for the regression coefficients per edge ordered depending on whether they are truly non-influential edges (top of each panel) or truly influential edges (bottom of each panel). The color of the intervals depends on whether it intersects zero (light) and hence estimated to be non-influential or does not intersect zero (dark) and hence estimated to be influential by the model. These panels allow us to visualize false positives (dark intervals on the top panel) or false negatives (light intervals on the bottom panel). The model has a low false positive rate of influential edges for all settings of  $n, k, \pi, \mu$ , except for  $n = 500, \pi = 0.3, \mu = 1.6$ . This behavior is similar for  $k = 22$  sampled microbes (Fig. 25) and for phylogenetic coefficients (Fig. 26 for  $k = 8$  and Fig. 27 for  $k = 22$ ). Accuracy to detect influential edges (dark intervals on the lower “True influential edges” panels) is also similar across all simulation settings.



**Figure 12: Posterior probability of influential nodes (functional redundancy model with random coefficients).** Different panels represent different number of sampled microbes ( $k = 8, 22$ ) which controls the sparsity of the adjacency matrix and different sample sizes ( $n = 100, 500$ ). Within each panel, we have four plots corresponding to the two values of edge effect size ( $\mu = 0.8, 1.6$ ) and two values of probability of influential edge ( $\pi = 0.3, 0.8$ ) which controls the sparsity of the regression coefficient matrix  $\mathbf{B}$ . Each bar corresponds to one node (microbe) and the bar are colored depending on whether the node is truly influential (dark) or not influential (light). The model shows high false positive rate in all settings except for low sparsity ( $\pi = 0.8$ ) in small number of sampled microbes ( $k = 8$ ), or high sparsity with small effect ( $\pi = 0.3, \mu = 0.8$ ) with large number of sampled nodes ( $k = 22$ ). This behavior is similar with phylogenetic coefficients (Fig. 28).

truly non-influential edges. Under the additive model, false positive rate of nodes (dark purple bars) appear to be the concern when there are few nodes sampled ( $k = 8$ ). High false positive rates of nodes are evident in most setting of the functional redundancy model except for  $\pi = 0.8, k = 8$  and  $\pi = 0.3, \mu = 0.8, k = 22$ . In general, the BNR model with random coefficients is able to accurately detect influential nodes and edges when there are truly interactions effects (Fig. 32 middle: interaction model), especially when there is low sparsity of the coefficient matrix  $\mathbf{B}$  ( $\pi = 0.8$ ). Under the additive model, the BNR suffers from high false positive rate of nodes.

Fig. 33 shows the false positive and false negative rates for edges and nodes for different simulation settings in terms of  $n, k, \pi, \mu$  for additive (top), interaction (middle) and functional redundancy (bottom) models with phylogenetic coefficients. Again, an interaction model shows the best performance in terms of controlled false positive and false negative rates for all settings of  $\pi, n$  and  $\mu$ . Under the interaction model (middle), there is inflated false negative rate of edges which could be due to the fact that the model does not include main (node) effects. Furthermore, there is better controlled false positive rate of nodes (dark purple bars) in the  $\pi = 0.3$  case than in the random coefficients case (Fig.

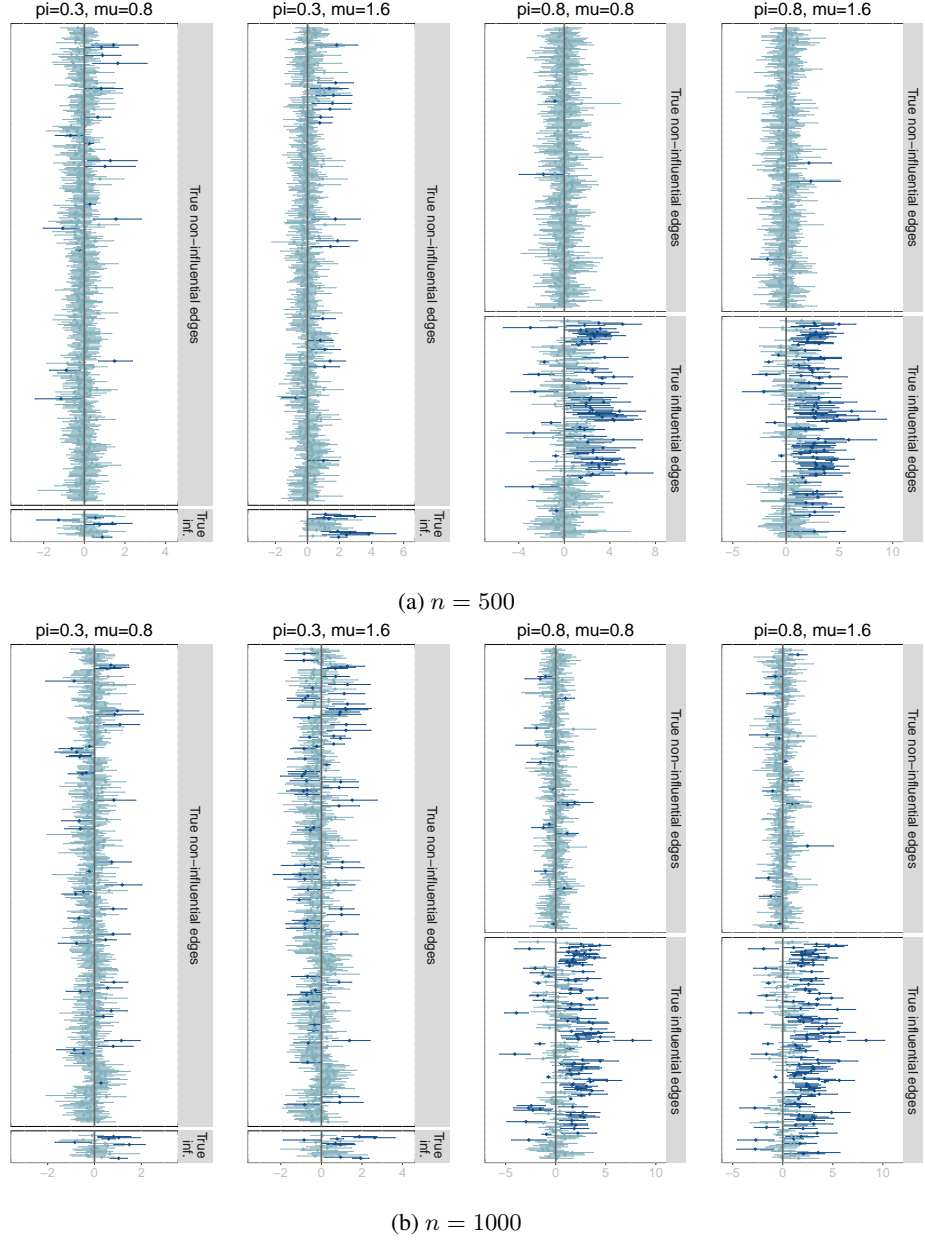


Figure 13: **95 % credible intervals for edge effects (functional redundancy model with random coefficients) with  $k = 8$  sampled nodes.** Top (a): Sample size of  $n = 500$ . Bottom (b): Sample size of  $n = 1000$ . Each panel corresponds to a scenario of  $\pi = 0.3, 0.8$  (which controls the sparsity of the regression coefficient matrix  $\mathbf{B}$ ) and  $\mu = 0.8, 1.6$ . We plot the 95 % credible intervals for the regression coefficients per edge ordered depending on whether they are truly non-influential edges (top of each panel) or truly influential edges (bottom of each panel). The color of the intervals depends on whether it intersects zero (light) and hence estimated to be non-influential or does not intersect zero (dark) and hence estimated to be influential by the model. These panels allow us to visualize false positives (dark intervals on the top panel) or false negatives (light intervals on the bottom panel).

32) which means that when the effects of microbes are expected to be phylogenetically-informed, the BNR model is able to accurately identify the influential nodes compared to effects of microbes that are randomly assigned. Under the additive model (top), there is controlled false positive rate of nodes in all settings of  $k = 22$  which is not true when coefficients are random (Fig. 32) The results for the functional redundancy model (bottom) are very similar to those

with the random coefficients (Fig. 32). Namely, there are inflated false positive and false negative rates on all settings of  $k = 22$ , and only controlled rates under the  $k = 8$  sampled microbes with low sparsity  $\pi = 0.8$ .

### Bacterial drivers of Phosphorous Leaching in Soil

Fig. 14 shows the posterior probabilities of being influential nodes for the OTUs in the augmented bacterial microbiome dataset (Wagg et al., 2019). Likely due to the limited number of samples, the model is not able to accurately differentiate the strength of the effect of different OTUs. We use 0.65 as the arbitrary cutoff probability to determine whether an OTU is identified as influential by the BNR model. With this cutoff, we find five OTUs whose presence is influential on the amount of phosphorous leaching in the soil (Table 3). We include also the reported association in the original study (Wagg et al., 2019).

Genus	Class	Wagg et al. (2019)
<i>Sporolituus</i>	Negativicutes	No association
<i>Mesorhizobium</i>	Alphaproteobacteria	Positive/Negative
<i>Paucibacter</i>	Betaproteobacteria	No association
<i>Cohnella</i>	Bacilli	Negative
<i>Brevibacillus</i>	Bacilli	Negative

Table 3: Bacterial genus identified by our BNR model as key drivers of P leaching in soil (posterior probability of influential node greater than 0.65). The original study Wagg et al. (2019) reported bacterial classes that were positively or negatively associated with P leaching (third column). No association means that the original study did not find any connection between the bacterial class and the response whereas Not shown means that the original study did not report anything about this class. There is one row with "Positive/Negative" status because the original study found positive association with some species in the class and negative association with others.

We unfortunately could not find any influential edges (interactions among bacterial genera) with our model (Fig. 34 in the Appendix) as all posterior 95% credible intervals for the edge effects intersect zero. This is consistent with the simulation study. The model typically requires more than 100 samples to reach the statistical power to identify key interactions. Furthermore, we note that this phenotype (P leaching) probably falls under the functional redundancy setting as it is known that several taxa can indeed support the same function (Wagg et al., 2019). Our simulation study showed that under a functional redundancy model, the BNR has good performance only when there are few microbes sampled and many are expected to be influential (low sparsity in  $\mathbf{B}$ ). The data collection setting in Wagg et al. (2019) was expected to produce high sampling rates which is in disagreement with the ideal setting for the BNR model which also explains the low statistical power to detect influential nodes. However, the requirement of low sampling could be an artifact of flaws in the simulation study. High sampling would artificially create more response values that surpass the threshold, inducing low variability in the response, and thus, restricting the power of the model. As a point of comparison, we present the histograms of both the simulated "functional redundancy" response and the actual phosphorous leaching response (Fig. 37 in the Appendix). For the simulation case of  $k = 8$  microbes in each sample, the mean response value is 6.9 with a standard deviation of 4.25, and out of the 500 samples in this case, just one is truncated. For the phosphorous leaching data (actual and augmented data), the mean amount of P leaching was 0.17 mg/L with a standard deviation of 0.16. Both histograms show sufficient spread and variability, yet the visual perception can be deceiving and the model could potentially require more samples for accurate estimation of parameters.

We conclude that for cases of functional redundancy, presence/absence of microbes does not appear to be a suitable predictor of phenotype variability, and other measures like diversity can be more relevant (as those used in the original study (Wagg et al., 2019)).

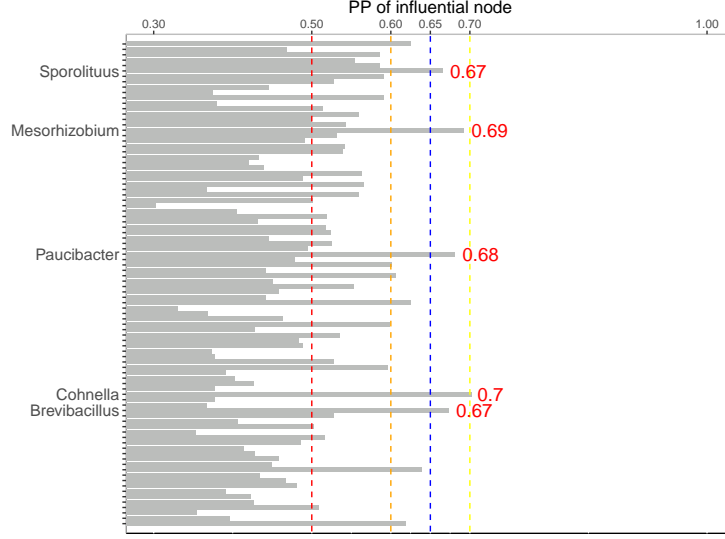


**Figure 14: Posterior probability of influential nodes (bacterial microbiome data)** We consider genus OTUs with a posterior probability of being influential nodes greater than or equal to 0.65 to be considered influential. We present other thresholds for comparison on which OTUs would be influential: red dashed line for 0.5, orange dashed line for 0.6, blue dashed line for 0.65 significance cutoff, and yellow dashed line for 0.7. For the arbitrary threshold of 0.65, 5 bacterial genera are identified as influential to the P leaching response.

### Convergence checks

For each simulation setting, we run three MCMC chains and assess convergence using the  $\hat{R}$  convergence criterion proposed in Vehtari et al. (2019). We consider convergence to have been achieved if  $\hat{R} \leq 1.2$  for all of the  $\gamma$  and  $\xi$  parameters. For the theoretical simulations, the maximum  $\hat{R}$  is 1.18 for  $\xi$  and 1.19 for  $\gamma$ . For the realistic simulations, the maximum  $\hat{R}$  value is 1.20 for  $\gamma$  and 1.13 for  $\xi$ . Maximum  $\hat{R}$  values for each realistic simulation type are given in Table 5 (Appendix). For the real data, the final  $\hat{R}$  value was 1.18 for the  $\xi$  variables and 1.18 for the  $\gamma$  variables.

### Computational speed

All simulations were run on Julia 1.7.1 with compiler optimization level set to 0, IEEE math, and bounds-checking on, on servers provided by the Wisconsin Institute for Discovery. These servers run a Linux-based operating system on Intel Xeon Gold 6254 CPUs. For the theoretical simulations performing 50,000 generations (burn-in and retained), the inference took an average of 6 minutes 24 seconds for sample size of  $n = 100$  and 19 minutes 54 seconds for sample size of  $n = 500$ . For the realistic simulations performing 50,000 generations (burn-in and retained), the inference took an average of 19 minutes 52 seconds for sample size of  $n = 500$  and 56 minutes 45 seconds for sample size of  $n = 1000$ . Note that the cases which required more burn-in samples are excluded from these averages (see Tables 1 and

2). For the real data analysis, performing 20,000 generations took 1 hour and 53 minutes. Note the time per generation is much higher for the real data due to the higher dimension of the coefficient matrix.

## Discussion

In this work, we present the first deep investigation of the applicability of the Bayesian Network Regression (BNR) model on microbiome data. In addition, we introduce the first user-friendly implementation of the BNR model in an open source well-documented Julia package `BayesianNetworkRegression.jl` available on GitHub <https://github.com/solislemuslab/BayesianNetworkRegression.jl>.

The model performs well under a variety of settings of data sparsity (sparsity in network adjacency matrix **A**) and sparsity of influential drivers (sparsity in the coefficient regression matrix **B**) when the model generating the simulated data matches the BNR model (denoted theoretical simulations). Indeed, the model is able to identify influential nodes (microbes) and influential edges (interactions of microbes) regardless of the sparsity of **A** and **B** for sample sizes of  $n = 500$ , and more surprisingly, in spite of not including main (node) effects. For smaller sample sizes ( $n = 100$ ), influential nodes and edges can still be detected as long as the effect sizes are large ( $\mu = 1.6$ ). It is important to note that the model has a low false positive rate in all settings which prevents the identification of spurious microbial drivers in the phenotypes of interest.

When the model generating the simulated data did not match the BNR model (realistic simulations), the model performance varied depending on the specific generating model. For example, if the biological phenotype is generated under an additive model with random or phylogenetic coefficients, the BNR model is able to successfully detect influential nodes only under large sample sizes ( $n = 1000$ ), large number of sampled microbes ( $k = 22$ ) and low sparsity in the regression coefficient matrix ( $\pi = 0.8$ ). Under this same additive model, there are no influential edges (interactions of microbes) and the BNR model is able to control the false positive rate of edges only when sufficiently microbes have been sampled ( $k = 22$ ). This result is important as it highlights that the model is able to identify influential nodes even in the absence of main (node) effects.

When the biological phenotype is generated under an interaction model, the BNR method is able to accurately identify influential microbes under low sparsity settings ( $\pi = 0.8$ ) regardless of the type of coefficients (random vs phylogenetic), regardless of number of sampled microbes ( $k = 8, 22$ ) and regardless of sample size ( $n = 500, 1000$ ). For high sparsity settings ( $\pi = 0.3$ ), phylogenetic coefficients appear to have more signal than random coefficients to identify influential nodes regardless of sample size ( $n$ ), number of microbes sampled ( $k$ ), or effect sizes ( $\mu$ ), yet there is an inflated false positive rate with larger sample sizes ( $n = 1000$ ) for the case of large effect size ( $\mu = 1.6$ ) with few sampled microbes ( $k = 8$ ). Random coefficients provide no strong signal to detect the influential nodes (high false positive rate) under high sparsity ( $\pi = 0.3$ ) unless there are  $k = 22$  microbes sampled with large sample size ( $n = 1000$ ). In addition, the BNR has good performance to identify the influential edges regardless of the sample size ( $n$ ), the number of

microbes sampled ( $k$ ), the sparsity level ( $\pi$ ), node effect sizes ( $\mu$ ), and type of coefficient (random vs phylogenetic) with controlled false positive and false negative rates in all settings.

Lastly, under the functional redundancy model, the BNR model is unable to identify influential microbes unless there are very few sampled microbes ( $k = 8$ ), but many expected to be influential ( $\pi = 0.8$ ). This result could be explained by the fact that multiple sampled microbes could cause the phenotype to reach the threshold more easily and thus, there is less information on the variability of the response to estimate the effects and influential probabilities. Similarly, the BNR model has good performance to identify influential nodes and influential edges only when there are few microbes sampled ( $k = 8$ ) and low sparsity in  $\mathbf{B}$  ( $\pi = 0.8$ ).

The main take-home message is that the current version of the BNR model (Equation 1), even without including main (node) effects, can accurately identify influential nodes (microbes) and influential edges (interactions among microbes) under most realistic biological settings, but it requires large sample sizes (e.g.  $n = 1000$  tested here). Future work will involve the extension of the model to incorporate main (node) effects as well as environmental predictors that can also have an effect on the phenotype of interest. Furthermore, future work will incorporate downstream estimation error of the adjacency matrix which is currently taken as perfectly reconstructed from the phylogenetic tree.

In terms of the real data analysis, we investigated the connections between the bacterial soil microbiome data and phosphorous leaching as in Wagg et al. (2019). Unlike in our simulation study, the sample size was merely 50 samples which we augmented to 100. The augmented sample was still not sufficient to achieve statistical power to detect influential edges (interactions), yet it was enough to identify influential nodes (microbes). Five bacterial genera were identified as key drivers of P leaching in soil, three of those had already been identified as significantly associated with the response in the previous study (Wagg et al., 2019).

While most existing public datasets do not have equivalent sample sizes to the ones tested in our simulation study, we believe that this is a case of “build it and they will come”. Until now, real data analyses of microbiome data involved *one* matrix of relative abundances which is used to estimate *one* co-occurrence microbial network. The assumption behind this one co-occurrence matrix is that correlations represent interactions, and these interactions are *global*. That is, the interactions will appear in all contexts and all samples.

In recent years, microbiome researchers believe that the interactions are context-dependent and that there will be different interactions on different environmental conditions. These different interactions would produce different microbial networks, each in turn associated with a specific biological phenotype of interest. BNR is the ideal model to represent this setting as it requires a sample of networks with edge variability (which violates the global interactions assumption of most public microbiome datasets) and it requires each of the microbial networks to be associated with a phenotype value. The downside is that the model requires hundreds of these network-phenotype samples. While these large sample conditions appear to be outside the norm of current observational microbiome research, we believe that the BNR model could be quite useful to identify key microbial drivers of biological phenotypes in experimental settings. Indeed, scientists can design experiments with  $k$  microbes and then, measure the phenotype of interest. Different

samples would correspond to different replicates under the same set (or different) of microbes. This setup actually aligns with our simulation study where we have  $k$  microbes per sample and the true phenotype value is computed only using those  $k$  microbes. Future work will incorporate other covariates into the model corresponding to replicate, experimental or environmental conditions. Furthermore, in conjunction with data augmentation techniques, the BNR model could be applied on a variety of real datasets, as this will be another line of future work. Despite its limitations, we view the BNR model as one novel tool that microbiome researchers could utilize to identify key microbiome drivers in biological phenotypes of interest given its robustness and accuracy under a variety of biologically relevant conditions.

## Acknowledgments

This work was supported by the Department of Energy [DE-SC0021016 to CSL] and by the National Institute of Food and Agriculture, United States Department of Agriculture [Hatch project 1023699 to CSL]. We thank Sharmistha Guha and Abel Rodriguez for communications to clarify specifics of their model implementation, and we thank Richard Lankau for meaningful conversations about microbial communities.

## Conflicts of interest

The authors declare no conflicts of interest.

## Author contributions

SO implemented the Julia package, ran the simulations and real data analysis and wrote the first draft of the manuscript. CSL devised the idea of the project, chose the model, and produced the first iteration of figures for the manuscript. All authors contributed critically to the drafts and gave final approval for publication.

## References

Cassandra Allsup and Richard Lankau. Migration of soil microbes may promote tree seedling tolerance to drying conditions. *Ecology*, 100:e02729, 04 2019. doi: 10.1002/ecy.2729.

Loubna Benidire, Fatima El Khaloufi, Khalid Oufdou, Mohamed Barakat, Joris Tulumello, Philippe Ortet, Thierry Heulin, and Wafa Achouak. Phytoprobiotic bacteria improve saline stress tolerance in *Vicia faba* and modulate microbial interaction network. *Science of the Total Environment*, 729:139020, 2020.

F Guillaume Blanchet, Kevin Cazelles, and Dominique Gravel. Co-occurrence is not evidence of ecological interactions. *Ecology Letters*, 23(7):1050–1063, 2020.

K Alaine Broadaway, Richard Duncan, Karen N Conneely, Lynn M Almli, Bekh Bradley, Kerry J Ressler, and Michael P Epstein. Kernel Approach for Modeling Interaction Effects in Genetic Association Studies of Complex

Quantitative Traits. *Genetic epidemiology*, 39(5):366–375, 2015. ISSN 0741-0395. doi: 10.1002/gepi.21901. URL <http://www.ncbi.nlm.nih.gov/pmc/articles/PMC4469530/>.

Chris Callewaert, Katia Ravard Helffer, and Philippe Lebaron. Skin microbiome and its interplay with the environment. *American Journal of Clinical Dermatology*, pages 1–8, 2020.

Anna M. Cates, Michael J. Braus, Thea L. Whitman, and Randall D. Jackson. Separate drivers for microbial carbon mineralization and physical protection of carbon. *Soil Biology and Biochemistry*, 133:72–82, 2019.

Heather J Cordell. Detecting gene-gene interactions that underlie human diseases. *Nature Reviews Genetics*, 10:392, 2009.

Herbert L Dupont, Zhi-Dong Jiang, Andrew W Dupont, and Netanya S Utay. The intestinal microbiome in human health and disease. *Transactions of the American Clinical and Climatological Association*, 131:178, 2020.

Daniele Durante and David B Dunson. Bayesian inference and testing of group differences in brain networks. *Bayesian Analysis*, 13(1):29–58, 2018.

Daniele Durante, David B Dunson, and Joshua T Vogelstein. Nonparametric bayes modeling of populations of networks. *Journal of the American Statistical Association*, 112(520):1516–1530, 2017.

R Fan, M Zhong, S Wang, Y Zhang, A Andrew, M Karagas, H Chen, C I Amos, M Xiong, and J Moore. Entropy-Based Information Gain Approaches to Detect and to Characterize Gene-Gene and Gene-Environment Interactions/Correlations of Complex Diseases. *Genetic Epidemiology*, 35(7):706–721, 2011.

Huaying Fang, Chengcheng Huang, Hongyu Zhao, and Minghua Deng. gcoda: Conditional dependence network inference for compositional data. *J. Comput. Biol.*, 24(7):699–708, July 2017.

Noah Fierer, Christian L Lauber, Kelly S Ramirez, Jesse Zaneveld, Mark A Bradford, and Rob Knight. Comparative metagenomic, phylogenetic and physiological analyses of soil microbial communities across nitrogen gradients. *The ISME Journal*, 6(5):1007–1017, 2012.

Jonathan Friedman and Eric J Alm. Inferring correlation networks from genomic survey data. *PLoS Comput. Biol.*, 8(9):e1002687, September 2012.

Neal S Grantham, Yawen Guan, Brian J Reich, Elizabeth T Borer, and Kevin Gross. MIMIX: A bayesian Mixed-Effects model for microbiome data from designed experiments. *J. Am. Stat. Assoc.*, 115(530):599–609, April 2020.

Sharmistha Guha and Rajarshi Guhaniyogi. Bayesian supervised clustering of undirected networks with cluster specific inference on significant nodes and edges related to predictors. *submitted*, 2021.

Sharmistha Guha and Abel Rodriguez. Bayesian regression with undirected network predictors with an application to brain connectome data. *Journal of the American Statistical Association*, 116(534):581–593, 2021.

Ian Holmes, Keith Harris, and Christopher Quince. Dirichlet multinomial mixtures: Generative models for microbial metagenomics. *PLOS ONE*, 7(2):e30126–, 02 2012.

Susan Holmes. Successful strategies for human microbiome data generation, storage and analyses. *Journal of Biosciences*, 44(5):111, 2019.

Ryan H Hsu, Ryan L Clark, Jin Wen Tan, John C Ahn, Sonali Gupta, Philip A Romero, and Ophelia S Venturelli. Microbial interaction network inference in microfluidic droplets. *Cell systems*, 9(3):229–242, 2019.

Hemant Ishwaran and J Sunil Rao. Spike and slab variable selection: frequentist and bayesian strategies. *The Annals of Statistics*, 33(2):730–773, 2005.

P Kraft, Y.-C. Yen, D O Stram, J Morrison, and W J Gauderman. Exploiting Gene-Environment Interaction to Detect Genetic Associations. *Human Heredity*, 63(2):111–119, 2007. ISSN 0001-5652. URL <https://www.karger.com/DOI/10.1159/000099183>.

Christina Kranz and Thea Whitman. Short communication: Surface charring from prescribed burning has minimal effects on soil bacterial community composition two weeks post-fire in jack pine barrens. *Applied Soil Ecology*, 144: 134–138, 2019.

Victor Kunin, Alex Copeland, Alla Lapidus, Konstantinos Mavromatis, and Philip Hugenholtz. A bioinformatician’s guide to metagenomics. *Microbiology and Molecular Biology Reviews*, 72(4):557, 12 2008.

Zachary D Kurtz, Christian L Müller, Emily R Miraldi, Dan R Littman, Martin J Blaser, and Richard A Bonneau. Sparse and compositionally robust inference of microbial ecological networks. *PLoS Comput. Biol.*, 11(5):e1004226, May 2015a.

Zachary D. Kurtz, Christian L. Müller, Emily R. Miraldi, Dan R. Littman, Martin J. Blaser, and Richard A. Bonneau. Sparse and compositionally robust inference of microbial ecological networks. *PLOS Computational Biology*, 11: 1–25, 05 2015b. URL <https://doi.org/10.1371/journal.pcbi.1004226>.

Emily W Lankau, Diane Xue, Rachel Chrisensen, Amanda J Gevens, and Richard A Lankau. Management and soil conditions influence common scab severity on potato tubers via indirect effects on soil microbial communities. *Phytopathology*™, 2020/02/27 2020a.

Richard Lankau, Isabelle George, and Max Miao. Crop health optimized by microbial diversity across phylogenetic scales. *Submitted*, 2020b.

Wei Lin, Pixu Shi, Rui Feng, and Hongzhe Li. Variable selection in regression with compositional covariates. *Biometrika*, 101(4):785–797, August 2014.

Xin Ma, Suprateek Kundu, and Jennifer Stevens. Semi-parametric bayes regression with network valued covariates. *arXiv preprint arXiv:1910.03772*, 2019.

Bryan D Martin, Daniela Witten, and Amy D Willis. Modeling microbial abundances and dysbiosis with beta-binomial regression. *The annals of applied statistics*, 14(1):94, 2020.

Brett Mckinney and Nicholas Pajewski. Six degrees of epistasis: Statistical network models for gwas. *Frontiers in Genetics*, 2:109, 2012.

Brett A. McKinney, James E. Crowe, Jr, Jingyu Guo, and Dehua Tian. Capturing the spectrum of interaction effects in genetic association studies by simulated evaporative cooling network analysis. *PLOS Genetics*, 5(3):1–12, 2009.

Samuel S. Minot and Amy D. Willis. Clustering co-abundant genes identifies components of the gut microbiome that are reproducibly associated with colorectal cancer and inflammatory bowel disease. *Microbiome*, 7(1):110, 2019.

E. Paradis and K. Schliep. ape 5.0: an environment for modern phylogenetics and evolutionary analyses in R. *Bioinformatics*, 35:526–528, 2019.

Tiago P Peixoto. Network reconstruction and community detection from dynamics. *Phys. Rev. Lett.*, 123(12):128301, September 2019.

R. A. Rioux, C. M. Stephens, and J. P. Kerns. Factors affecting pathogenicity of the turfgrass dollar spot pathogen in natural and model hosts. *bioRxiv*, page 630582, 01 2019.

Jordan S Rosenfeld. Functional redundancy in ecology and conservation. *Oikos*, 98(1):156–162, 2002.

Kris Sankaran and Susan P Holmes. Latent variable modeling for the microbiome. *Biostatistics*, 20(4):599–614, 06 2018. ISSN 1465-4644. doi: 10.1093/biostatistics/kxy018. URL <https://doi.org/10.1093/biostatistics/kxy018>.

Kris Sankaran and Susan P Holmes. Multitable methods for microbiome data integration. *Frontiers in genetics*, 10: 627–627, 08 2019.

Ruqaiyyah Siddiqui, Noor Akbar, and Naveed Ahmed Khan. Gut microbiome and human health under the space environment. *Journal of Applied Microbiology*, 130(1):14–24, 2021.

C. Solís-Lemus, P. Bastide, and C. Ané. PhyloNetworks: a package for phylogenetic networks. *Molecular Biology and Evolution*, 34(12):3292–3298, 2017.

Elisavet Stavropoulou, Konstantia Kantartzzi, Christina Tsigalou, Theocharis Konstantinidis, Chrissoula Voidarou, Theodoros Konstantinidis, and Eugenia Bezirtzoglou. Unraveling the interconnection patterns across lung microbiome, respiratory diseases, and covid-19. *Frontiers in cellular and infection microbiology*, 10:892, 2021.

Sanjeena Subedi, Drew Neish, Stephen Bak, and Zeny Feng. Cluster analysis of microbiome data by using mixtures of dirichlet–multinomial regression models. *J. R. Stat. Soc. Ser. C Appl. Stat.*, 69(5):1163–1187, November 2020.

Imran Sulaiman, Sheeba Schuster, and Leopoldo N Segal. Perspectives in lung microbiome research. *Current Opinion in Microbiology*, 56:24–29, 2020.

Zheng-Zheng Tang and Guanhua Chen. Zero-inflated generalized dirichlet multinomial regression model for microbiome compositional data analysis. *Biostatistics*, 20(4):698–713, October 2019.

Aki Vehtari, Andrew Gelman, Daniel Simpson, Bob Carpenter, and Paul-Christian Bürkner. Rank-normalization, folding, and localization: An improved r for assessing convergence of mcmc. *arXiv preprint arXiv:1903.08008*, 2019.

Cameron Wagg, Klaus Schlaeppi, Samiran Banerjee, Eiko E Kuramae, and Marcel GA van der Heijden. Fungal-bacterial diversity and microbiome complexity predict ecosystem functioning. *Nature communications*, 10(1):1–10, 2019.

Lu Wang, Zhengwu Zhang, and David Dunson. Symmetric bilinear regression for signal subgraph estimation. *IEEE Transactions on Signal Processing*, 67(7):1929–1940, 2019.

Thea Whitman, Rachel Neurath, Adele Perera, Ilexis Chu-Jacoby, Daliang Ning, Jizhong Zhou, Peter Nico, Jennifer Pett-Ridge, and Mary Firestone. Microbial community assembly differs across minerals in a rhizosphere microcosm. *Environmental Microbiology*, 20(12):4444–4460, 2018. doi: 10.1111/1462-2920.14366. URL <https://sfamjournals.onlinelibrary.wiley.com/doi/abs/10.1111/1462-2920.14366>.

Thea Whitman, Ellen Whitman, Jamie Woolet, Mike D. Flannigan, Dan K. Thompson, and Marc-André Parisien. Soil bacterial and fungal response to wildfires in the canadian boreal forest across a burn severity gradient. *Soil Biology and Biochemistry*, 138:107571, 2019.

Brian D Williamson, James P Hughes, and Amy D Willis. A multi-view model for relative and absolute microbial abundances. *Biometrics*, 2019.

Fan Xia, Jun Chen, Wing Kam Fung, and Hongzhe Li. A logistic normal multinomial regression model for microbiome compositional data analysis. *Biometrics*, 69(4):1053–1063, December 2013.

Vincent B Young. The role of the microbiome in human health and disease: an introduction for clinicians. *Bmj*, 356, 2017.

Zhaojing Zhang, Yuanyuan Qu, Shuzhen Li, Kai Feng, Weiwei Cai, Huaqun Yin, Shang Wang, Wenzong Liu, Aijie Wang, and Ye Deng. Florfenicol restructured the microbial interaction network for wastewater treatment by microbial electrolysis cells. *Environmental research*, 183:109145, 2020.

Jie Zhou, Weston D Viles, Boran Lu, Zhigang Li, Juliette C Madan, Margaret R Karagas, Jiang Gui, and Anne G Hoen. Identification of microbial interaction network: zero-inflated latent ising model based approach. *BioData mining*, 13(1):1–15, 2020.

Hui Zou and Trevor Hastie. Regularization and variable selection via the elastic net. *Journal of the Royal Statistical Society: Series B (Statistical Methodology)*, 67(2):301–320, 2005.

## A Appendix

### A.1 Table of parameters

Table 4: Parameters in the model and in the priors

Parameter	Description
$V$	number of nodes
$q$	number of edges
$\tau^2 \in \mathbb{R}$	variance of error term
$\mathbf{u} \in \mathbb{R}^{R \times V}$	$R$ -dimensional latent variables for each node
$\xi \in \{0, 1\}^V$	binary vector to denote if a node is influential
$\gamma \in \mathbb{R}^q$	regression coefficients for edge effects
$\mathbf{s} \in \mathbb{R}^q$	scale parameters for the variance of $\gamma$
$\theta \in \mathbb{R}$	exponential parameter for the scale $\mathbf{s}$
$\Delta \in \mathbb{R}$	Bernoulli parameter for $\xi$
$\mathbf{M} \in \mathbb{R}^{R \times R}$	covariance matrix for latent variables $\mathbf{u}$
$\mu \in \mathbb{R}$	overall mean
$\lambda \in \{0, 1, -1\}^R$	vector that governs which entries in the latent variables are informative
$\tilde{\pi} \in \mathbb{R}^{R \times 3}$	Dirichlet prior probability for $\lambda$ being 0, 1, -1

### A.2 Mathematical description of theoretical simulations

Graphical description of the theoretical simulations is in Fig. 2. Here, we list the variables:

- $n$ : sample size ( $n = 100, 500$ )
- $d$ : number of total microbes ( $d = 30$ )
- $k$ : number of microbes sampled ( $k = 8, 15, 22$ ) which controls the sparsity in  $\mathbf{A}$
- $R$ : dimension of latent variables  $\mathbf{u}$  ( $R = 5, 7, 9$ )
- $\pi$ : probability of Bernoulli per node ( $\pi = 0.3, 0.8$ ) which controls the sparsity in  $\mathbf{B}$
- $\mu$ : mean of effect size in  $\mathbf{B}$  ( $\mu = 0.8, 1.6$ ) which controls the magnitude in  $\mathbf{B}$

Then, the simulating algorithm is:

1. Simulate a 30-taxon phylogenetic tree using the `rtree` function from the R package `ape` (Paradis and Schliep, 2019)
2. Simulate whether each node is influential and the true effects of each interaction for  $i = 1, \dots, d$  and  $j = 1, \dots, 30$

$$\begin{aligned} \xi_i &\sim \text{Bernoulli}(\pi) \\ \mathbf{B}_{ij} &\sim \xi_i \xi_j \text{Normal}(\mu, 1) \end{aligned}$$

3. For every sample  $i = 1, \dots, n$ , calculate the adjacency matrix  $\mathbf{A}_i$  as follows
  - (a) Select  $k$  microbes randomly  $K^* = \{j_1, j_2, \dots, j_k\}$
  - (b) For  $p, q \in K^*$ , let  $d_{p,q}$  be the phylogenetic distance between microbes  $p$  and  $q$ , so that the  $(p, q)$  entry in the adjacency matrix is given by

$$\mathbf{A}_i[p, q] = \frac{1}{d_{p,q}}$$

4. For every sample  $i = 1, \dots, n$ , calculate the response value as follows

$$y_i = \langle \mathbf{A}_i, \mathbf{B} \rangle_F + \epsilon, \quad \epsilon \sim \text{Normal}(0, 1)$$

At the end of the simulating algorithm, we have a collection of pairs  $(y_1, \mathbf{A}_1), \dots, (y_n, \mathbf{A}_n)$  to be used as data in the BNR implementation.

### A.3 Mathematical description of realistic simulations

Graphical description of the realistic simulations is in Fig. 3. Here, we list the variables:

- $n$ : sample size ( $n = 500, 1000$ )
- $d$ : number of total microbes ( $d = 30$ )
- $k$ : number of microbes sampled ( $k = 8, 22$ ) which controls the sparsity in  $\mathbf{A}$
- $R$ : dimension of latent variables  $\mathbf{u}$  ( $R = 7$ )
- $\pi$ : probability of Bernoulli per node ( $\pi = 0.3, 0.8$ ) which controls the sparsity in  $\mathbf{B}$
- $\mu_b$ : mean of main effect size in  $\mathbf{B}$  ( $\mu_b = 0.8, 1.6$ ) which controls the magnitude in  $\mathbf{B}$
- $L$ : limit for response  $y$  under the functional redundancy model

$\mu$	$\pi$	$L$
0.8	0.3	3
1.6	0.3	7
0.8	0.8	22
1.6	0.8	30

Next, we describe the simulating algorithm for the three models.

#### A.3.1 Additive Simulations

1. Simulate a 30-taxon phylogenetic tree using the `rtree` function from the R package `ape` (Paradis and Schliep, 2019)
2. Simulate whether a specific node is influential and its true main effect for  $i = 1, \dots, 30$ :
  - (a)  $\xi_i \sim \text{Bernoulli}(\pi)$
  - (b)  $b_i \sim \text{Normal}(\mu_b, \Sigma)$ 
    - $\Sigma = \mathbb{I}_{30}$  (case of random coefficients)
    - $\Sigma$  governed by the phylogenetic tree using the Julia package `PhyloNetworks` (Solís-Lemus et al., 2017) (case of phylogenetic coefficients)
3. For every sample  $i = 1, \dots, n$  calculate the adjacency matrix ( $\mathbf{A}_i$ ) as follows
  - (a) Select  $k$  microbes randomly  $K^* = \{j_1, j_2, \dots, j_k\}$
  - (b) For  $p, q \in K^*$ , let  $d_{p,q}$  be the phylogenetic distance between microbes  $p$  and  $q$  so that the  $(p, q)$  entry in the adjacency matrix is given by

$$\mathbf{A}_i[p, q] = \frac{1}{d_{p,q}}$$

4. For every sample  $i = 1, \dots, n$ , calculate the response value as follows

$$y_i = \sum_{i=1}^d b_i m_i \xi_i + \epsilon, \quad \epsilon \sim \text{Normal}(0, 1)$$

$$m_i = \mathbf{1}(i \in K^*)$$

where  $\mathbf{1}(\cdot)$  is the indicator function.

At the end of the simulating algorithm, we have a collection of pairs  $(y_1, \mathbf{A}_1), \dots, (y_n, \mathbf{A}_n)$  to be used as data in the BNR implementation.

#### A.3.2 Interaction Simulations

1. Simulate a 30-taxon phylogenetic tree using the `rtree` function from the R package `ape` (Paradis and Schliep, 2019)
2. Simulate whether a specific node is influential, its true main effect for  $i = 1, \dots, 30$  and all interaction effects  $j = 1, \dots, 30$ :

- (a)  $\xi_i \sim \text{Bernoulli}(\pi)$
- (b)  $b_i \sim \text{Normal}(\mu_b, \Sigma)$ 
  - $\Sigma = \mathbb{I}_{30}$  (case of random coefficients)
  - $\Sigma$  governed by the phylogenetic tree using the Julia package `PhyloNetworks` (Solís-Lemus et al., 2017) (case of phylogenetic coefficients)
- (c)  $b_{ij} \sim \text{Normal}(0.4, 1)$

3. For every sample  $i = 1, \dots, n$  calculate the adjacency matrix ( $\mathbf{A}_i$ ) as follows

- (a) Select  $k$  microbes randomly  $K^* = \{j_1, j_2, \dots, j_k\}$
- (b) For  $p, q \in K^*$ , let  $d_{p,q}$  be the phylogenetic distance between microbes  $p$  and  $q$  so that the  $(p, q)$  entry in the adjacency matrix is given by

$$\mathbf{A}_i[p, q] = \frac{1}{d_{p,q}}$$

4. For every sample  $i = 1, \dots, n$ , calculate the response value as follows:

$$y_i = \sum_{l=1}^d b_l m_l \xi_l + \sum_{l=1}^d \sum_{j=1}^d b_{lj} (\mathbf{A}_i[l, j]) \xi_l \xi_j + \epsilon, \quad \epsilon \sim \text{Normal}(0, 1)$$

$$m_i = \mathbf{1}(i \in K^*)$$

where  $\mathbf{1}(\cdot)$  is the indicator function.

At the end of the simulating algorithm, we have a collection of pairs  $(y_1, \mathbf{A}_1), \dots, (y_n, \mathbf{A}_n)$  to be used as data in the BNR implementation.

### A.3.3 Functional Redundancy Simulations

1. Simulate a 30-taxon phylogenetic tree using the `rtree` function from the R package `ape` (Paradis and Schliep, 2019)
2. Simulate whether a specific node is influential, its true main effect for  $i = 1, \dots, 30$  and all interaction effects  $j = 1, \dots, 30$ :
  - (a)  $\xi_i \sim \text{Bernoulli}(\pi)$
  - (b)  $b_i \sim \text{Normal}(\mu_b, \Sigma)$ 
    - $\Sigma = \mathbb{I}_{30}$  (case of random coefficients)
    - $\Sigma$  governed by the phylogenetic tree using the Julia package `PhyloNetworks` (Solís-Lemus et al., 2017) (case of phylogenetic coefficients)
  - (c)  $b_{ij} \sim \text{Normal}(0.4, 1)$
3. For every sample  $i = 1, \dots, n$  calculate the adjacency matrix ( $\mathbf{A}_i$ ) as follows
  - (a) Select  $k$  microbes randomly  $K^* = \{j_1, j_2, \dots, j_k\}$
  - (b) For  $p, q \in K^*$ , let  $d_{p,q}$  be the phylogenetic distance between microbes  $p$  and  $q$  so that the  $(p, q)$  entry in the adjacency matrix is given by

$$\mathbf{A}_i[p, q] = \frac{1}{d_{p,q}}$$

4. For every sample  $i = 1, \dots, n$ , calculate the response value as follows:

$$y_i = \min \left\{ \sum_{l=1}^d b_l m_l \xi_l + \sum_{l=1}^d \sum_{j=1}^d b_{lj} (\mathbf{A}_i[l, j]) \xi_l \xi_j + \epsilon, L \right\}, \quad \epsilon \sim \text{Normal}(0, 1)$$

$$m_l = \mathbf{1}(l \in K^*)$$

where  $\mathbf{1}(\cdot)$  is the indicator function.

At the end of the simulating algorithm, we have a collection of pairs  $(y_1, \mathbf{A}_1), \dots, (y_n, \mathbf{A}_n)$  to be used as data in the BNR implementation.

#### A.4 Simulation plots

#### List of Tables

4	Parameters in the model and in the priors	36
5	Convergence for realistic simulations. Maximum $\hat{R}$ convergence statistics for the realistic simulations by simulation type.	56

#### List of Figures

15	Posterior probability of influential nodes (theoretical simulations $R = 5$ )	40
16	Posterior probability of influential nodes (theoretical simulations $R = 9$ )	41
17	Posterior probability of influential nodes (theoretical simulations $k = 15, R = 5, 9$ )	42
18	False positive and false negative rates for influential edges and nodes (theoretical simulations)	43
19	Mean Square Error for regression coefficients and response	43
20	95 % credible intervals for edge effects (additive model with random coefficients) with $k = 8$ sampled nodes	44
21	Posterior probability of influential nodes (additive model with phylogenetic coefficients)	45
22	95 % credible intervals for edge effects (additive model with phylogenetic coefficients) with $k = 8$ sampled nodes	46
23	95 % credible intervals for edge effects (additive model with phylogenetic coefficients) with $k = 22$ sampled nodes	47
24	Posterior probability of influential nodes (interaction model with random coefficients)	48
25	95 % credible intervals for edge effects (interaction model with random coefficients) with $k = 22$ sampled nodes	49
26	95 % credible intervals for edge effects (interaction model with phylogenetic coefficients) with $k = 8$ sampled nodes	50
27	95 % credible intervals for edge effects (interaction model with phylogenetic coefficients) with $k = 22$ sampled nodes	51
28	Posterior probability of influential nodes (functional redundancy model with phylogenetic coefficients)	52
29	95 % credible intervals for edge effects (functional redundancy model with phylogenetic coefficients) with $k = 8$ sampled nodes	53
30	95 % credible intervals for edge effects (functional redundancy model with random coefficients) with $k = 22$ sampled nodes	54
31	95 % credible intervals for edge effects (functional redundancy model with phylogenetic coefficients) with $k = 22$ sampled nodes	55
32	False positive and false negative rates for influential edges and nodes for additive (top), interaction (middle) and functional redundancy (bottom) models with random coefficients	57
33	False positive and false negative rates for influential edges and nodes for additive (top), interaction (middle) and functional redundancy (bottom) models with phylogenetic coefficients	58
34	Posterior 95% credible intervals for edge effects (real-world data)	59
35	Posterior probability of influential nodes (bacterial microbiome data)	59
36	Posterior 95% credible intervals for edge effects (real-world data)	60
37	Histogram of response values for simulated "functional redundancy" data	60

#### A.4.1 Theoretical case

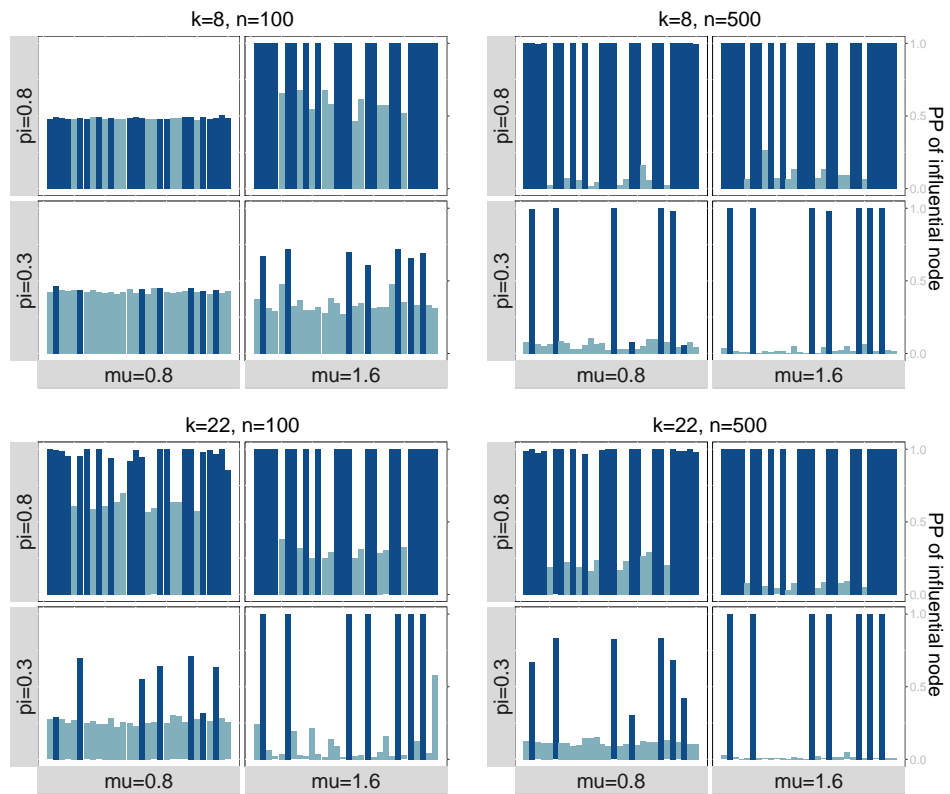


Figure 15: **Posterior probability of influential nodes (theoretical simulations  $R = 5$ )**. Different panels represent different number of sampled microbes ( $k = 8, 22$ ) which controls the sparsity of the adjacency matrix and different sample sizes ( $n = 100, 500$ ). Latent dimension of  $R = 5$ . Within each panel, we have four plots corresponding to the two values of edge effect size ( $\mu = 0.8, 1.6$ ) and two values of probability of influential node ( $\pi = 0.3, 0.8$ ) which controls the sparsity of the regression coefficient matrix ( $\mathbf{B}$ ). Each bar corresponds to one node (microbe) and the bar are colored depending on whether the node is truly influential (dark) or not influential (light). As expected, the model has a high PP for truly influential nodes (tall dark bars) and a low PP for non-influential nodes (short light bars) with best performance for  $n = 500$ , or for high coefficients  $\mu = 1.6$  for  $n = 100$ .

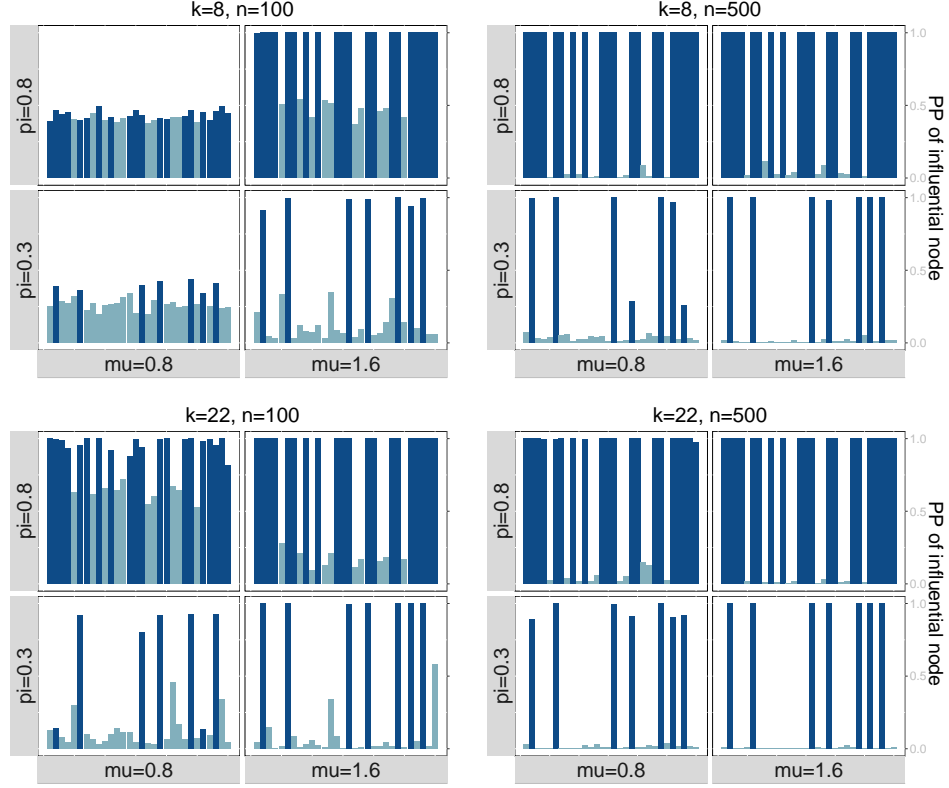


Figure 16: **Posterior probability of influential nodes (theoretical simulations  $R = 9$ )**. Different panels represent different number of sampled microbes ( $k = 8, 22$ ) which controls the sparsity of the adjacency matrix and different sample sizes ( $n = 100, 500$ ). Latent dimension of  $R = 9$ . Within each panel, we have four plots corresponding to the two values of edge effect size ( $\mu = 0.8, 1.6$ ) and two values of probability of influential node ( $\pi = 0.3, 0.8$ ) which controls the sparsity of the regression coefficient matrix ( $\mathbf{B}$ ). Each bar corresponds to one node (microbe) and the bar are colored depending on whether the node is truly influential (dark) or not influential (light). As expected, the model has a high PP for truly influential nodes (tall dark bars) and a low PP for non-influential nodes (short light bars) with best performance for  $n = 500$ , or for high coefficients  $\mu = 1.6$  for  $n = 100$ . We also notice here that a higher  $R$  ( $R = 9$ ) helps identify influential microbes on smaller effect sizes ( $\mu = 0.8, k = 22, n = 100$ ) compared to the same setting in Fig. 15. The downside of a larger latent dimension is less floating-point stability.

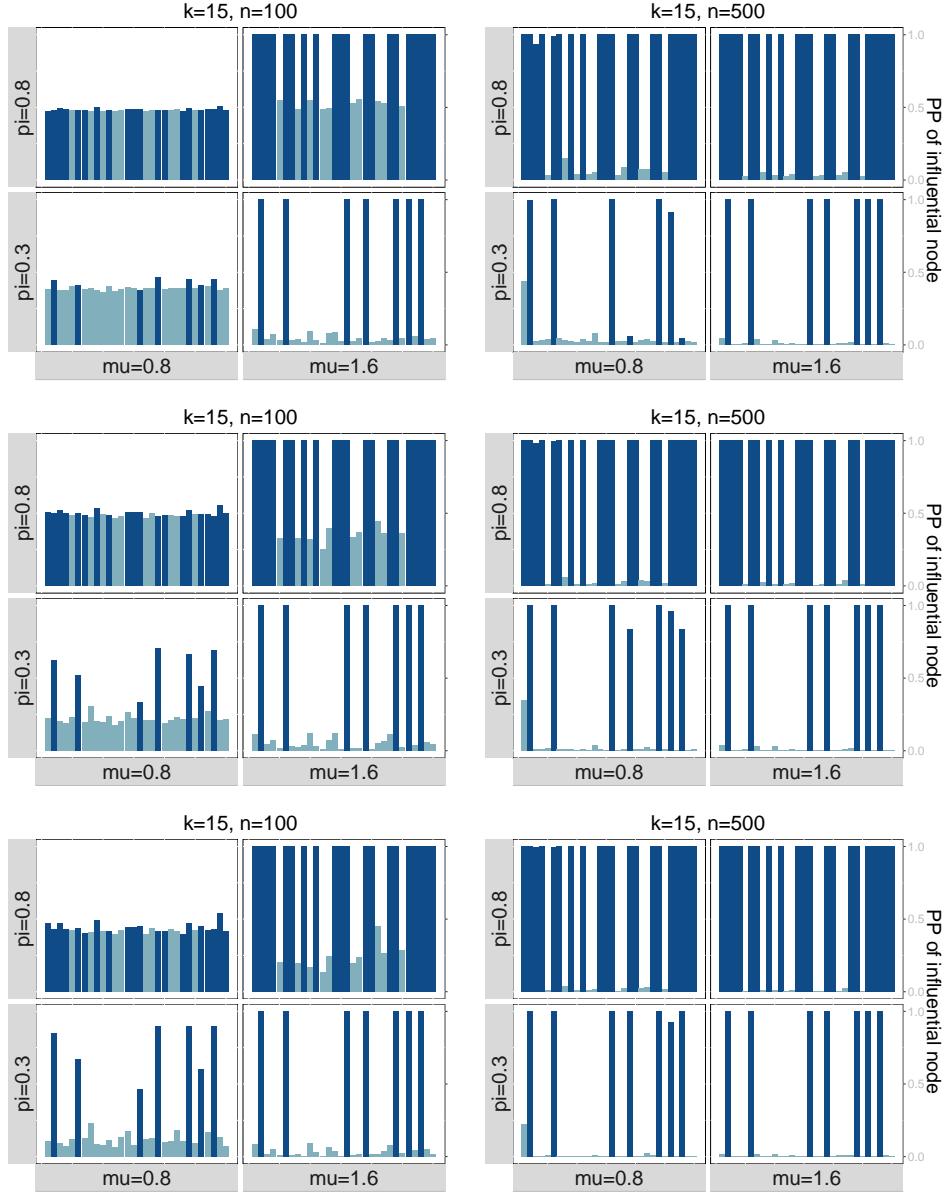


Figure 17: **Posterior probability of influential nodes (theoretical simulations  $k = 15, R = 5, 9$ ).** Top: Latent dimension of  $R = 5$ . Middle: Latent dimension of  $R = 7$ . Bottom: Latent dimension of  $R = 9$ . Different panels represent different number of sampled microbes ( $k = 15$ ) which controls the sparsity of the adjacency matrix and different sample sizes ( $n = 100, 500$ ). Within each panel, we have four plots corresponding to the two values of edge effect size ( $\mu = 0.8, 1.6$ ) and two values of probability of influential node ( $\pi = 0.3, 0.8$ ) which controls the sparsity of the regression coefficient matrix ( $\mathbf{B}$ ). Each bar corresponds to one node (microbe) and the bar are colored depending on whether the node is truly influential (dark) or not influential (light). As expected, the model has a high PP for truly influential nodes (tall dark bars) and a low PP for non-influential nodes (short light bars) with best performance for  $n = 500$ , or for high coefficients  $\mu = 1.6$  or high sparsity  $\pi = 0.3$  for  $n = 100$ . There appear to be no differences by the latent dimension  $R$ .

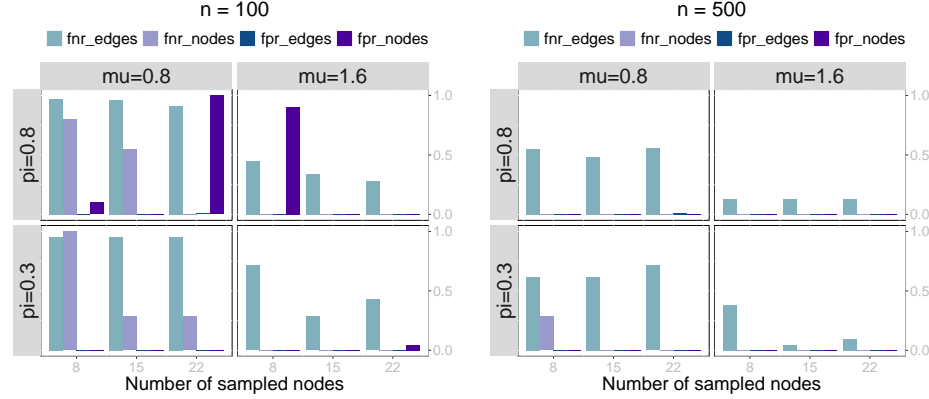


Figure 18: **False positive and false negative rates for influential edges and nodes (theoretical simulations).** X axis corresponds to the number of sampled nodes (microbes) which relates to the sparsity of the adjacency matrices  $\mathbf{A}_i$ . Y axis corresponds to false positive or false negative rates for edges or nodes (depending on the color of the bar). Decisions to reject for edges are based on 95% posterior credible intervals, and for nodes are based on whether the posterior probability of influence is greater than 0.5. Within each panel, we have four plots corresponding to the two values of edge effect size ( $\mu = 0.8, 1.6$ ) and two values of probability of influential node ( $\pi = 0.3, 0.8$ ) which controls the sparsity of the regression coefficient matrix ( $\mathbf{B}$ ). Each bar corresponds to one rate: false positive rate and false negative rate for edges (dark and light blue) and false positive rate and false negative rate for nodes (dark and light purple). With increased sample size ( $n = 500$ ), there are no more false positives for edges and for nodes and there are no false negatives for nodes. Only the false negative rate for edges remains high for  $n = 500$  for the case of small effect size ( $\mu = 0.8$ ).

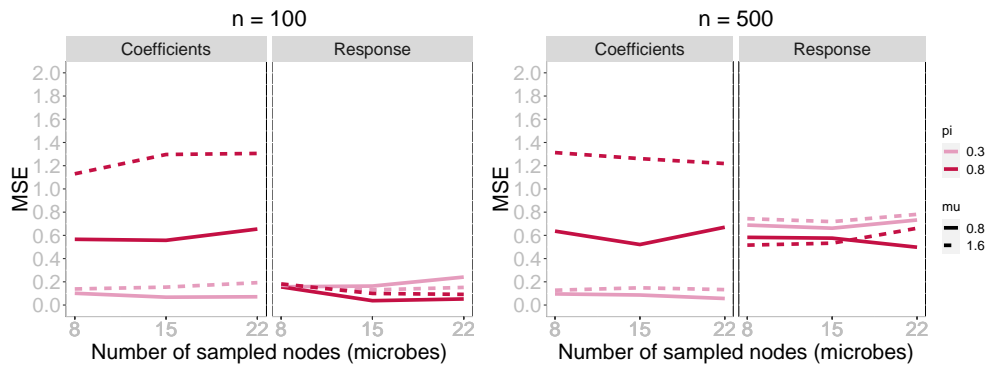
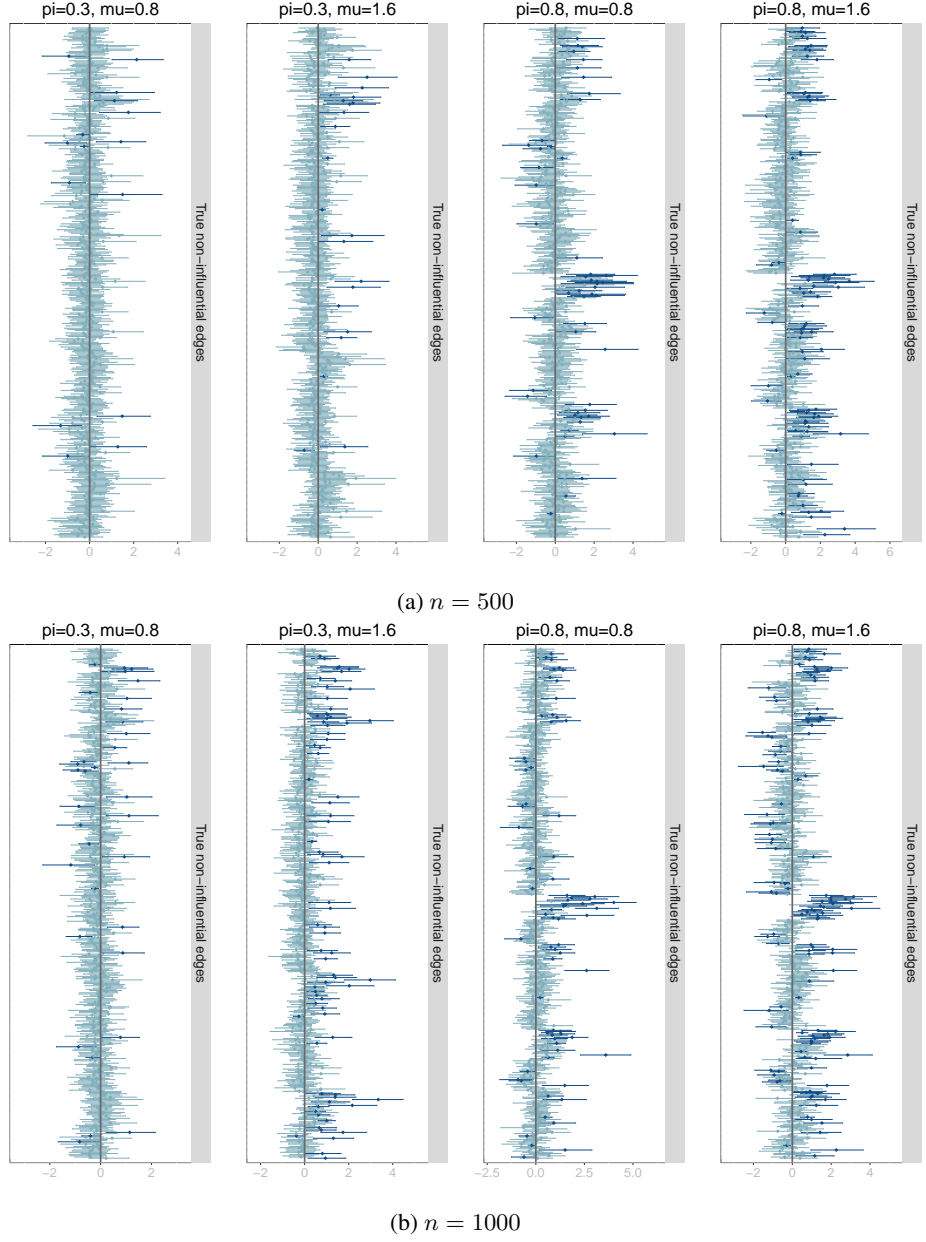


Figure 19: **Mean Square Error for regression coefficients and response.** X axis corresponds to the number of sampled nodes (microbes) which relates to the sparsity of the adjacency matrix  $\mathbf{X}$ . Dashed lines correspond to different values of the true mean for edge effects ( $\mu = 0.8, 1.6$ ) and different colors correspond to different sparsity levels on the regression coefficient matrix  $\mathbf{B}$  ( $\pi = 0.3, 0.8$ ). The MSE does not seem to be affected by the sampling proportion, and it is more impacted in the case of the regression coefficients to the value of  $\mu$ .



**Figure 20: 95 % credible intervals for edge effects (additive model with random coefficients) with  $k = 8$  sampled nodes.** Top (a): Sample size of  $n = 500$ . Bottom (b): Sample size of  $n = 1000$ . Each panel corresponds to a scenario of  $\pi = 0.3, 0.8$  (which controls the sparsity of the regression coefficient matrix  $\mathbf{B}$ ) and  $\mu = 0.8, 1.6$ . We plot the 95 % credible intervals for the regression coefficients per edge. In the additive model, all edges are non-influential. The color of the intervals depends on whether it intersects zero (light) and hence estimated to be non-influential or does not intersect zero (dark) and hence estimated to be influential by the model. Given that the additive model does not have interaction (edge) effects, these panels allow us to visualize false positives (dark intervals). The false positive rate does not appear to be affected by sample size (top vs bottom) with higher rate for the cases of larger effect sizes ( $\mu = 1.6$ ) or less sparsity ( $\pi = 0.8$ ).

#### A.4.2 Realistic case: Additive model

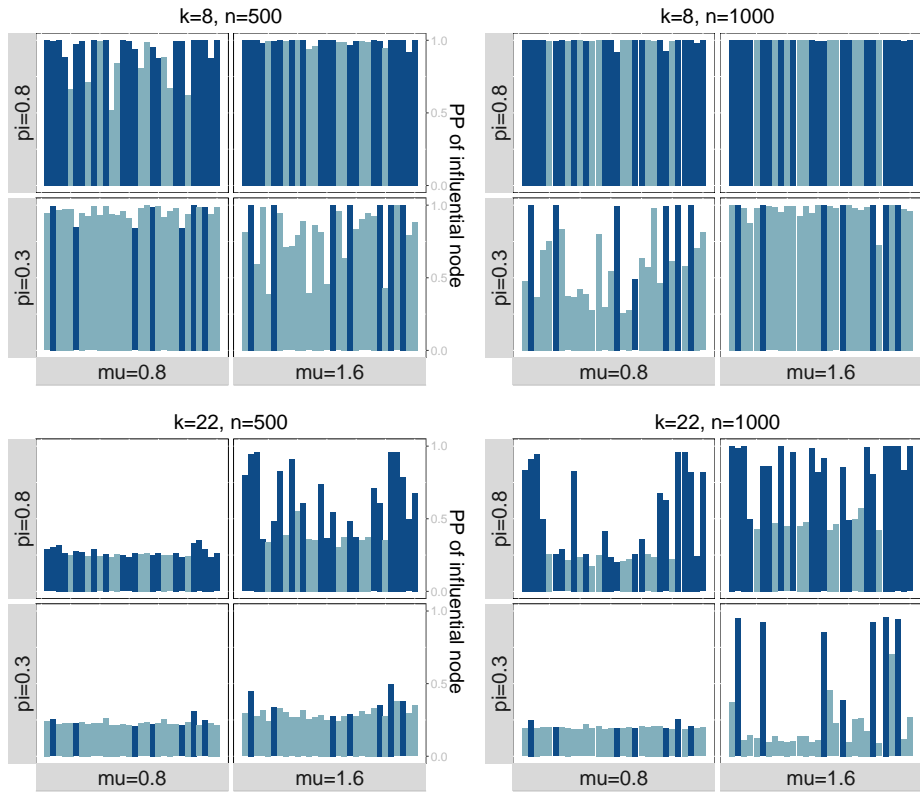


Figure 21: **Posterior probability of influential nodes (additive model with phylogenetic coefficients).** Different panels represent different number of sampled microbes ( $k = 8, 22$ ) which controls the sparsity of the adjacency matrix and different sample sizes ( $n = 500, 1000$ ). Within each panel, we have four plots corresponding to the two values of edge effect size ( $\mu = 0.8, 1.6$ ) and two values of probability of influential node ( $\pi = 0.3, 0.8$ ) which controls the sparsity of the regression coefficient matrix ( $\mathbf{B}$ ). Each bar corresponds to one node (microbe) and the bar are colored depending on whether the node is truly influential (dark) or not influential (light). As with random coefficients (Fig. 8), the model performs poorly for  $k = 8$  sampled nodes as it is unable to identify influential nodes regardless of sample size ( $n$ ) and characteristics of  $\mathbf{B}$  ( $\pi, \mu$ ). For  $k = 22$  sampled microbes, the model behaves better for increased sample size ( $n = 1000$ ) except for high sparsity and small effects ( $\pi = 0.3, \mu = 0.8$ ).

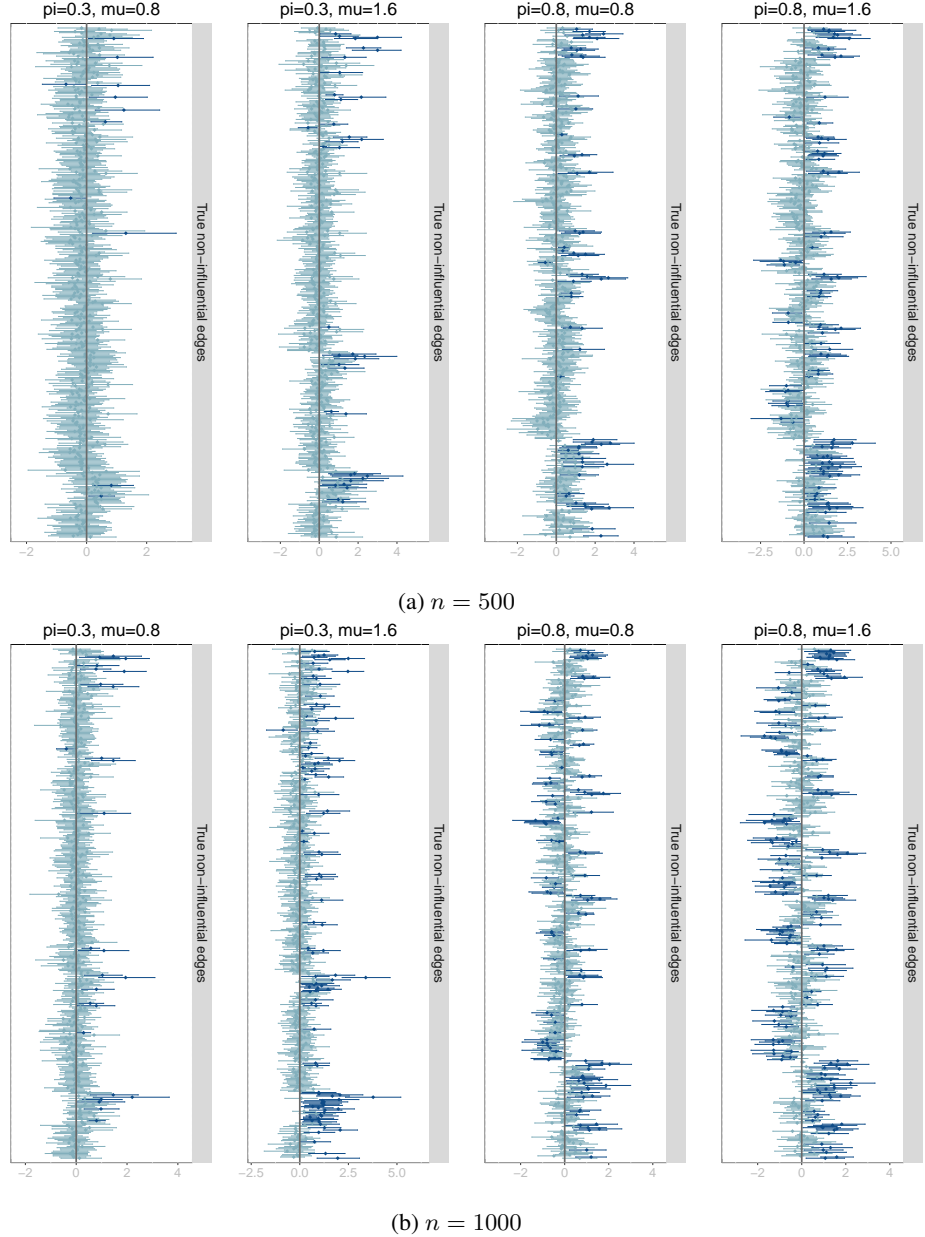


Figure 22: **95 % credible intervals for edge effects (additive model with phylogenetic coefficients) with  $k = 8$  sampled nodes.** Top (a): Sample size of  $n = 500$ . Bottom (b): Sample size of  $n = 1000$ . Each panel corresponds to a scenario of  $\pi = 0.3, 0.8$  (which controls the sparsity of the regression coefficient matrix  $\mathbf{B}$ ) and  $\mu = 0.8, 1.6$ . We plot the 95 % credible intervals for the regression coefficients per edge. In the additive model, all edges are non-influential. The color of the intervals depends on whether it intersects zero (light) and hence estimated to be non-influential or does not intersect zero (dark) and hence estimated to be influential by the model. Given that the additive model does not have interaction (edge) effects, these panels allow us to visualize false positives (dark intervals). Same results as with random coefficients (Fig. 20). Namely, the false positive rates is increased with larger effect sizes ( $\mu = 1.6$ ) or less sparsity ( $\pi = 0.8$ ).

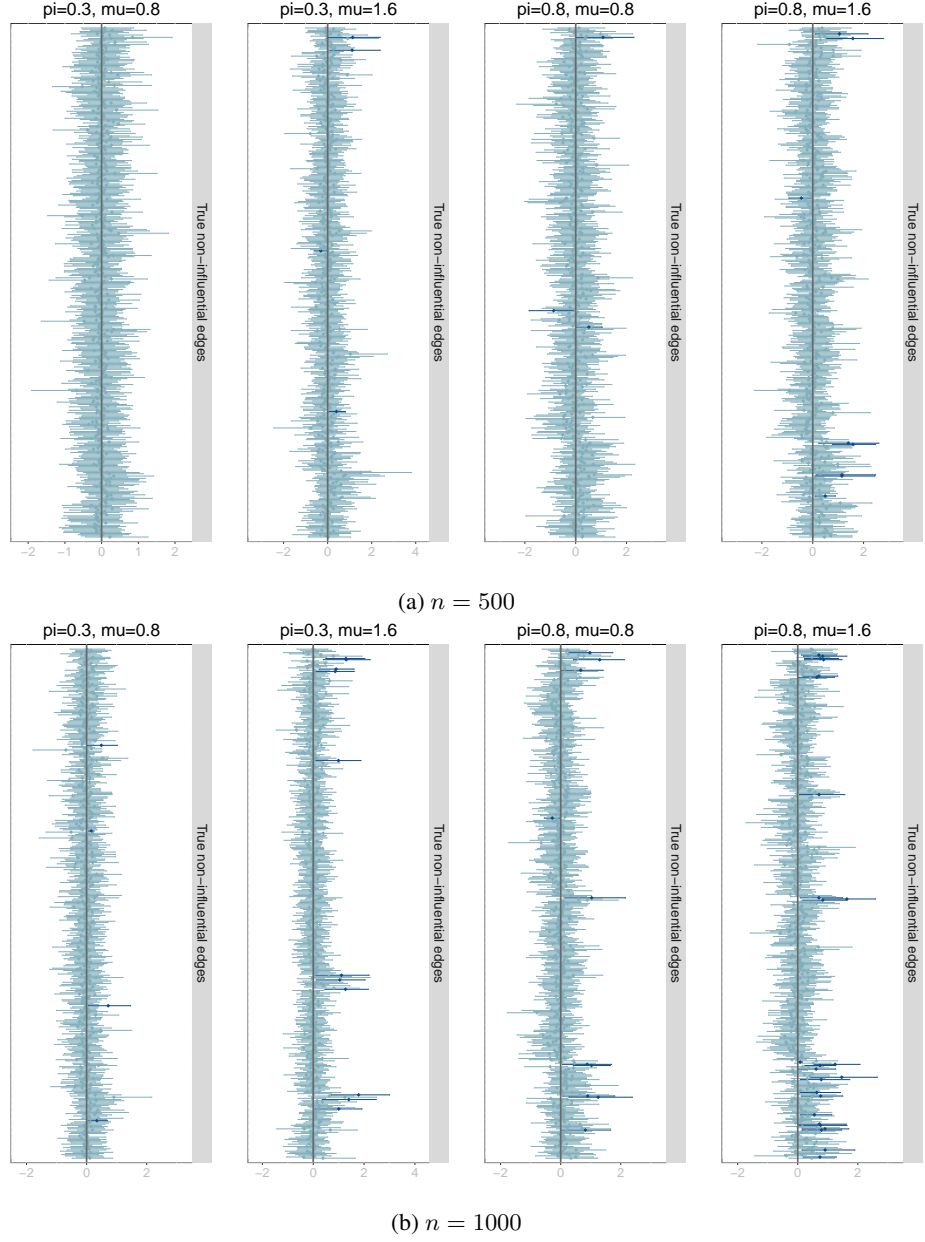
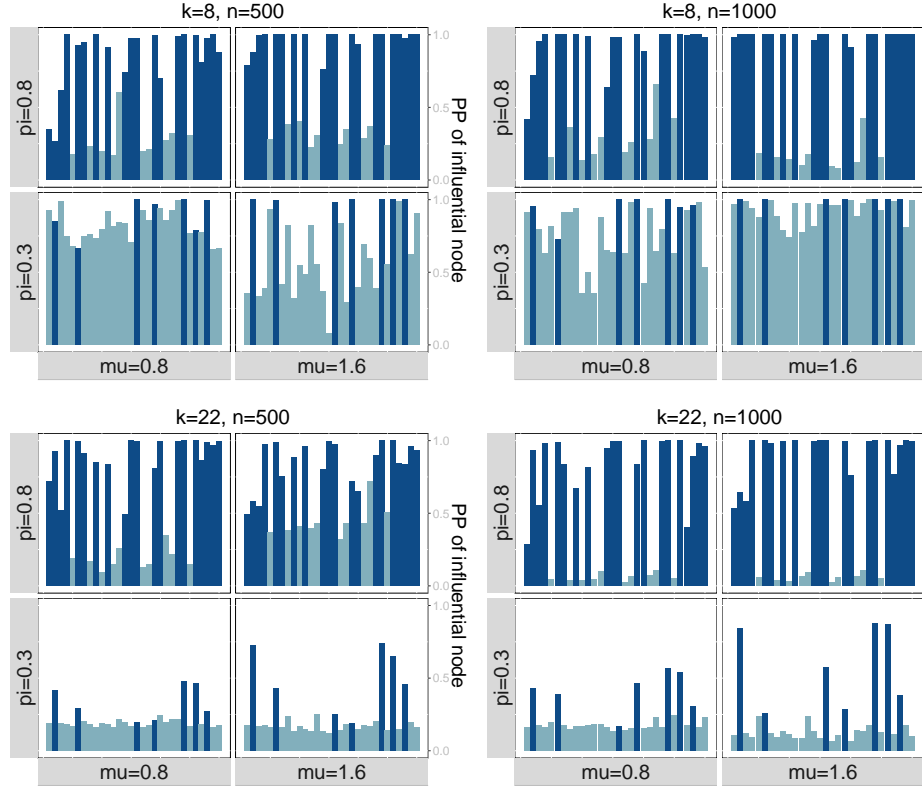


Figure 23: **95 % credible intervals for edge effects (additive model with phylogenetic coefficients) with  $k = 22$  sampled nodes.** Top (a): Sample size of  $n = 500$ . Bottom (b): Sample size of  $n = 1000$ . Each panel corresponds to a scenario of  $\pi = 0.3, 0.8$  (which controls the sparsity of the regression coefficient matrix  $\mathbf{B}$ ) and  $\mu = 0.8, 1.6$ . We plot the 95 % credible intervals for the regression coefficients per edge. In the additive model, all edges are non-influential. The color of the intervals depends on whether it intersects zero (light) and hence estimated to be non-influential or does not intersect zero (dark) and hence estimated to be influential by the model. Given that the additive model does not have interaction (edge) effects, these panels allow us to visualize false positives (dark intervals). As with random coefficients, we observe a decreased false positive rate when compared to  $k = 8$  sampled microbes (Fig. 22).



**Figure 24: Posterior probability of influential nodes (interaction model with random coefficients).** Different panels represent different number of sampled microbes ( $k = 8, 22$ ) which controls the sparsity of the adjacency matrix and different sample sizes ( $n = 100, 500$ ). Within each panel, we have four plots corresponding to the two values of edge effect size ( $\mu = 0.8, 1.6$ ) and two values of probability of influential edge ( $\pi = 0.3, 0.8$ ) which controls the sparsity of the regression coefficient matrix ( $\mathbf{B}$ ). Each bar corresponds to one node (microbe) and the bar are colored depending on whether the node is truly influential (dark) or not influential (light). The model has a high PP for truly influential nodes (tall dark bars) a low PP for non-influential nodes (short light bars) for all cases of low sparsity in  $\mathbf{B}$  ( $\pi = 0.8$ ) regardless of sample size ( $n$ ), number of sampled microbes ( $k$ ) or effect size ( $\mu$ ). For high sparsity in  $\mathbf{B}$  ( $\pi = 0.3$ ), there is a high false positive rate (tall light bars) when  $k = 8$  microbes are sampled (top) for both values of effect size ( $\mu = 0.8, 1.6$ ) and both sample sizes ( $n = 500, 1000$ ). In this setting ( $\pi = 0.3$ ), there is a high false negative rate (short dark bars) for  $k = 22, n = 500$  which is improved with larger sample size ( $k = 22, n = 1000$ ). Interestingly, all cases of high sparsity ( $\pi = 0.3$ ) for  $k = 22, n = 500$  have good performance with phylogenetic coefficients (Fig. 10).

#### A.4.3 Realistic case: Interaction model

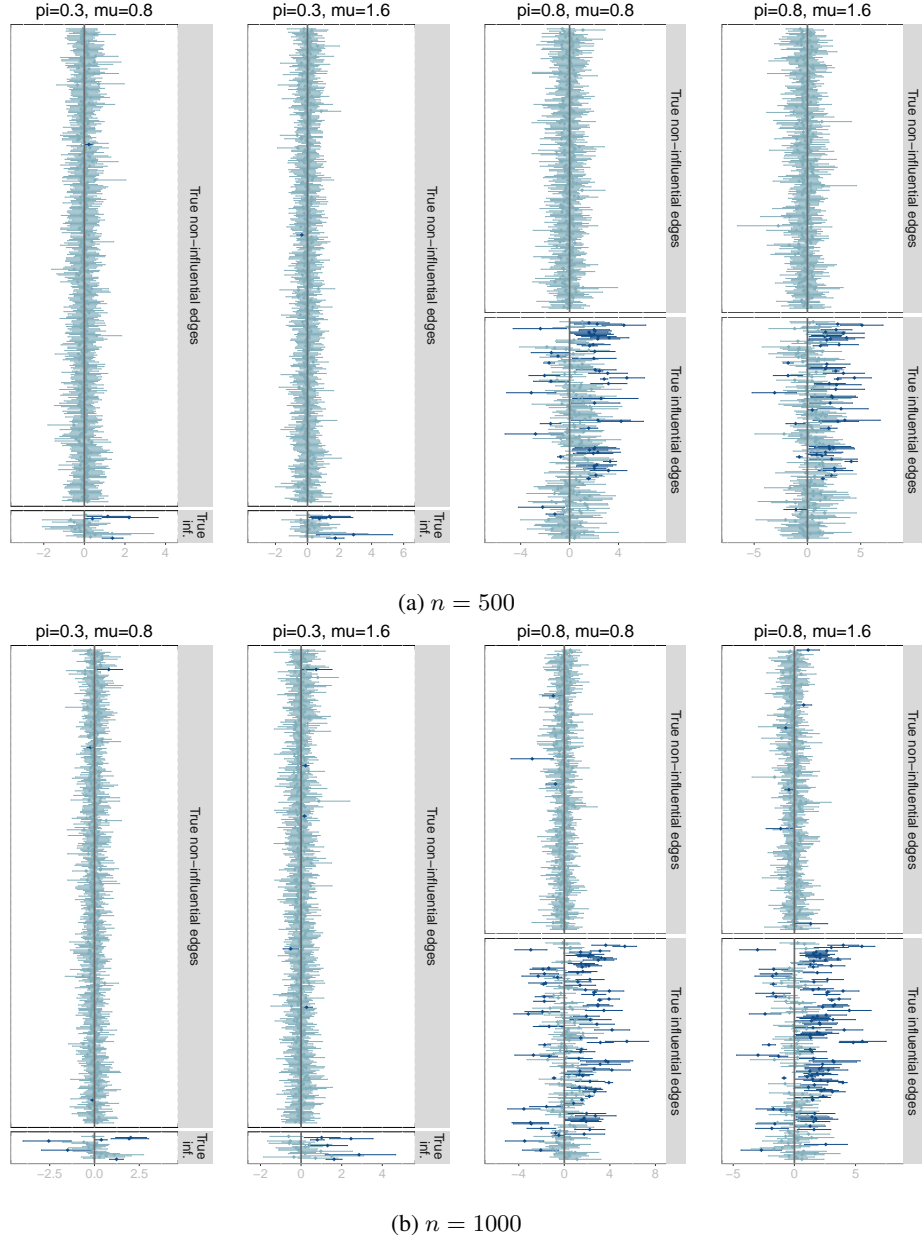


Figure 25: **95 % credible intervals for edge effects (interaction model with random coefficients) with  $k = 22$  sampled nodes.** Top (a): Sample size of  $n = 500$ . Bottom (b): Sample size of  $n = 1000$ . Each panel corresponds to a scenario of  $\pi = 0.3, 0.8$  (which controls the sparsity of the regression coefficient matrix  $\mathbf{B}$ ) and  $\mu = 0.8, 1.6$ . We plot the 95 % credible intervals for the regression coefficients per edge ordered depending on whether they are truly non-influential edges (top of each panel) or truly influential edges (bottom of each panel). The color of the intervals depends on whether it intersects zero (light) and hence estimated to be non-influential or does not intersect zero (dark) and hence estimated to be influential by the model. These panels allow us to visualize false positives (dark intervals on the top panel) or false negatives (light intervals on the bottom panel).

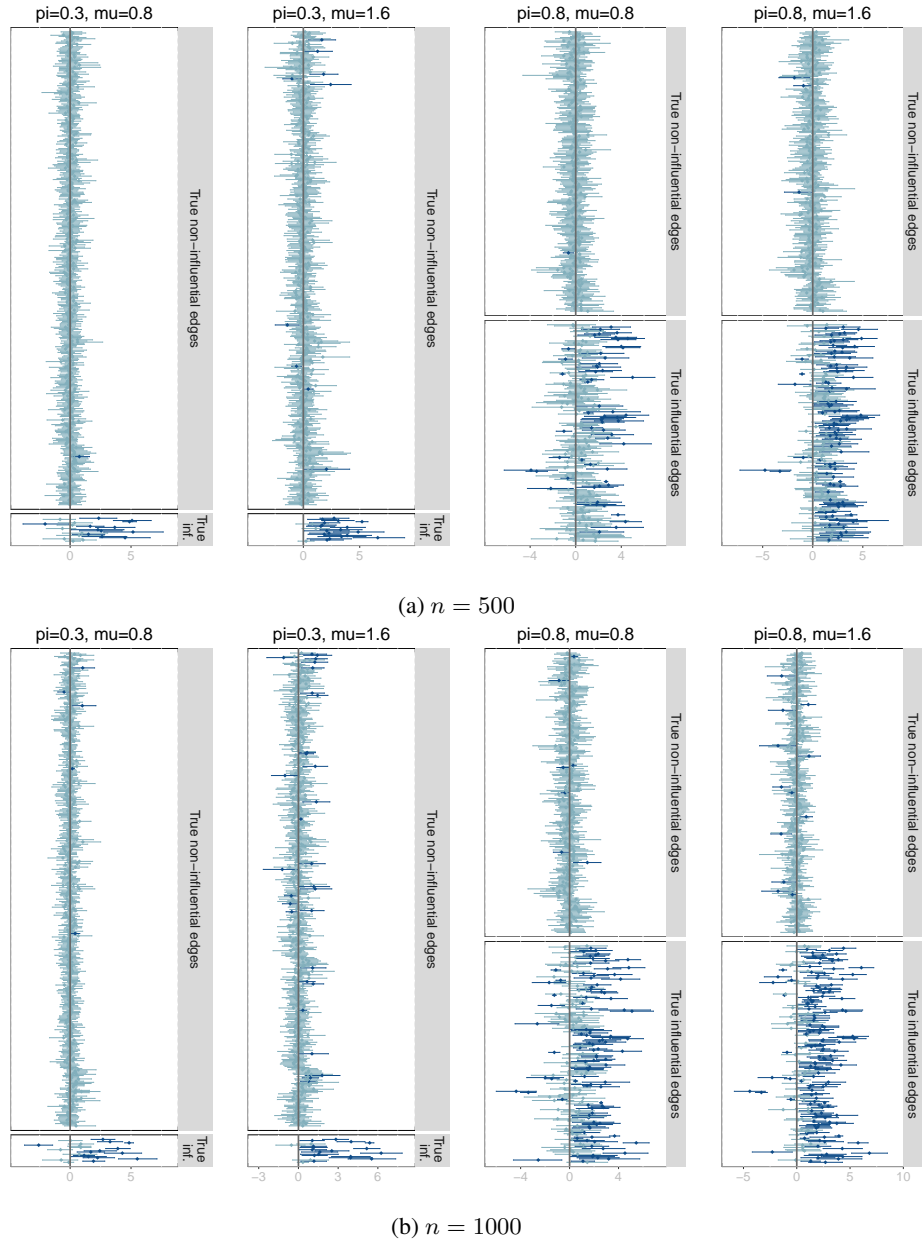


Figure 26: **95 % credible intervals for edge effects (interaction model with phylogenetic coefficients) with  $k = 8$  sampled nodes.** Top (a): Sample size of  $n = 500$ . Bottom (b): Sample size of  $n = 1000$ . Each panel corresponds to a scenario of  $\pi = 0.3, 0.8$  (which controls the sparsity of the regression coefficient matrix  $\mathbf{B}$ ) and  $\mu = 0.8, 1.6$ . We plot the 95 % credible intervals for the regression coefficients per edge ordered depending on whether they are truly non-influential edges (top of each panel) or truly influential edges (bottom of each panel). The color of the intervals depends on whether it intersects zero (light) and hence estimated to be non-influential or does not intersect zero (dark) and hence estimated to be influential by the model. These panels allow us to visualize false positives (dark intervals on the top panel) or false negatives (light intervals on the bottom panel).

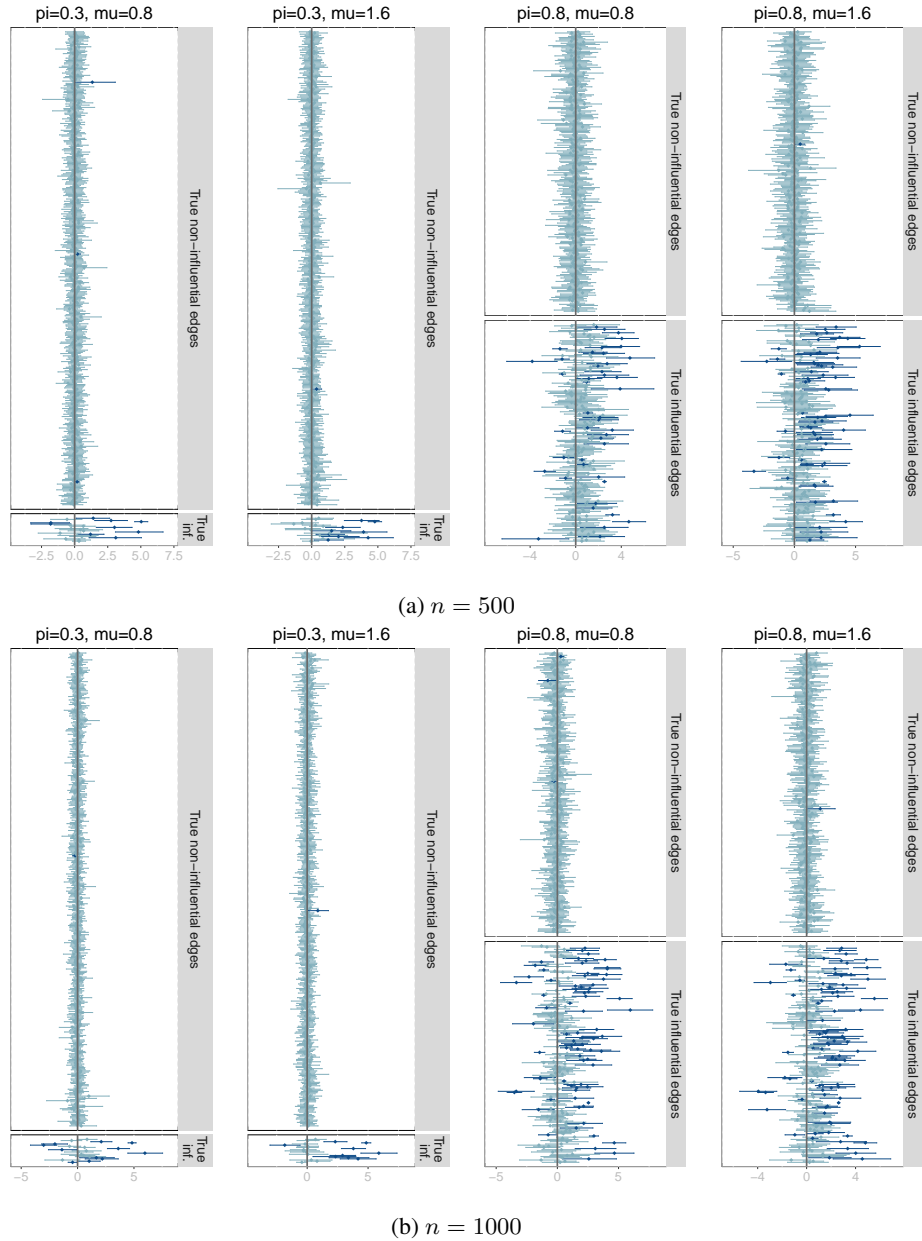


Figure 27: **95 % credible intervals for edge effects (interaction model with phylogenetic coefficients) with  $k = 22$  sampled nodes.** Top (a): Sample size of  $n = 500$ . Bottom (b): Sample size of  $n = 1000$ . Each panel corresponds to a scenario of  $\pi = 0.3, 0.8$  (which controls the sparsity of the regression coefficient matrix  $\mathbf{B}$ ) and  $\mu = 0.8, 1.6$ . We plot the 95 % credible intervals for the regression coefficients per edge ordered depending on whether they are truly non-influential edges (top of each panel) or truly influential edges (bottom of each panel). The color of the intervals depends on whether it intersects zero (light) and hence estimated to be non-influential or does not intersect zero (dark) and hence estimated to be influential by the model. These panels allow us to visualize false positives (dark intervals on the top panel) or false negatives (light intervals on the bottom panel).

#### A.4.4 Realistic case: Functional redundancy

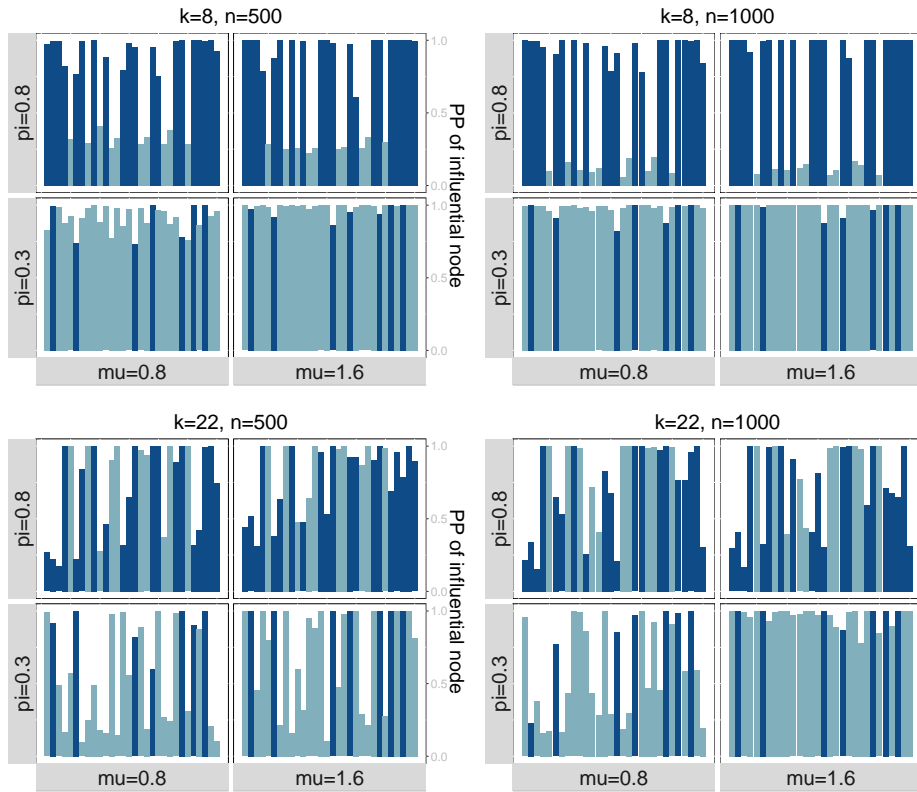


Figure 28: **Posterior probability of influential nodes (functional redundancy model with phylogenetic coefficients).** Different panels represent different number of sampled microbes ( $k = 8, 22$ ) which controls the sparsity of the adjacency matrix and different sample sizes ( $n = 100, 500$ ). Within each panel, we have four plots corresponding to the two values of edge effect size ( $\mu = 0.8, 1.6$ ) and two values of probability of influential edge ( $\pi = 0.3, 0.8$ ) which controls the sparsity of the regression coefficient matrix ( $\mathbf{B}$ ). Each bar corresponds to one node (microbe) and the bar are colored depending on whether the node is truly influential (dark) or not influential (light). The model has a high PP for truly influential nodes (tall dark bars) a low PP for non-influential nodes (short light bars) only when  $n = 1000$  and  $\pi = 0.3$  (high sparsity in  $\mathbf{B}$ ). The model shows high false positive rate in all settings except for low sparsity ( $\pi = 0.8$ ) with small number of sampled nodes ( $k = 8$ ). This behavior is similar with random coefficients (Fig. 12).

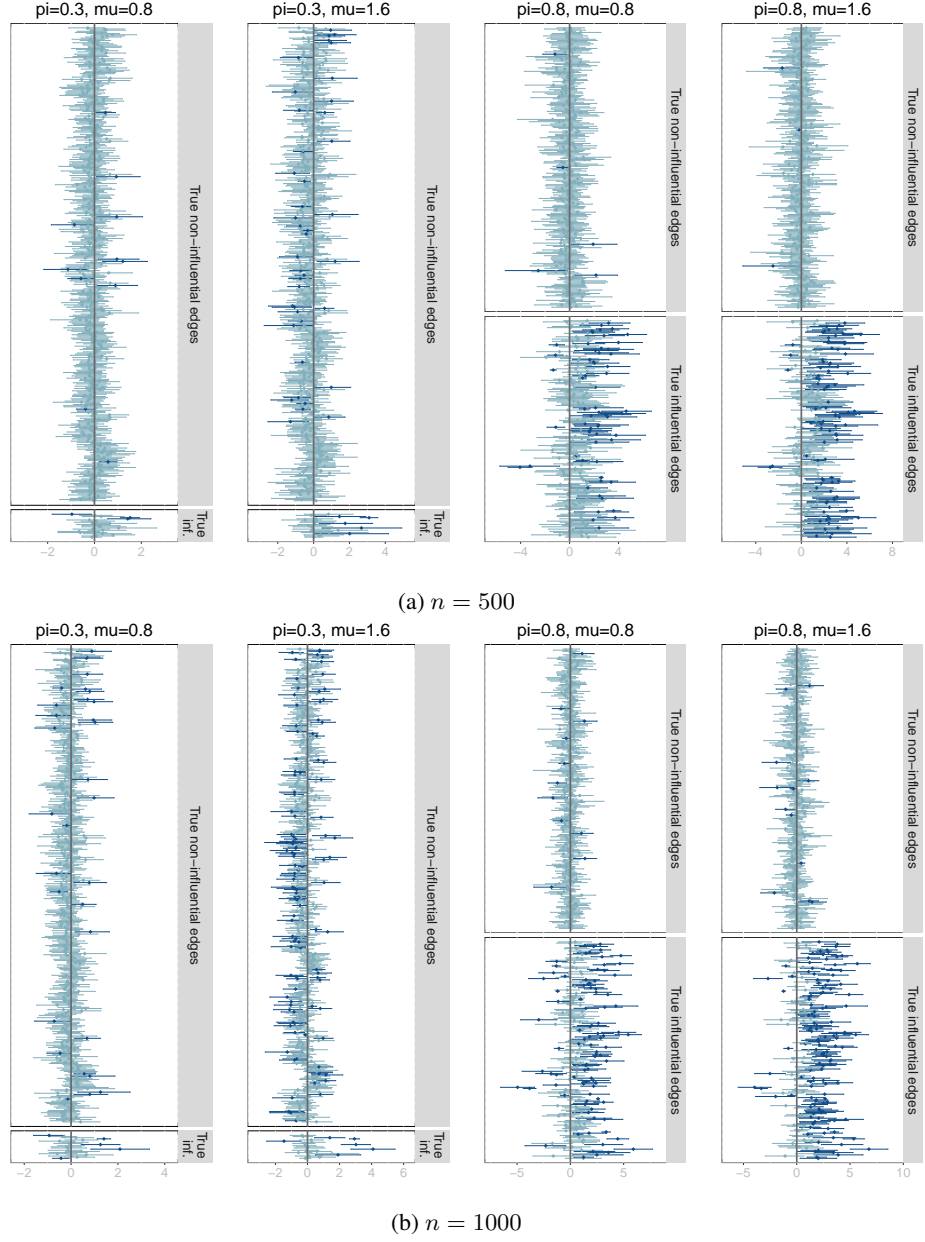


Figure 29: **95 % credible intervals for edge effects (functional redundancy model with phylogenetic coefficients) with  $k = 8$  sampled nodes.** Top (a): Sample size of  $n = 500$ . Bottom (b): Sample size of  $n = 1000$ . Each panel corresponds to a scenario of  $\pi = 0.3, 0.8$  (which controls the sparsity of the regression coefficient matrix  $B$ ) and  $\mu = 0.8, 1.6$ . We plot the 95 % credible intervals for the regression coefficients per edge ordered depending on whether they are truly non-influential edges (top of each panel) or truly influential edges (bottom of each panel). The color of the intervals depends on whether it intersects zero (light) and hence estimated to be non-influential or does not intersect zero (dark) and hence estimated to be influential by the model. These panels allow us to visualize false positives (dark intervals on the top panel) or false negatives (light intervals on the bottom panel).

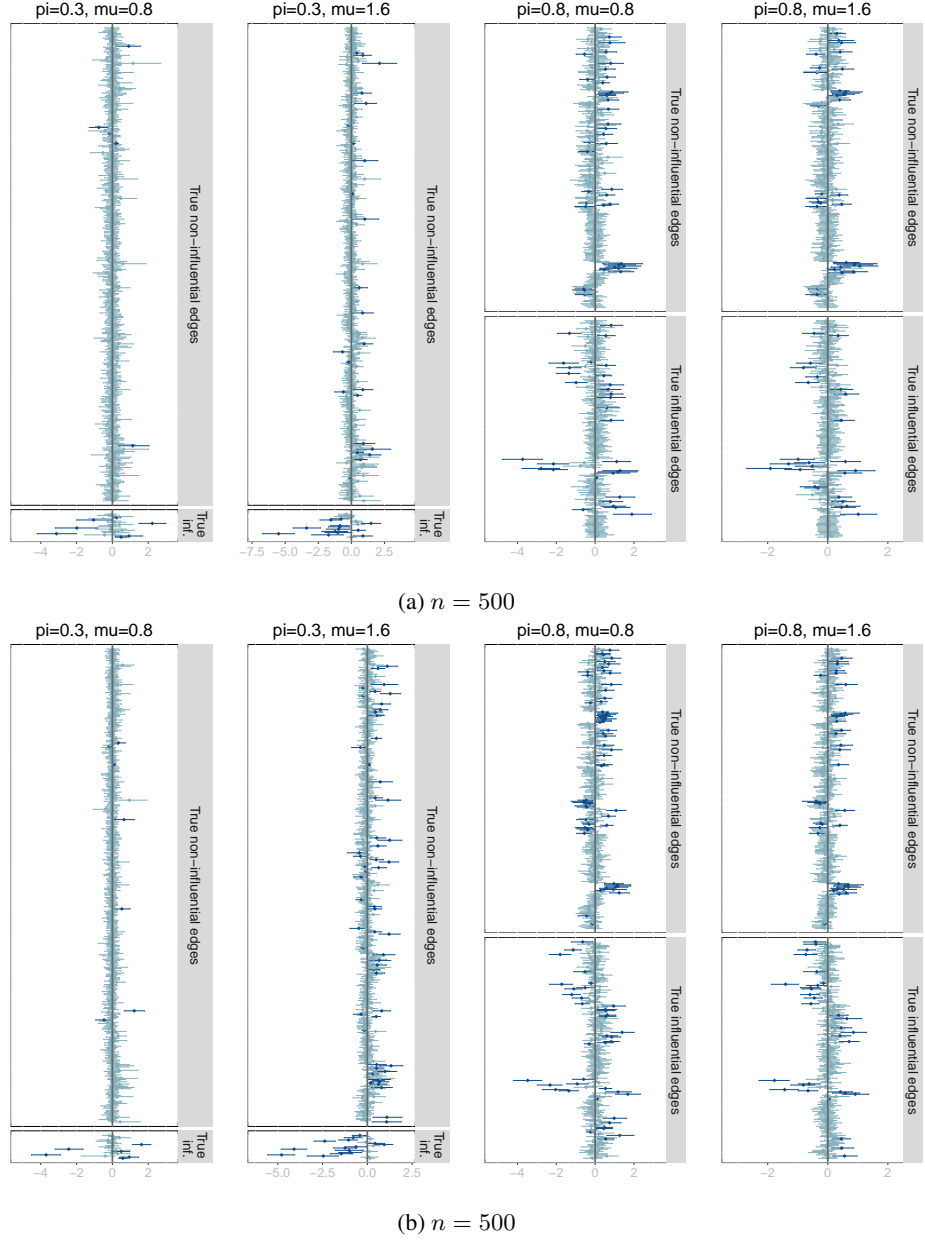
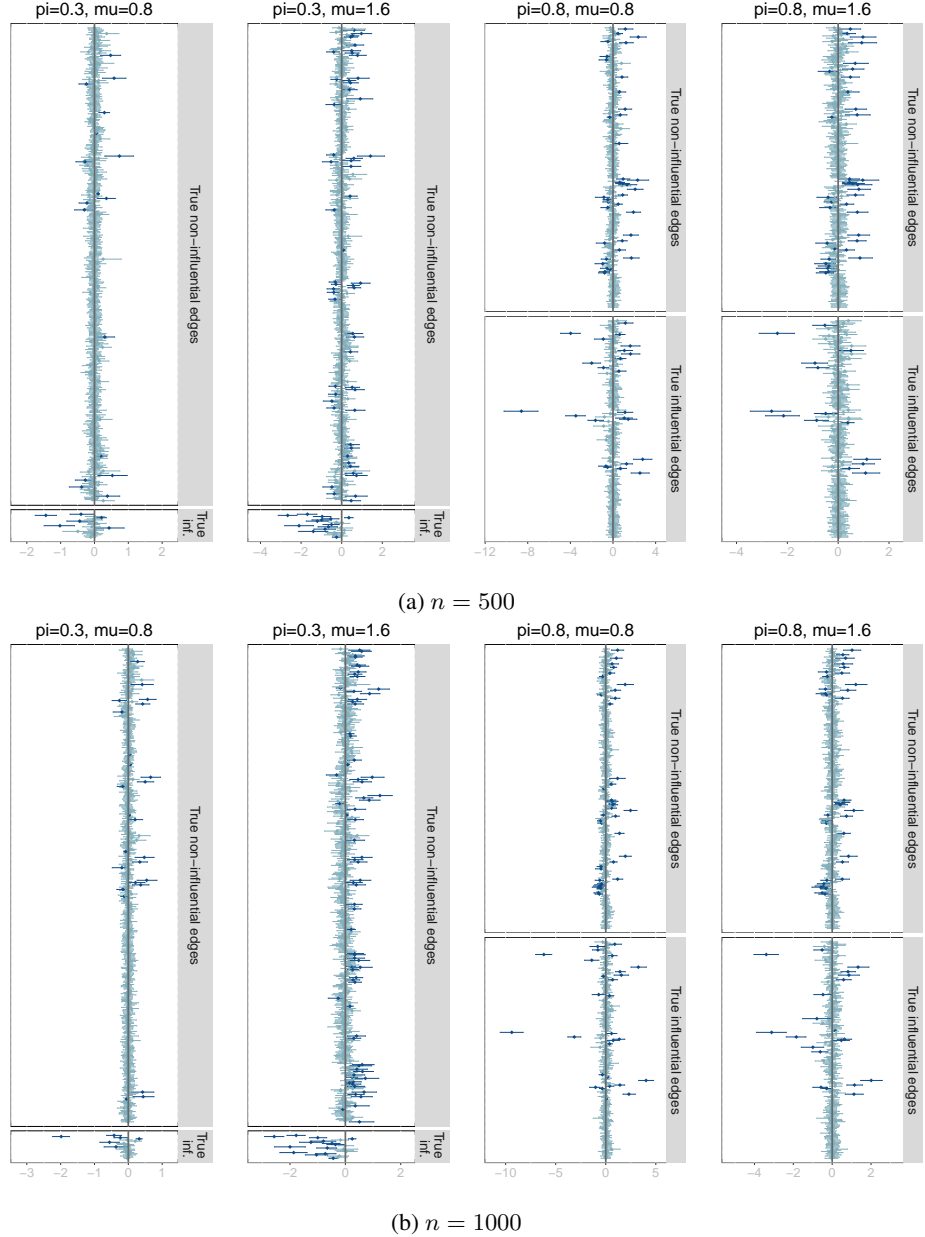


Figure 30: **95 % credible intervals for edge effects (functional redundancy model with random coefficients) with  $k = 22$  sampled nodes.** Top (a): Sample size of  $n = 500$ . Bottom (b): Sample size of  $n = 1000$ . Each panel corresponds to a scenario of  $\pi = 0.3, 0.8$  (which controls the sparsity of the regression coefficient matrix  $\mathbf{B}$ ) and  $\mu = 0.8, 1.6$ . We plot the 95 % credible intervals for the regression coefficients per edge ordered depending on whether they are truly non-influential edges (top of each panel) or truly influential edges (bottom of each panel). The color of the intervals depends on whether it intersects zero (light) and hence estimated to be non-influential or does not intersect zero (dark) and hence estimated to be influential by the model. These panels allow us to visualize false positives (dark intervals on the top panel) or false negatives (light intervals on the bottom panel).



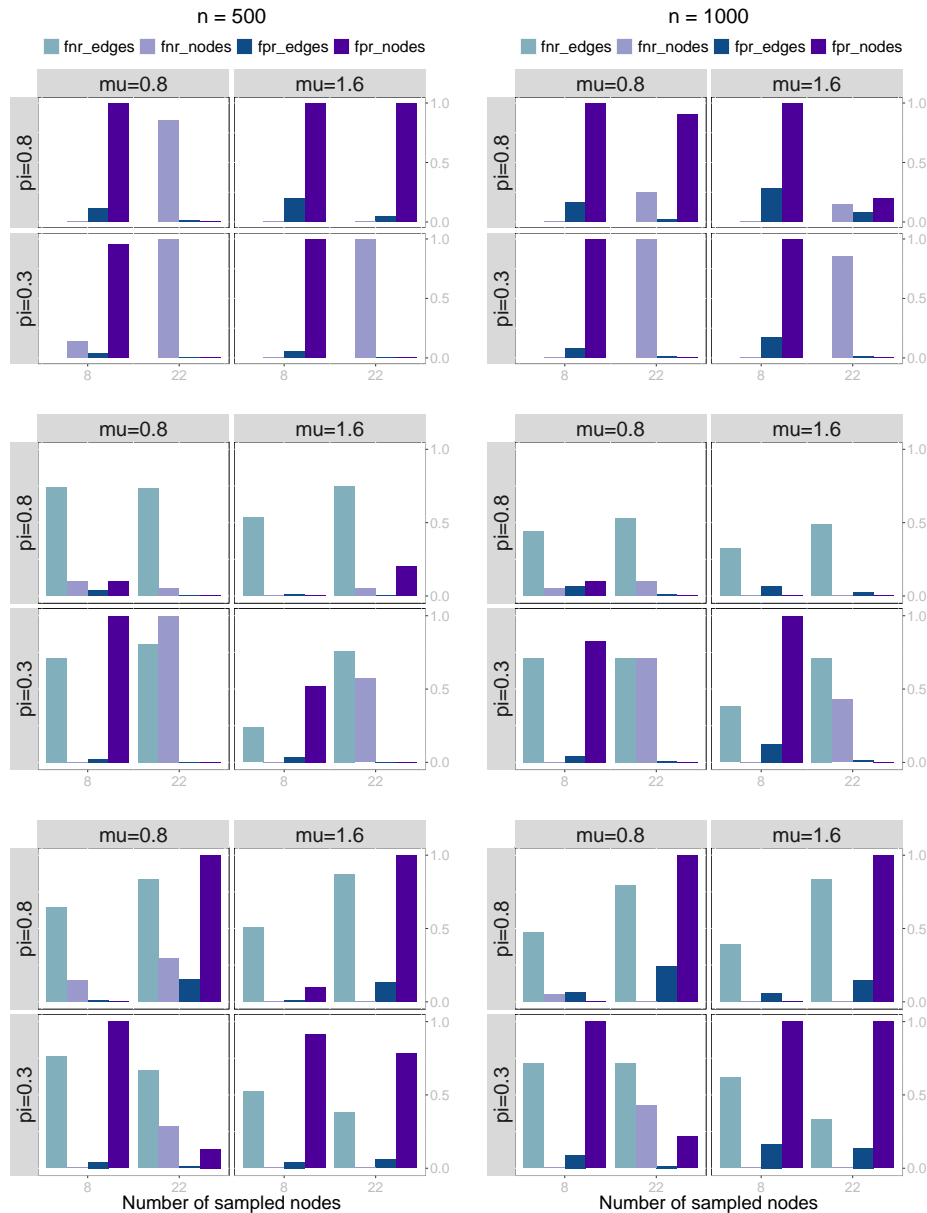
**Figure 31: 95 % credible intervals for edge effects (functional redundancy model with phylogenetic coefficients) with  $k = 22$  sampled nodes.** Top (a): Sample size of  $n = 500$ . Bottom (b): Sample size of  $n = 1000$ . Each panel corresponds to a scenario of  $\pi = 0.3, 0.8$  (which controls the sparsity of the regression coefficient matrix  $B$ ) and  $\mu = 0.8, 1.6$ . We plot the 95 % credible intervals for the regression coefficients per edge ordered depending on whether they are truly non-influential edges (top of each panel) or truly influential edges (bottom of each panel). The color of the intervals depends on whether it intersects zero (light) and hence estimated to be non-influential or does not intersect zero (dark) and hence estimated to be influential by the model. These panels allow us to visualize false positives (dark intervals on the top panel) or false negatives (light intervals on the bottom panel).

#### A.4.5 Convergence checks

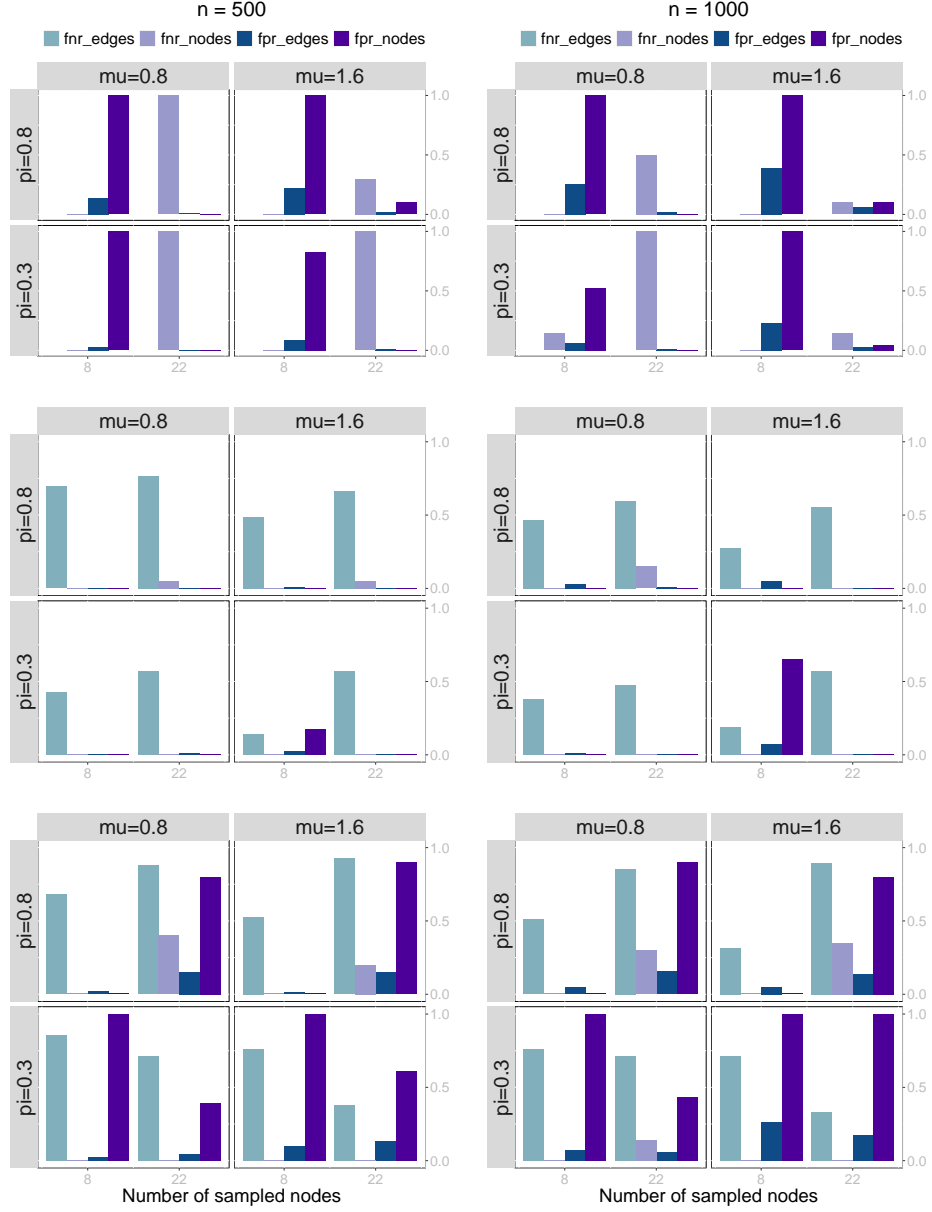
Sample size	Simulation Type	$\hat{R}(\xi)$	$\hat{R}(\gamma)$
500	additive random	1.06	1.08
500	interaction random	1.02	1.02
500	redundant random	1.02	1.05
500	additive phylogenetic	1.09	1.04
500	interaction phylogenetic	1.09	1.08
500	redundant phylogenetic	1.01	1.02
1000	additive random	1.13	1.20
1000	interaction random	1.04	1.07
1000	redundant random	1.07	1.10
1000	additive phylogenetic	1.04	1.02
1000	interaction phylogenetic	1.09	1.09
1000	redundant phylogenetic	1.01	1.03

Table 5: Convergence for realistic simulations. Maximum  $\hat{R}$  convergence statistics for the realistic simulations by simulation type.

#### A.4.6 False positive and negative rates



**Figure 32: False positive and false negative rates for influential edges and nodes for additive (top), interaction (middle) and functional redundancy (bottom) models with random coefficients.** X axis corresponds to the number of sampled nodes (microbes) which relates to the sparsity of the adjacency matrix  $\mathbf{X}$ . Decisions to reject for edges are based on 95% posterior credible intervals, and for nodes are based on whether the posterior probability of influence is greater than 0.5. Within each panel, we have four plots corresponding to the two values of edge effect size ( $\mu = 0.8, 1.6$ ) and two values of probability of influential edge ( $\pi = 0.3, 0.8$ ) which controls the sparsity of the regression coefficient matrix ( $\mathbf{B}$ ). Each bar corresponds to one rate: false positive rate and false negative rate for edges (dark and light blue) and false positive rate and false negative rate for nodes (dark and light purple). An interaction model with low sparsity ( $\pi = 0.8$ ) shows the best performance in terms of controlled false positive and false negative rates for all setting of  $n$  and  $\mu$ .



**Figure 33: False positive and false negative rates for influential edges and nodes for additive (top), interaction (middle) and functional redundancy (bottom) models with phylogenetic coefficients.** X axis corresponds to the number of sampled nodes (microbes) which relates to the sparsity of the adjacency matrix  $\mathbf{X}$ . Decisions to reject for edges are based on 95% posterior credible intervals, and for nodes are based on whether the posterior probability of influence is greater than 0.5. Within each panel, we have four plots corresponding to the two values of edge effect size ( $\mu = 0.8, 1.6$ ) and two values of probability of influential edge ( $\pi = 0.3, 0.8$ ) which controls the sparsity of the regression coefficient matrix ( $\mathbf{B}$ ). Each bar corresponds to one rate: false positive rate and false negative rate for edges (dark and light blue) and false positive rate and false negative rate for nodes (dark and light purple). Again, an interaction model shows the best performance in terms of controlled false positive and false negative rates for all settings of  $\pi$ ,  $n$  and  $\mu$ .

### A.5 Fungal and bacterial drivers of Phosphorous Leaching in Soil

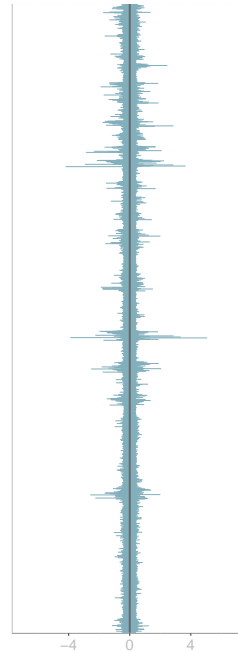


Figure 34: **Posterior 95% credible intervals for edge effects (real-world data)**. The color of the intervals depends on whether it intersects zero (light) and hence estimated to be non-influential or does not intersect zero (dark) and hence estimated to be influential by the model. Note that there are no dark intervals: no edges are found to be influential.

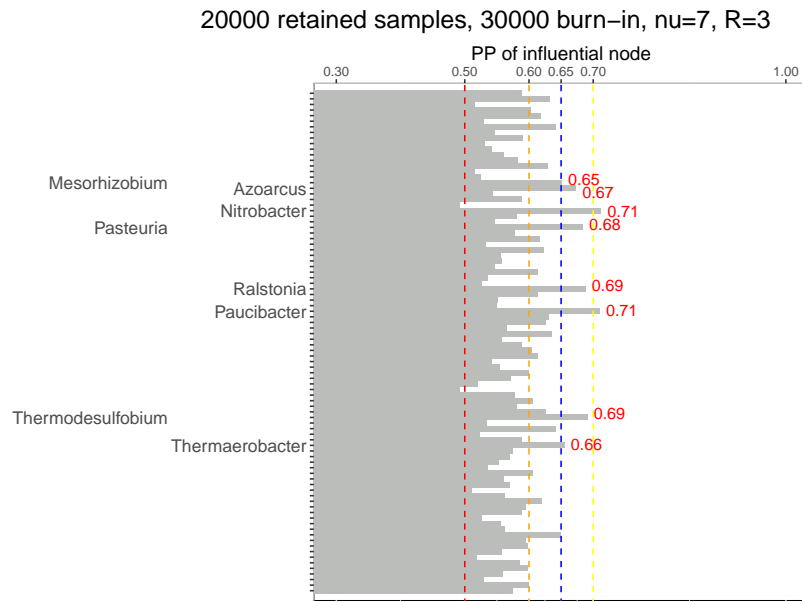


Figure 35: **Posterior probability of influential nodes (bacterial microbiome data)**. We consider genus OTUs with a posterior probability of being influential nodes greater than or equal to 0.65 to be considered influential. We present other thresholds for comparison on which OTUs would be influential: red dashed line for 0.5, orange dashed line for 0.6, blue dashed line for 0.65 significance cutoff, and yellow dashed line for 0.7. For the arbitrary threshold of 0.65, 8 bacterial genera are identified as influential to the P leaching response

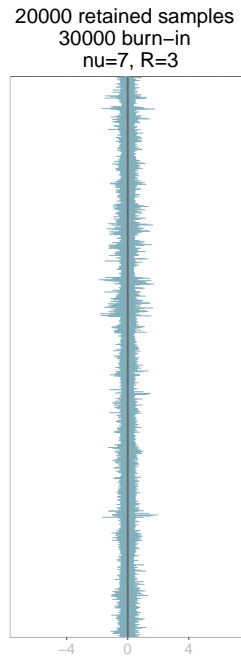


Figure 36: **Posterior 95% credible intervals for edge effects (real-world data).** The color of the intervals depends on whether it intersects zero (light) and hence estimated to be non-influential or does not intersect zero (dark) and hence estimated to be influential by the model. Note that there are no dark intervals: no edges are found to be influential.

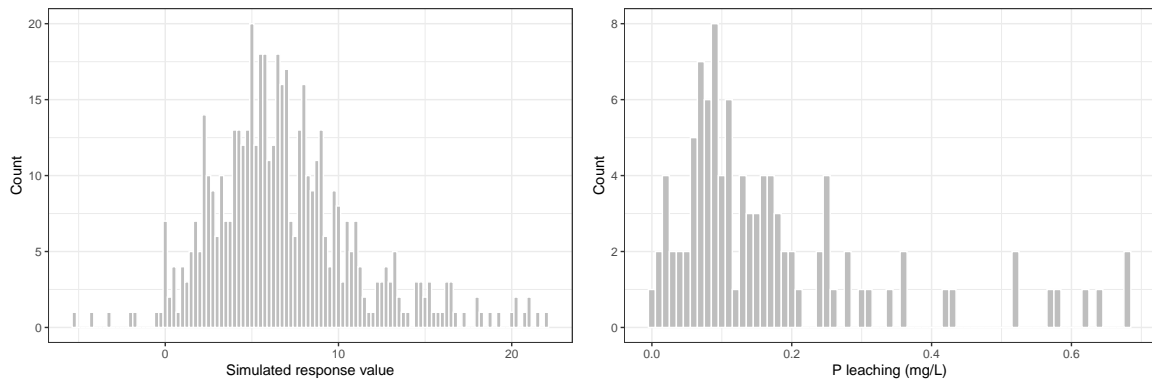


Figure 37: Histogram of response values for simulated "functional redundancy" data with  $\pi = 0.8$ ,  $\mu = 0.8$ ,  $n = 500$  samples,  $k = 8$  sampled nodes (left) and for the phosphorous leaching data, including augmented samples (right).